UNIVERSIDADE FEDERAL DE PERNAMBUCO

CENTRO DE TECNOLOGIA E GEOCIÊNCIAS

DEPARTAMENTO DE GEOLOGIA

PROGRAMA DE PÓS-GRADUAÇÃO EM GEOCIÊNCIAS

BIANCA THALITA ARAÚJO DE LIMA ALBUQUERQUE

PETROLOGIA E GEOQUÍMICA DO GRANITO COM EPÍDOTO MAGMÁTICO CARMO, TERRENO CACHOEIRINHA-SALGUEIRO, PERNAMBUCO

Recife

2021

BIANCA THALITA ARAÚJO DE LIMA ALBUQUERQUE

PETROLOGIA E GEOQUÍMICA DO GRANITO COM EPÍDOTO MAGMÁTICO CARMO, TERRENO CACHOEIRINHA-SALGUEIRO, PERNAMBUCO

Dissertação apresentada ao Programa de Pós-graduação em Geociências, Centro de Tecnologia e Geociências da Universidade Federal de Pernambuco como parte dos requisitos parciais para obtenção do título de mestre em Geociências.

Área de concentração: Geoquímica, Geofísica e Evolução Crustal

Orientadora: Profª. Drª. Valderez Pinto Ferreira

Coorientador: Prof. Dr. Alcides Nóbrega Sial

Recife

2021

Catalogação na fonte
Bibliotecária Maria Luiza de Moura Ferreira, CRB-4 / 1469

A345p Albuquerque, Bianca Thalita Araújo de Lima.
Petrologia e geoquímica do granito com epídoto magmático Carmo, terreno Cachoeirinha-Salgueiro, Pernambuco / Bianca Thalita Araújo de Lima Albuquerque. - 2021.
116 folhas, il.

Orientadora: Profa. Dra. Valderez Pinto Ferreira.
Coorientador: Prof. Dr. Alcides Nóbrega Sial.

Dissertação (Mestrado) – Universidade Federal de Pernambuco. CTG. Programa de Pós-Graduação em Geociências, 2021.
Inclui Referências e Anexo.

1. Geociências. 2. Magmatismo sin-colisional. 3. Fusão da placa. 4. Contribuição de sedimentos. 5. Enclaves microgranulares máficos. 6. granitos tipo I. 7. Província Borborema. I. Ferreira, Valderez Pinto (Orientadora). II. Sial, Alcides Nóbrega (Coorientador). III. Título.

UFPE

551 CDD (22. ed.) BCTG/2022-308

BIANCA THALITA ARAÚJO DE LIMA ALBUQUERQUE

PETROLOGIA E GEOQUÍMICA DO GRANITO COM EPÍDOTO MAGMÁTICO CARMO, TERRENO CACHOEIRINHA-SALGUEIRO, PERNAMBUCO

Dissertação apresentada ao Programa de Pós-graduação em Geociências, Centro de Tecnologia e Geociências da Universidade Federal de Pernambuco como parte dos requisitos parciais para obtenção do título de mestre em Geociências.

Aprovada em 29 de julho de 2021.

BANCA EXAMINADORA

Prof. Drª. Valderez Pinto Ferreira (Orientadora)

Universidade Federal de Pernambuco

Prof. Drª Ignez Pinho Guimarães (Examinadora Interna)

Universidade Federal de Pernambuco

Prof. Dr. Hebert Conceição (Examinador Externo)

Universidade Federal de Sergipe

AGRADECIMENTO

Agradeço primeiramente a Deus pela dádiva da vida e por ter me sustentado e guiado meus caminhos durante essa jornada. Todos os momentos de alegria e difíceis percorridos me tornaram mais forte. A minha família por sempre está ao meu lado e ser fonte de inspiração, agradeço cada palavra e atitude de apoio diário. Em especial a minha mãe Lúcia Maria por ser a luz da minha vida e todo o sacrifício feito pela minha educação. Aos grandes amigos que fiz no curso de Geologia da UFPE, pela força, diversas conversas e cuidados. Em especial agradeço ao amigo Diego pela atenção e paciência, e incontáveis horas dedicadas para me incentivar e ensinar.

Agradeço aos professores do Departamento de Geologia (DGEO) que contribuíram para a minha formação acadêmica. À minha orientadora prof.ª Valderez Pinto Ferreira e coorientador prof. Alcides Nóbrega Sial, pelo apoio e ensinamentos de geologia contribuindo para minha formação como profissional. À equipe do NEG-LABISE, Anderson pelas análises de fluorescência de raios-X e Gerlany Lins por sempre está disposta a ajudar. Agradeço também aos professores Ignez Guimarães e Hebert Conceição por terem aceitado participar da banca examinadora da defesa de dissertação.

Agradeço ao Conselho Nacional de Desenvolvimento Científico e Tecnológico (CNPq, processo número 404472/2016-8) pelo auxílio financeiro para o desenvolvimento desta dissertação. À Fundação de Amparo à Ciência e Tecnologia do estado de Pernambuco (FACEPE, processo número IBPG 0780 1.07/18), pela concessão da bolsa de mestrado.

RESUMO

Durante a Orogênese Brasiliana, extenso magmatismo granítico foi gerado na Província Borborema, nordeste do Brasil. No Domínio Central desta província, os granitóides que correspondem ao pulso mais antigo (640 – 620 Ma) são principalmente granodioritos e tonalitos, cálcio-alcalinos de alto K, metaluminosos, com epidoto magmático. Novos dados do pluton Carmo, intrusivo nas rochas metassedimentares do Domínio Cachoeirinha-Salgueiro são apresentados neste trabalho. O stock Carmo é constituído por monzogranitos e granodioritos porfiríticos, com megacristais de plagioclásio. As rochas contêm abundantes enclaves microgranulares máficos (MMEs) de composição quartzo monzodioritica e clots ricos em anfibólio, ambos distribuídos aleatoriamente no pluton. Dados U-Pb LA-ICP-MS em grãos de zircão indicam cristalização em torno de 615 para os granitóides Carmo. Pressões de solidificação de 6 a 7 kbar, temperaturas (TZr) próximas ao *liquidus* (749 a 776°C), e condições moderadamente oxidantes, ligeiramente abaixo do tampão NNO (ΔNNO de -1,2 a -0,4), foram estimadas para o granodiorito Carmo, e são consistentes com a presença de epidoto magmático cristalizando a altas pressões. Granitóides e MMEs apresentam padrões de REE normalizados em relação a condrito enriquecidos em LREE e empobrecidos em HREE, sendo moderadamente fracionados para os granitóides ([La/Yb]N = 17,36 – 25,82) e mais horizontalizados para os MMEs ([La/Yb]N = 5,33 – 12,39). As rochas apresentam enriquecimento em elementos LILE (e.x., U, K e Ba) e empobrecimento em HFSE (e.x., Nb, Ti e P) em diagramas multielementares normalizados em relação ao manto primitivo. As composições isotópicas são sobrepostas para os MMEs e granitóides hospedeiros, com altas razões (87Sr/86Sr)i (0,70786 – 0,70968), εNd(t) fracamente negativo (-2,1 a -3,1) e idades modelo TDM de 1,31 – 1,40 Ga. A similaridade dos valores isotópicos junto com evidências petrográficas, tais como a presença de megacristais de feldspato inclusos nos MMEs, apatita acicular, quartzo ocelli e plagioclásio com zonação oscilatória, indica que MMEs representam bolhas de magma máfico derivado do manto injetado em uma câmara magmática félsica evoluindo. Dados de química dos minerais ferromagnesianos, geoquímica de rocha total e isotópicos sugerem que a fonte do granodiorito Carmo tem componentes do manto e da crosta. As composições isotópicas de Sr-Nd-O são sugestivas de crosta oceânica alterada hidrotermalmente como a fonte máfica, enquanto que as altas razões de Th/La e (La/Sm)N, bem como a presença de *lumps* de quartzo nos granitóides, apontam para a participação de sedimentos na fonte. Assim, é concluído neste trabalho que os granitóides foram produzidos a partir da fusão parcial de crosta oceânica mais sedimentos. O

conjunto de dados petrológicos, geocronológicos e geoquímicos combinados com as características geológicas regionais sugerem que o stock Carmo foi mais provavelmente gerado em um ambiente sin-colisional após o rompimento cedo de uma placa oceânica relativamente fraca.

Palavras-chave: magmatismo sin-colisional; fusão da placa; contribuição de sedimentos; enclaves microgranulares máficos; granitos tipo I; Província Borborema

ABSTRACT

During the Brasiliano Orogeny, extensive granitic magmatism was generated in the Borborema Province, northeastern Brazil. In the Central Domain of this province, granitoids that correspond to the oldest pulse (640 – 620 Ma) are mainly magmatic epidote-bearing metaluminous, high-K calc-alkalic granodiorites and tonalites. New data from the Carmo pluton, intrusive in metasedimentary rocks of the Cachoeirinha-Salgueiro Domain are presented in this work. The Carmo stock consists of porphyritic monzogranites and granodiorites, with plagioclase megacrysts. The rocks contain abundant mafic microgranular enclaves (MMEs) of quartz monzodioritic composition and amphibole-rich clots, both randomly distributed in the pluton. LA-ICP-MS U-Pb data on zircon grains indicate crystallization ages around 615 for Carmo granitoids. Solidification pressures of 6 to 7 kbar, temperatures (TZr) close to liquidus (749 to 776°C), and moderately oxidizing conditions, slightly below the NNO buffer (ΔNNO from -1.2 to -0.4), were estimated for the Carmo granodiorites, and are consistent with the presence of magmatic epidote crystallizing at high pressures. Granitoids and MMEs show chondrite-normalized REE patterns enriched in LREE and depleted in HREE, with moderately fractioned patterns for granitoids ([La/Yb]N = 17.36 – 25.82) and more horizontalized patterns for MMEs ([La/Yb]N = 5.33 - 12.39). Both rock types show enrichment in LILE (e.g., U, K and Ba) and depletion in HFSE (e.g., Nb, Ti and P) in primitive mantle-normalized multielement diagrams. The Sr-Nd isotopic compositions are superimposed for host MMEs and granitoids, with high initial 87Sr/86Sr (0.70786 – 0.70968) ratios, weakly negative εNd(t) (-2.1 to -3.1) values and TDM model ages from 1.31 to 1.40 Ga. The similarity of isotopic compositions together with petrographic evidence, such as the presence of megacrysts of feldspar included in MMEs, acicular apatite, quartz “ocelli” and plagioclase with oscillatory zonation, indicates that MMEs represent blobs of mafic magma derived from the mantle injected into a felsic magma chamber evolving. Ferromagnesian mineral chemistry, whole-rock geochemistry and isotopic data suggest that the Carmo granodiorite source has both mantle and crustal components. The Sr-Nd-O isotopic signatures are suggestive of hydrothermally altered oceanic crust as the mafic source, while the high Th/La and (La/Sm)N ratios, as well as the presence of quartz lumps in the granitoids, point out for the participation of sediments in the source. Thus, it is concluded in this work that the granitoids were produced from the partial melting of oceanic crust and sediments. The petrological, geochronological and geochemical data, combined with

regional geological features, suggest that the Carmo stock was most likely generated in a syn-collisional tectonic setting following the early break-off of a relatively weak oceanic slab.

Keywords: syn-collisional magmatism; slab melting; sediment contribution; mafic microgranular enclave; I-type granitoids; Borborema Province

LISTA DE FIGURAS

-

SUMÁRIO

1 INTRODUÇÃO

Epidoto é um mineral que ocorre comumente em rochas ígneas plutônicas intermediárias a ácidas. No entanto, sua importância como um mineral magmático somente foi reconhecida a partir do estudo experimental conduzido por Naney (1983), no qual foi demonstrado que em pressões de 6 a 8 kbar esse mineral se cristaliza como fase primária em magmas de composições graníticas e granodioríticas. Posteriormente, estudos experimentais e naturais mostraram que dependendo da fugacidade de oxigênio, o campo de estabilidade do epidoto pode ser expandido para pressões de cristalização em torno de 3 kbar (e.x., Schmidt & Thompson, 1996; Sial et al., 1999; Ferreira et al., 2011). Além disso, tem sido reconhecido que a dissolução de epidoto em magmas graníticos é relativamente rápida, pelo que a sua sobrevivência nesse tipo de magmas implica transporte ascendente rápido (e.x., Brandon et al., 1996; Sial et al., 2008; Silva et al., 2020). Portanto, a presença de epidoto magmático em rochas graníticas tem sido estudada como um possível indicador para restringir condições de cristalização específicas, tais como pressão de solidificação, estado de oxidação e taxas de ascensão dos magmas.

Volumoso magmatismo granítico foi gerado na Província Borborema durante os diferentes estágios de evolução da Orogênese Brasiliana/Pan Africana (Brito Neves et al., 2000). Granodioritos e tonalitos cálcio-alcalinos de alto K, metaluminosos, com epidoto magmático, também chamados de plutons tipo Conceição (Almeida et al., 1967; Sial, 1986), são os principais representantes do pulso magmático mais antigo (640 – 620 Ma) gerados durante o Neoproterozoico tardio, na Subprovíncia Central. Estudos petrológicos, geoquímicos e isotópicos sistemáticos desenvolvidos nas últimas décadas têm sugerido que componentes crustais e juvenis estiveram envolvidas na formação desses granitóides (e.x., Ferreira et al., 2004; Guimarães et al., 2011). Nesse cenário, diversos ambientes tectônicos têm sido propostos para explicar a gênese dos granitos tipo Conceição. Estudos recentes frequentemente associam a gêneses desse magmatismo a um ambiente de arco magmático continental (Brito Neves et al., 2016; Santos et al., 2019, 2020; Caxito et al., 2021). As principais evidências citadas por esses autores para o modelo de subducção são: ocorrência local de retroeclogitos, granitóides com assinatura geoquímica de arco magmático e possível participação de uma componente juvenil na geração desses magmas. No entanto, o modelo de arco magmático continental é ainda questionado, devido à ausência de características geológicas típicas de zonas de subducção, tais como complexos acrescionários e/ou rochas

metamórficas de alta pressão. Alternativamente, um cenário sin colisional poderia explicar a geração desse magmatismo (Neves, 2018), contudo esse modelo tectônico não tem sido abordado até agora.

Esta dissertação apresenta dois artigos científicos, os quais foram submetidos em periódicos internacionais como parte dos requisitos para a obtenção do título de Mestre em Geociências, na área de Geoquímica, Geofísica e Evolução Crustal do Programa de Pós-Graduação em Geociências da Universidade Federal de Pernambuco. O primeiro artigo intitulado: "Crystallization conditions of the Carmo stock, NE Brazil: Implications for magmatic epidote-bearing granitoids petrogenesis" aborda observações de campo e petrográficas, juntamente com dados de química mineral do stock Carmo, os quais são usados para restringir suas condições de cristalização e alojamento. O trabalho também aborda uma discussão sobre as implicações petrogenéticas na geração de granitóides cálcio-alcalinos com epidoto magmático na Província Borborema, nordeste do Brasil. O segundo artigo intitulado: "Petrogenesis of the Late Neoproterozoic Carmo stock, northeastern Brazil: Implications for partial melting of oceanic crust and sediments in a syn-collisional setting" apresenta novos dados geoquímicos de rocha total, isotópicos (Rb-Sr e Sm-Nd) e geocronológicos (zircão U-Pb) dos granodioritos e monzogranito do stock Carmo, para restringir os processos petrogenéticos que atuaram na formação dos granitóides tipo Conceição no Domínio Cachoeirinha-Salgueiro. Este artigo também discute as implicações tectônicas no contexto geológico da Província Borborema e propõe que um cenário sin colisional após o rompimento cedo de uma placa oceânica relativamente fraca é o modelo tectônico mais viável para explicar a evolução geológica desta região.

1. 1 CONTEXTO GEOLÓGICO REGIONAL

A Província Borborema, localizada no nordeste do Brasil, foi inicialmente definida por Almeida et al. (1977) e descrita como um complexo sistema de dobramentos Brasilianos. As principais características tectonoestruturais da província foram desenvolvidas no Neoproterozoico, como resultado da convergência dos crátons São Francisco-Congo, África Ocidental e Amazônia que deu origem ao oeste de Gondwana durante a Orogênese Brasiliana/Pan-Africana (Almeida et al., 1981; Brito Neves et al., 2002; Van Schmus et al., 2011). Extensas zonas de cisalhamento transcorrentes com tendências E-W e cinemática destral, geradas durante o estágio tardio da

orogenia, são usadas para dividir a Província Borborema nas subprovíncias Norte, Central e Sul (Brito Neves et al., 2000; Neves, 2003; Van Schmus et al., 2011).

A Subprovíncia Central (Fig.1) (também chamada de Zona Transversal; Ebert 1970; Jardim de Sá, 1994), localizada entre as zonas de cisalhamento Patos e Pernambuco, é constituída por rochas gnáissicas Paleoproterozoicas, sequências metavulcânicas e metassedimentares Neoproterozoicas e raros núcleos Arqueanos, que foram posteriormente retrabalhadas e intrudidas por numerosos batólitos e plutons durante o Neoproterozoico tardio (Van Schmus et al., 2011; Neves, 2015). Um complexo sistema de zonas de cisalhamento com tendência NE-SW divide a subprovíncia em cinco terrenos ou domínios tectonoestratigráficos, os quais de leste a oeste são: Rio Capibaribe, Alto Moxotó, Alto Pajeú, Cachoeirinha-Salgueiro e São José do Caiano (Brito Neves et al., 2000; Santos et al., 2010; Van Schmus et al., 2011).

Figura 1. Mapa geológico simplificado da Província Borborema mostrando os principais domínios e distribuição dos plutons graníticos Brasilianos. A localização aproximada da área de estudo no contexto regional está destacada pelo retângulo verde.

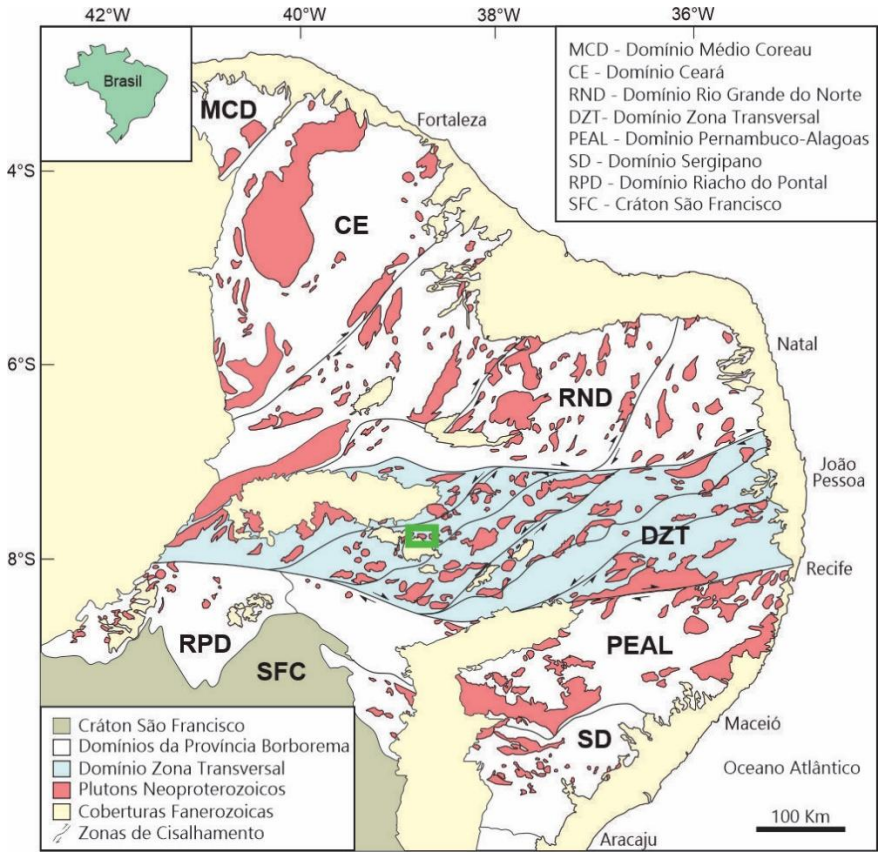

Fonte: Medeiros (2004)

A área de estudo desta pesquisa está localizada no Domínio Cachoeirinha-Salgueiro (também chamado de Piancó-Alto Brígida; Brito Neves, 1975). Este domínio compreende duas principais unidades litológicas: (I) Sequências metavulcanossedimentares de baixo a médio grau metamórfico (Grupos Cachoeirinha e Salgueiro); (II) Numerosos plutons graníticos intrudidos nas rochas metassedimentares como pequenos stocks (Sial, 1990, 1993; Brito Neves et al., 2016; Sial & Ferreira, 2016). O Grupo Cachoeirinha tem sido interpretado como uma antiga bacia de sedimentação marinha costeira que sofreu acresção seguida de colisão durante o Criogeniano-Ediacariano (Brito Neves et al., 2018). Esse grupo é constituído pelas formações Serra do Olho D´Água e Santana dos Garrotes. Apesar de que a relação espacial e temporal entre as duas formações ainda é debatida, estudos geocronológicos em populações de zircão detrítico tem mostrado que a deposição da Formação Santana dos Garrotes (690 – 620 Ma; Van Schmus et al., 2011; Marulanda, 2013; Brito Neves et al., 2018) provavelmente sucedeu a deposição da Formação Serra do Olho D'Água (1080 – 950 Ma; Marulanda, 2013). A Formação Serra do Olho D'Água é composta por metaconglomerados e metarenitos polimíticos, enquanto que a Formação Santana dos Garrotes é composta principalmente por metassiltitos e metarenitos, com ocorrências locais de carbonatos, formações ferríferas bandadas e rochas metavulcânicas (Bittar, 1998; Medeiros, 2004; Marulanda, 2013; Brito Neves et al., 2018; Usma et al., 2021).

1. 2 OBJETIVOS

A presente dissertação tem como objetivo geral contribuir para o conhecimento da gênese de granitos cálcio-alcalinos com epidoto magmático, através do estudo petrológico, geoquímico e geocronológico do stock Carmo no Domínio Cachoeirinha-Salgueiro.

Os objetivos específicos são:

I. Identificar e mapear diferentes domínios petrográficos/texturais das litologias presentes e suas relações de contato;

II. Caracterizar a petrogênese e parâmetros intensivos de geração do magma e sua cristalização através de estudos de química mineral, geoquímicos, isotópicos e geocronológicos;

III. Correlacionar os dados geoquímicos e isotópicos do stock Carmo com os de outros granitos com epidoto magmático de 640 – 620 Ma localizados na Subprovíncia Central.

1.3 LOCALIZAÇÃO E VIAS DE ACESSO

A área de estudo está inserida no município de São José do Belmonte, localizado a aproximadamente 472 km a oeste de Recife (Fig. 2), capital do estado de Pernambuco. Partindo de Recife, percorre-se pela rodovia pavimentada BR-232, sentido oeste, até a cidade de Bom Nome, onde o sentido muda para noroeste, trafegando pela PE-361 até São José do Belmonte. O município de São José do Belmonte ocupa uma área de 1484,2 km², compreendido na folha topográfica SUDENE de São José do Belmonte (SB.24-V-III) na escala 1:100.000. A área estudada é limitada pelas coordenadas UTM, segundo o datum WGS 84 e zona 24L: 519117m e 539117m, 9147429m e 9137429m, e coordenadas geográficas 38°49’35,91” e 38°38’42,73’’ a oeste da linha de Greenwich, e 7°42’46,71” e 7°48’11,95” a sul da linha do Equador.

Figura 2. Mapa esquemático de localização e principais vias de acesso a área de estudo (retângulo preto).

Fonte: A autora (2021)

1.4 METODOLOGIA

Para alcançar os objetivos previamente mencionados, as principais atividades realizadas durante o desenvolvimento desta dissertação são descritas abaixo:

- Aquisição de Dados Preliminares

A revisão bibliográfica é uma etapa fundamental desta pesquisa e foi realizada ao longo do seu progresso, a fim de melhorar as discussões referentes aos temas abordados e técnicas utilizadas. Durante essa fase foram realizadas leituras de artigos, livros, teses de doutorados e dissertações de mestrado sobre a geologia da Província Borborema e trabalhos específicos publicados em revistas de alta qualidade pertinentes aos temas tratados no desenvolvimento deste trabalho.

- Trabalho de Campo

A realização desta etapa ocorreu durante três trabalhos de campo, onde foram anotados detalhes característicos de cada afloramento, tais como litologia, mineralogia, características texturais, e quando possível, foram feitas medições estruturais com o auxílio de uma bússula tipo Clar. Todos os afloramentos visitados tiveram suas coordenadas (UTM) anotadas segundo o datum WGS 84 e fotografados. Amostras de litologias representativas foram coletadas e etiquetadas com a sigla BCAR seguida do número da ordem na qual os afloramentos foram visitados.

- Trabalho de Laboratório

Após etapas de campo, foram separadas amostras para a confecção de lâminas petrográficas no Laboratório de Preparação de Lâmina Delgada do Departamento de Geologia – UFPE. A partir do estudo das fases minerais primárias e secundárias, e suas relações texturais foram selecionadas algumas amostras para confecção de seções polidas na Universidade de São Paulo, e posteriormente análise química mineral por microssonda eletrônica na Universidade de Brasília.

Todas as amostras coletadas passaram pelas etapas de britagem, pulverização e quarteamento, no Laboratório de Preparação de Amostras do NEG-LABISE (Núcleo de Estudos Geoquímicos - Laboratório de Isótopos Estáveis, Universidade Federal de Pernambuco), para análises químicas de rocha total de elementos maiores. Amostras representativas dos granitóides e seus enclaves máficos associados foram selecionadas para análise de rocha total de elementos traços (SGS Geosol - Laboratórios Ltda) e isotópicas Rb-Sr e Sm-Nd (Centro de Pesquisa Geocronológicas – CPGeo, Universidade de São Paulo). Além disso, uma amostra foi selecionada para análise geocronológica U-Pb em zircão, realizada por LA-ICP-MS no CPGeo. Os dados analíticos obtidos foram tratados e usados para confeccionar diagramas de química mineral, geoquímicos e isotópicos utilizando os softwares Microsoft® Office Excel 2020, Grapher 12 e IsoplotR.

Finalmente, a interpretação e integração dos dados de campo, petrográficos, geoquímicos, isotópicos e geocronológicos obtidos durante esta pesquisa, junto com os dados disponíveis na literatura, resultaram na elaboração desta dissertação. Portanto, essa pesquisa constitui uma importante contribuição para evolução magmática dos granitóides cálcio-alcalinos com epidoto magmático (640 – 620 Ma) no Domínio Cachoeirinha-Salgueiro, e propõe um modelo de evolução geotectônica para esta região da Província Borborema.

2 RESULTADOS

Os resultados obtidos ao longo desta dissertação são discutidos através de dois artigos, o primeiro publicado na revista *Journal of South American Earth Sciences*, o segundo artigo também foi submetido no mesmo periódico científico. Os artigos são apresentados na integra neste tópico e as cartas de submissão e aceito de cada publicação encontram-se no ANEXO A.

3 ARTIGO 1 – JOURNAL of SOUTH AMERICAN EARTH SCIENCES

Volume 110, October 2021, 103427

Crystallization conditions of the Carmo stock, NE Brazil: Implications for magmatic epidote-bearing granitoids petrogenesis

Bianca T.A. Lima*, Valderez P. Ferreira, Diego H. Ardila, Charles H.F.S. Neves and Alcides N. Sial

NEG–LABISE, Department of Geology, Federal Univ. of Pernambuco, Recife, PE, 50740-530, Brazil

https://doi.org/10.1016/j.jsames.2021.103427

Abstract

The Carmo stock is part of a 650 – 620 Ma magmatic-epidote bearing metaluminous calc-alkalic magma association intruded within the Cachoeirinha-Salgueiro domain (CSD, Northeastern Brazil). The pluton consists mainly of granodiorites and monzogranites, with abundant mafic microgranular enclaves (MMEs). Textural and chemical evidence indicate that epidote is magmatic, while titanite was partially re-equilibrated during subsolidus processes. Amphibole in granitoids is hastingsite, and varies in composition from edenite to pargasite in the MMEs. Biotite exhibits similar values of Al^{IV} (2.3 – 2.5 apfu) in the MMEs and host rocks, but shows lower Fe/(Fe+Mg) ratios in the former than in the host granitoids (0.53 – 0.56 and 0.56 – 0.60, respectively). Pressures between 6 and 7 kbar and temperatures between 656 and 735 °C were estimated from the Al-in-hornblende geobarometer and the amphibole-plagioclase geothermometer, which are consistent with presence of magmatic epidote. The zircon saturation thermometer provided higher temperatures, between 749 and 776 °C, and are interpreted as near-liquidus temperatures. Estimative of fO_2 indicates moderately oxidizing crystallization conditions slightly below the NNO buffer (ΔNNO from -1.2 to -0.4). The initial water content estimated for these magmas suggests that they were highly hydrated (~ 5 – 6 wt%), consistent with presence of early-crystallized hornblende. The chemical composition of ferromagnesian minerals indicates that the rocks of Carmo stock crystallized from I-type calc-alkalic magma and suggests interaction between juvenile and crustal components. Based on these new data, in combination with previously published data, we suggest that magmatic epidote-bearing granitoids from CSD were likely derived from partial melting of mantle-like sources along with recycled terrigenous sediment.

Keywords: Magmatic epidote, Crystallization conditions, Sediment contribution, Mineral chemistry, I-type granitoids, Borborema Province

__Corresponding author__: biancathalitalima@gmail.com

1. Introduction

The presence of magmatic epidote (mEp) was first recognized by Keyes (1892), however for almost a century after publication of this work, epidote in igneous rocks was still considered as a mineral of metamorphic origin. The importance of this phase as a magmatic mineral was given from the experimental study by Naney (1983), who demonstrated that at pressures of 6 – 8 kbar, epidote can crystallize as a primary phase in magmas of granitic composition. Subsequently, natural and experimental studies have shown that the minimum crystallization pressure may be lower than that reported by Naney (1983), depending on the fugacity of oxygen (e.g., Schmidt & Thompson, 1996; Sial et al., 1999; Ferreira et al., 2011), and that dissolution of epidote in granitic magmas is relatively fast and, therefore, its survival in granitic magmas implies rapid upward transport (Brandon et al., 1996; Sial et al., 2008). Thus, magmatic epidote is not only useful for determining the solidification pressure, but also for providing information about the reducing and oxidizing states and ascension rates of magmas.

The generation of extensive granitic-syenitic magmatism in the Borborema Province during the Neoproterozoic constitutes one of the main characteristics of the Brasiliano/Pan-African Orogeny that affected northeast of Brazil (Fig. 1A; Almeida et al., 1981; Caby et al., 1990; Brito Neves et al., 2002; Van Schmus et al., 2011). Based on petrographic, geochemical and geochronological characteristics, this magmatism has been grouped into different time intervals and magma associations (e.g., Almeida et al., 1967; Sial, 1986; Ferreira et al., 2004; Guimarães et al., 2004; Sial & Ferreira, 2016). Among the associations, mEp-bearing calc-alkalic and high-K calc-alkalic tonalites/granodiorites plutons (650 – 620 Ma) have been strongly studied from a petrological and geochemical perspective, given the importance of the presence of mEp in determining the conditions of crystallization and relative rate of magma ascent (Sial, 1990; Sial et al., 2008; Ferreira et al., 2003, 2011; Brasilino et al., 2011; Silva et al., 2020).

The Carmo stock, as well as other intrusions in the CSD (Sial, 1986, 1990; Sial & Ferreira, 2016; Sial et al., 1998, Van Schmus et al., 1995; Kozuch, 2003; Ferreira et al., 2004; Siqueira et al., 2018; among others), consists mainly of granodiorites and monzogranites with mEp and abundant MMEs. The genesis of these granitoids has been linked by several authors to a subduction environment (Medeiros 2004; Caby et al. 2009; Brito Neves et al., 2016; Sial & Ferreira, 2016; Caxito et al., 2021). However, due to the scarcity of coeval mafic magmas and other typical characteristics of subduction zones, there is controversy about petrogenesis and the geodynamic setting of these granitoids (Neves, 2018).

Chemical composition of the minerals of a given mineral assemblage in equilibrium is related to the bulk composition of the melt and the conditions involved during the crystallization processes (Abbott & Clarke, 1979; Yousefi et al., 2017). The evaluation of the physical-chemical characteristics of granitic rocks, through analysis of mineral chemistry, provides useful information on the petrogenetic processes and evolution of the magma, such as pressure, temperature, depth of crystallization, oxygen fugacity and rates of magma ascent (Anderson, 1996; Ridolfi et al., 2010; Sial et al., 2008; Brasilino et al., 2011; Massawe & Lentz, 2020).

In this paper, we present petrographic aspects and mineral chemistry data, obtained by electron microprobe analyses from the Carmo granitoids and their MMEs. Based on these data, we infer the crystallization conditions (e.g., temperature, pressure, oxygen fugacity, and water content) associated with the evolution and emplacement of the Carmo stock and evaluate the petrogenetic implications in the generation of mEp-bearing granitoids in the Borborema Province, northeastern Brazil.

Figure 1. (A) Simplified geological map of the Borborema Province showing the main domains and distribution of Brasiliano granitic plutons (modified from Medeiros, 2004); (B) Geological sketch-map of the domains of the Transversal Zone Domain: SJCD = São José do Caiano Domain; CSD = Cachoeirinha-Salgueiro Domain; RGD = Riacho Gravatá subdomain; APD = Alto Pajeú Domain; AMD = Alto Moxotó Domain, and their main magma association with the studied area highlighted by the black rectangle (modified from Sial & Ferreira, 2016); (C) Detailed geological map showing facies distribution of the Carmo stock.

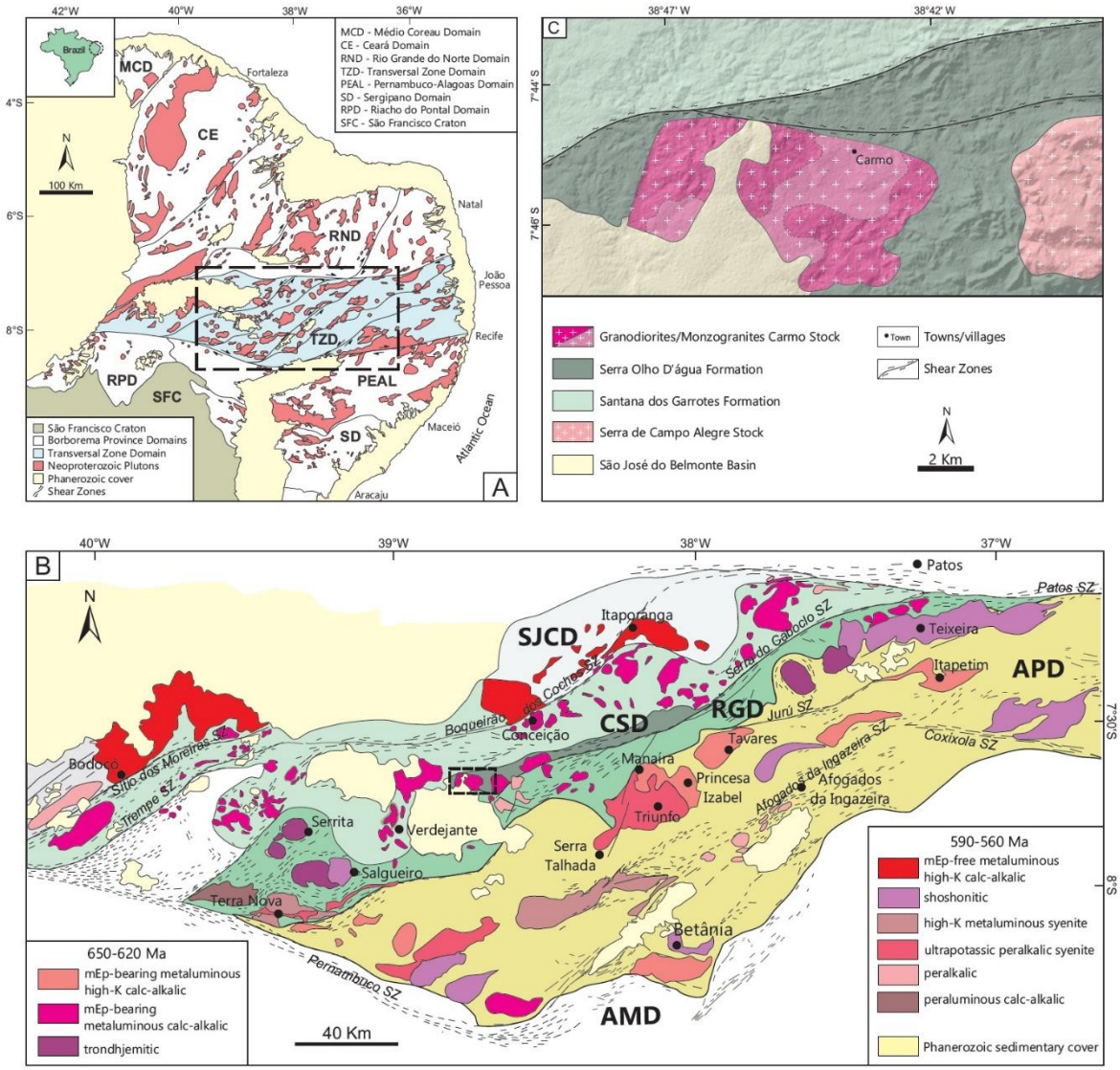

2. Geologic setting

The Borborema Province, as initially defined by Almeida et al. (1977), is located on the eastern edge of the South American Plate, north of the São Francisco Craton (Fig. 1A). It is limited to the east and north by the Atlantic Ocean and to the west by the Parnaíba Basin, with an extension of approximately 450,000 km². Its main characteristics were developed during the late Mesoproterozoic to early Neoproterozoic, during the so-called Cariris Velhos event, and the late Neoproterozoic, during the Brasiliano/Pan-African Orogeny (Brito Neves et al., 2000). This last tectono-thermal event was marked by regional low-angle foliation and by intense magmatic

activity, evidenced by numerous batholiths and small plutons intruded in the gneissic basement and metasedimentary cover, accompanied by the development of regional-scale transcurrent shear zones (Fig.1A; Neves et al., 2000; Neves, 2015).

The dextral Patos and Pernambuco shear zones have commonly been used as boundaries that divide the Borborema Province into three major subprovinces: Northern, Central, and Southern (Vauchez et al., 1995; Brito Neves et al., 2000; Neves, 2003; Van Schmus et al., 2011). In the Central Subprovince, also called Transversal Zone Domain (Jardim de Sá, 1994), NE-SW-striking sinistral shear zones separate five tectonostratigraphic terrains/ domains, which from east to west they are: Rio Capibaribe, Alto Moxotó, Alto Pajeú, Cachoeirinha-Salgueiro and São Pedro or São José do Caiano (Fig. 1B; Santos & Medeiros, 1999; Brito Neves et al., 2000; Van Schmus et al., 2011).

The CSD (Piancó-Alto Brígida belt, in the sense of Brito Neves, 1975), is considered as a coastal marine basin that during the Cryogenian-Ediacarian periods underwent accretion and collision processes (Brito Neves et al., 2018). The domain consists of a sequence of low grade metaturbidites from the Cachoeirinha Group and low to medium grade micaschists from the Salgueiro Group. The Cachoeirinha Group comprises the Serra do Olho D'Água and Santana dos Garrotes formations, but the stratigraphic relationship between them is still uncertain due to the deformation processes that affected these rocks during the evolution of the Brasiliano Orogeny. However, detrital zircon U-Pb ages suggest that the deposition of the Santana dos Garrotes Formation was latter than that of the Serra do Olho D'Água Formation, as constrained by the youngest detrital zircon populations (688 – 620 Ma and 1080 – 950 Ma, respectively; Marulanda, 2013). The Serra do Olho D'Água Formation is composed of polymitic metaconglomerates and metarenites, while the Santana dos Garrotes Formation predominantly comprises metasiltites and metarenites, with local occurrences of carbonates, banded iron formations and metavolcanic rocks (Bittar, 1998; Medeiros, 2004; Marulanda, 2013; Brito Neves et al., 2018; Usma et al., 2021). Detrital zircon grains dated at ca. 620 Ma in the Santana dos Garrotes Formation and crystallization ages of ca. 635 – 600 Ma obtained from metavolcanic rocks (Van Schmus et al., 1995, 2011; Kozuch, 2003; Medeiros, 2004; Brito Neves et al., 2018; Caxito et al., 2021), suggest that this sequence was deposited just before the metamorphic peak (610 – 590 Ma; Van Schmus et al. 2011) of the Brasiliano Orogeny.

The Brasiliano magmatic activity in the CSD was marked by intrusive igneous rocks composed mainly of metaluminous granodiorites to tonalites, containing biotite and calcic amphibole as the main mafic phases, as well as mEp occurring as crystals up to 2 mm in length (Sial, 1990; Sial et al. 1998, 2008; Sial & Ferreira, 2016). The presence of dioritic to quartz dioritic MMEs and amphibole clots is a characteristic commonly observed in these granitoids. In addition, unusual high-pressure thermal aureoles with a mineral assembly composed of garnet, kyanite, staurolite, muscovite, biotite, plagioclase ± quartz, were developed locally around these granites (Caby et al., 2009). The Carmo stock intrudes the metasedimentary rocks of the Serra do Olho D'Água Formation and is dominated by granodiorites and monzogranites enclosing mafic enclaves and minor amphibole clots.

3. Analytical methods

Petrographic description and modal analyses (ca. 1500 points per thin section) of representative samples was done using a transmitted light microscope. The rocks were classified following the recommendations of the Subcommission on the Systematics of Igneous Rocks of the IUGS (Le Maitre et al., 2002). Five representative samples of the granitoids and MMEs (BCAR-56; BCAR-57; BCAR-60; BCAR-20E; BCAR-25E) were selected for mineral chemistry analysis. Electron probe microanalyses (EPMA) of mineral assemblages were performed using a JEOL JXA-8230 Superprobe, equipped with five wavelength dispersive spectrometers (WDS) and an integrated Energy Dispersive Spectrometer (EDS) detector, at the Institute of Geosciences of the University of Brasília. The operating conditions were 15 kV accelerating voltage, 10 nA current, and 5 μm beam diameter. The analyzed minerals were feldspars, biotite, amphibole, titanite and epidote. Structural formula from analyzed minerals was calculated on the basis of 8, 22, 23, 5 and 12.5 oxygens, respectively. Amphibole and biotite structural formulas (including ferric contents) were calculated using the spreadsheets of Locock (2014) and Li et al. (2020), respectively. The Mica+ (Yavuz, 2003) computer program was used to calculates log ratios (e.g., X_F/X_{OH}, X_{Mg}/X_{Fe}) of the mica analyses.

The geobarometric calculation were obtained using Al-in-hornblende geobarometers proposed by Schmidt (1992), Anderson & Smith (1995) and Mutch et al. (2016). Amphibole-plagioclase pairs were used to estimate crystallization temperatures according to Holland & Blundy

(1994) method. Zircon saturation thermometers (Watson & Harrison, 1983 and Shao et al., 2019) were also used to calculate near-liquidus temperatures. The whole-rock geochemistry data used in this approach are from Lima & Ferreira (2019). The equation proposed by Wones (1989) and the spreadsheet of the Ridolfi et al. (2010) were used to estimate fO_2 values. In addition, also we estimate the initial water content of the magma using the models by Putirka (2005) and Ridolfi et al. (2010).

4. Results

4.1. Field relationships and petrography

The Carmo pluton is limited to the north by the western branch of the Juru-Belém shear zone and to the south it is partially covered by sandstones of the São José do Belmonte basin (Fig. 1C). This intrusion occurs as a stock, with an area of about 45 km², intruded into Neoproterozoic metasedimentary rocks of the Serra do Olho D'Água Formation at the CSD. The Carmo stock consists of porphyritic monzogranites to granodiorites (Fig. 3A) with plagioclase megacrysts up to 11 cm in length (Fig. 2C). These rocks are coarse-grained and have seriate texture in the central part, but they become finer-grained toward the margin.

Figure 2. (A) Contact between host granitoids and mafic enclave. Note the plagioclase and quartz xenocrysts within the enclave; (B) Amphibole-rich clot in granodiorite, showing their sharp boundaries; (C) Plagioclase megacryst of 11 cm in length; (D) Typical mineral assemblage of the host granodiorite-monzogranite containing plagioclase (Pl), quartz (Qz), alkali feldspar (Kfs), biotite (Bt), amphibole (Amp), epidote (Ep), titanite (Ttn) and allanite (Aln); (E) mEp with allanite core included in biotite. Note that euhedral faces are preferred in the Ep-Bt contacts contrasting with the irregular shape of the Ep-Qz contact; (F) mEp in contact with biotite and amphibole; (G) Plagioclase crystal with core partially altered to sericite and abundant Amp inclusions indicating that Amp was previous in the crystallization sequence; (H) Quartz xenocryst ('ocelli') with amphibole-rich rim in a mafic enclave; and (I) Presence of apatite with acicular shape in the MME, evidencing rapid cooling. Mineral abbreviations from Whitney & Evans (2010).

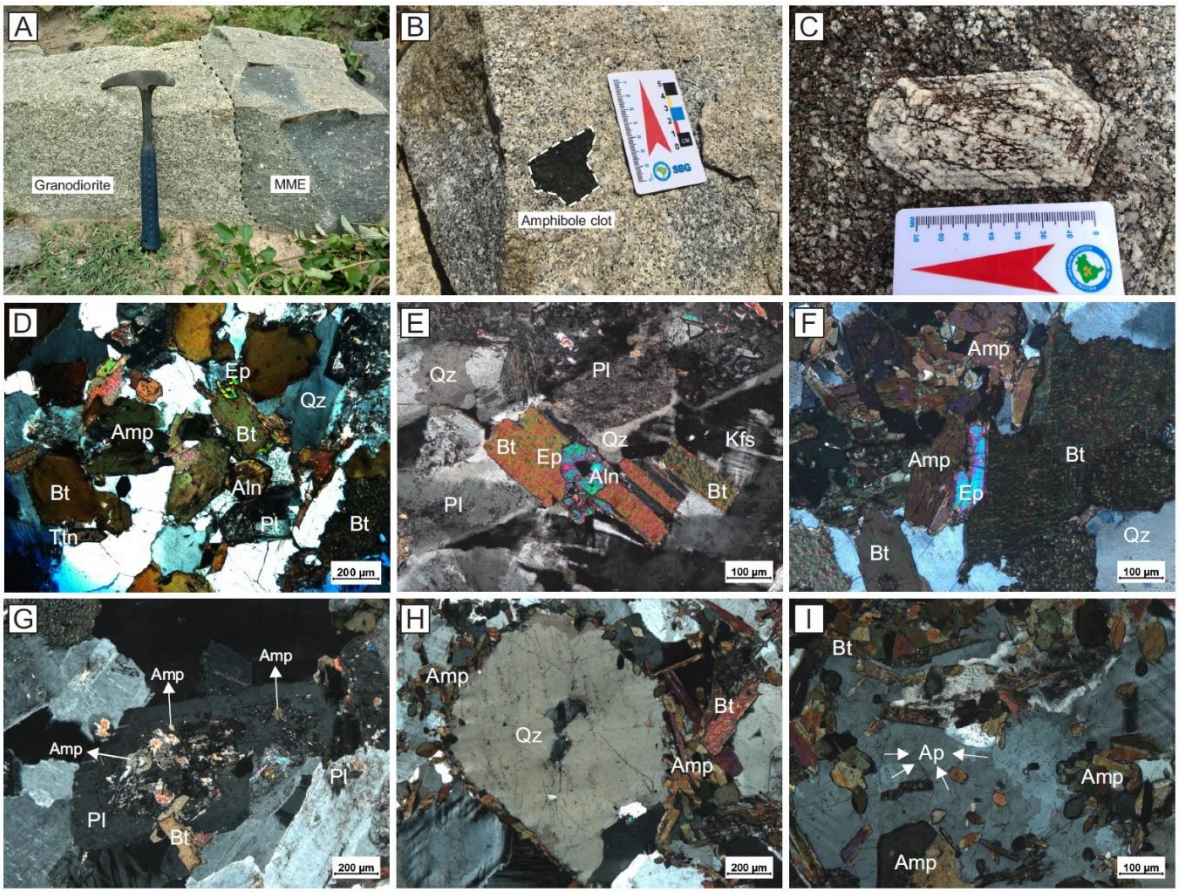

The granodiorites-monzogranites contain abundant quartz monzodioritic MMEs and amphibole-rich clots, both randomly distributed in the pluton. The quartz monzodioritic enclaves range from a few centimeters to almost one meter in size (Fig. 2A) and show spheroidal to ellipsoidal shapes. Most quartz monzodioritic MMEs shows rounded shape, irregular boundaries and gradual contacts with the host rock. The presence of plagioclase megacrysts from the host granite is a characteristic widely observed in these MMEs. The amphibole-rich clots have angular shapes up to 8 cm long and their contact with the host rock is often sharp (Fig. 2B).

The host granodiorite-monzogranite samples are mainly composed of plagioclase (32 – 40%), quartz (22 – 36%), alkali feldspar (11 – 28%), biotite (9 – 14%), amphibole (< 3%), with accessory minerals such as titanite, epidote, apatite, allanite and zircon (Fig. 2D), in decreasing order of abundance. The plagioclase megacrysts are euhedral to subhedral, sometimes zoned and often altered into sericite and clay minerals. Some plagioclase megacrysts exhibit poikilitic texture, with amphibole, biotite and apatite inclusions. Plagioclase crystals present in the matrix or included

in other minerals show a lower degree of alteration. Alkali feldspar is microcline and orthoclase, both occurring as large subhedral crystals and as small euhedral to subhedral crystals. A poikilitic texture is characteristic in samples that contain large alkali feldspar phenocrysts, with inclusions of biotite, amphibole, plagioclase, titanite and other accessory minerals. Quartz is anhedral and occurs as interstitial mineral phase. Biotite usually appears as subhedral crystals dispersed in the matrix or included in plagioclase and alkali feldspar. Some biotite crystals contain inclusions of epidote, zircon, titanite and rare opaque minerals, and sometimes is altered into chlorite, along its cleavages. Amphibole is present as small euhedral to subhedral crystals, with pleochroism that ranges from green to greenish brown, rarely showing inclusions. The modal content of amphibole decreases towards the center of the pluton, while the modal content of biotite and epidote increases. Titanite is predominantly euhedral and occurs as small diamond-shaped crystals, some of them with inclusions of Fe-Ti oxide minerals. They are included in other minerals, usually biotite, or dispersed in the matrix. Epidote is observed in all Carmo samples occurring as three different textural types. Type I epidote appears as euhedral to subhedral crystals with allanite cores and partially rimmed by biotite (Fig. 2E). Type II epidote occurs as smaller euhedral to subhedral crystals lacking allanite core and totally rimmed by biotite. Finally, type III epidote is subhedral to anhedral in shape and occurs in contact with biotite and less often with amphibole (Fig. 2F). Thus, type I and II epidote shows textural characteristic similar to those suggested by Zen & Hammarstrom (1984), Sial (1990) and Schmidt & Poli (2004) to represent a magmatic origin, while type III epidote possibly resulted from subsolidus reactions.

In comparison with the host granitoids, the MMEs present the same mineral assemblage but with different modal proportions. The MMEs have a fine-grained equigranular texture but occasionally is also observed a porphyritic texture. The enclaves consist of plagioclase (37 – 45%), amphibole (21 – 29%), biotite (12 – 14%), quartz (~ 12%), alkali feldspar (8 – 10%), and are classified as quartz monzodiorite (Fig. 3A). Accessory minerals include titanite, epidote, apatite and zircon. Plagioclase occurs as euhedral to subhedral crystals frequently zoned, sometimes with amphibole and biotite inclusions. Amphibole is subhedral to anhedral, in some samples occur as elongated and twinned crystals. Biotite is usually subhedral and contains inclusions of zircon, titanite and epidote. Quartz is an interstitial mineral phase and sometimes appears as ocelli quartz, surrounded by a reaction rim of biotite and hornblende (Fig. 2H). Alkali feldspar is mostly microcline but rare perthitic orthoclase is present. Apatite is a common mineral in the MMEs and

is predominantly acicular (Fig. 2I), although prismatic crystals also exist. The presence of ocelli quartz and acicular apatite in the MMEs are suggestive of an injection of hotter mafic magma into a cooler granitic magma (e.g., Didier & Barbarin, 1991).

Figure 3. (A) Modal classification of the Carmo stock in Q-A-P diagram (Streckeinsen, 1976). (B) An-Ab-Or ternary diagram showing composition of plagioclase and alkali feldspar, field boundaries are from Deer et al. (2013). (C) Biotite classification ternary diagram in terms of Mg, AlVI, Fe^{3+}, Ti, Fe^{2+} and Mn (Foster, 1960). (D) Diagram based on Fe/(Fe+Mg) versus Al^{IV} showing classification of biotite (Deer et al., 1992). (E) Mg versus Al_T diagram showing the composition of magma based on biotite composition (Nachit et al., 1985). (F) FeO versus MgO diagram showing the composition of magma based on biotite composition by Abdel-Rahman (1994).

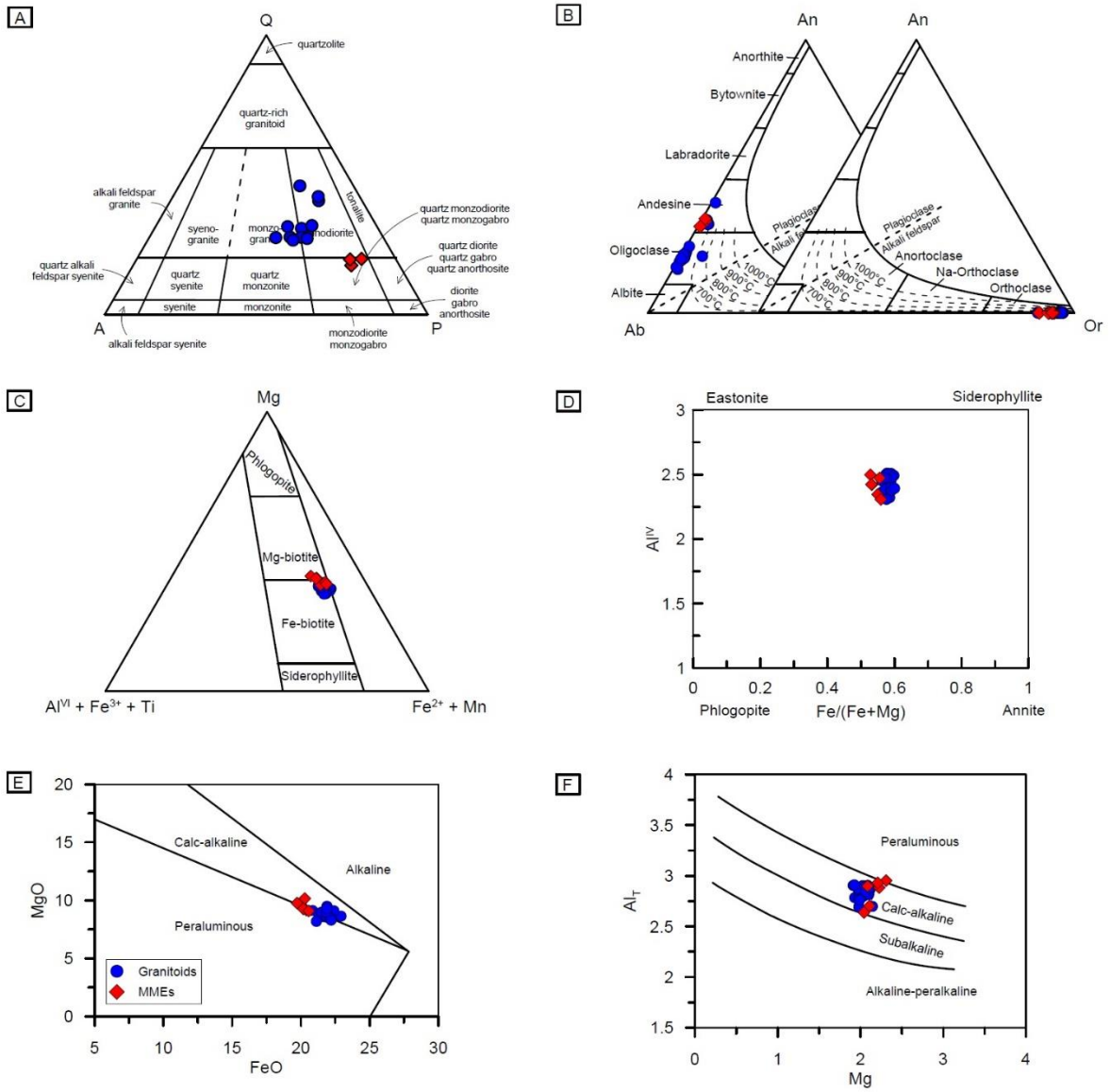

4.2. Mineral chemistry

In this section, results from the electron microprobe analyses are presented and the more interesting chemical features regarding feldspar, biotite, amphibole, titanite and epidote are discussed. The representative compositions of the analyzed minerals from MMEs and host granitoids are given in Table 1 to 5.

4.2.1. Feldspar

The composition of feldspars from granitoid rocks and their MMEs is relatively similar (Table 1 and Fig. 3B). Plagioclase from granitoids shows contents of 3.4 to 8.3 wt% CaO, 21.8 to 27.0 wt% Al_2O_3 and 6.6 to 9.7 wt% Na_2O, while MMEs have more restricted contents of CaO (6.6 – 7.0 wt%), Al_2O_3 (24.7 – 25.4 wt%) and Na_2O (7.2 – 7.63 wt%). Therefore, in the An-Ab-Or ternary diagram (Fig. 3B), plagioclases from granitoids show composition ranging from oligoclase to andesine ($An_{16–40}$), whereas most of the plagioclase from enclaves are andesine ($An_{32–34}$). The plagioclase crystals in the granitoids show compositional zoning with a calcium-rich core ($An_{19–40}$). Alkali feldspar in all samples falls within the orthoclase field ($Or_{89–96}$).

4.2.2. Biotite

Biotite from the granitoids is characterized by higher FeO contents (20.8 – 22.9 wt%) and lower MgO (8.2 – 9.5 wt%) than that from the MMEs (19.7 – 20.6 wt% and 9.1 – 10.1 wt%, respectively), but both exhibit similar Al_2O_3 contents (15.1 – 16.0 wt% and 14.8 –16.4wt%) (Table 2). According to the classification diagram proposed by Foster (1960), biotites from both granitoids and MMEs plot in the field of Fe-biotite, however due to the slightly higher MgO values of the MMEs, some their crystals plot in the field of magnesian biotite (Fig. 3C). The Fe/(Fe+Mg) ratios of biotite from granitoids (0.56 – 0.60) are slightly higher than that of the MMEs (0.53 – 0.56). Hence, in the classification diagram Fe/(Fe+Mg) versus Al^{IV}, the analyzed biotite crystals present compositions close to the siderophyllite end-member (Fig. 3D), reflecting the relatively high Fe and Al^{IV} values. All of the biotite analyses from both rock types plot within calc-alkaline field (Figs. 3E, 3F) in the discrimination diagram of Nachit et al. (1985) and Abdel-Rahman (1994).

4.2.3. Amphibole

Amphibole in rocks from the Carmo stock does not show significant compositional differences (Table 3). Electron microprobe analysis has shown that amphibole from the granitoids have slightly higher FeO contents (18.4 – 21.1 wt%) but lower MgO (6.9 – 9.0 wt%) than that from the MMEs (17.1 – 19.6 wt% and 8.2 – 10.1 wt%, respectively). These results indicate that amphibole from both rock types has compositions that suggest magmatic origin (Fig. 4A; Czamanske & Wones, 1973). All of the analyzed amphibole grains belong to the calcic-amphibole group with values of $(Ca + Na)_B = 2$ and similar Na_B values for the host granite (0.10 – 0.20) and MMEs (0.05 – 0.16). Based on the classification by Leake et al. (1997), amphiboles from the host granitoids are mostly hastingsite, with higher Fe^{3+} values (0.1 – 0.6 apfu) than Al^{VI} (0.3 – 0.5 apfu), whilst MMEs amphibole ranging from edenite to pargasite, and their ferro-end-members (Fig. 4B).

Figure 4. (A) Si versus Ca+Na+K classification diagram for amphibole, field boundary is from Czamanske & Wones (1973). (B) Amphibole composition classification diagram based on Si versus Mg/(Mg+Fe^{2+}) according to the nomenclature of Leake et al. (1997). (C) Al+Fe versus Ti diagram for compositional variations of titanite. (D) Al versus Fe diagram showing the compositional distribution of titanites, field boundaries defined by Kowallis et al. (1997).

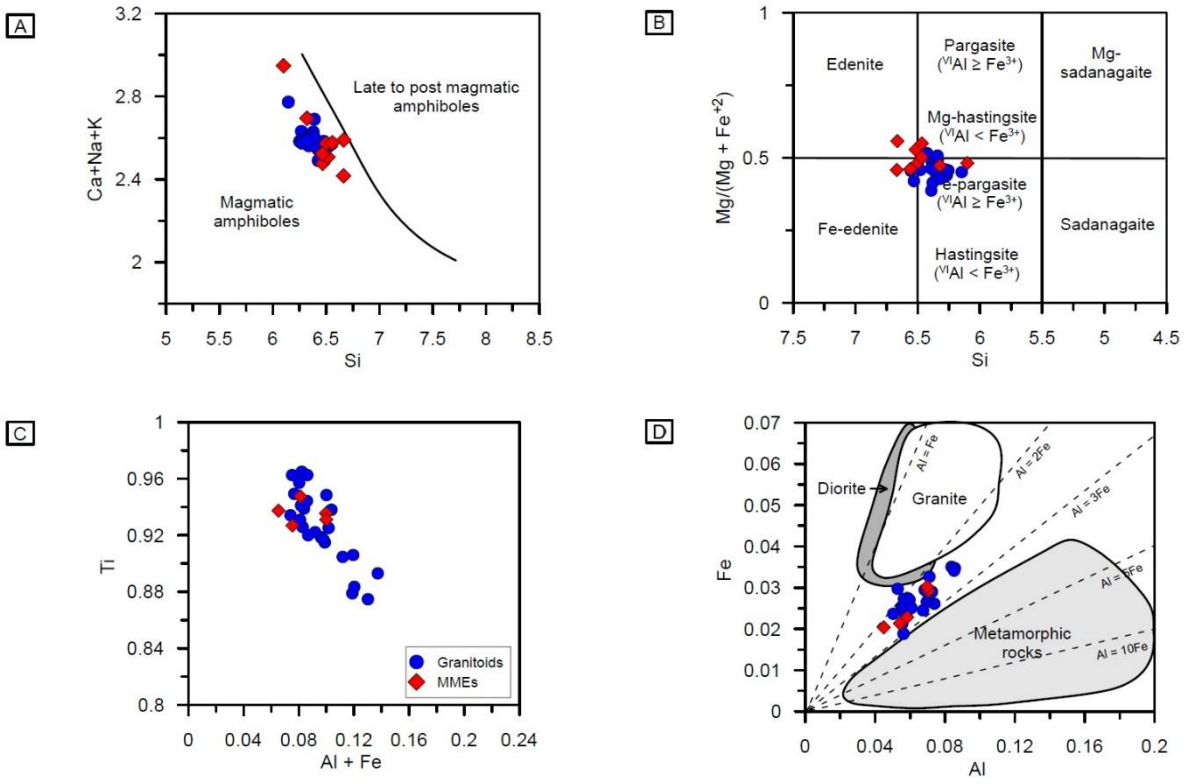

4.2.4. Titanite

Titanite from both granitoids and MMEs shows only few differences in the concentrations of the major elements and F (Table 4). Titanite from granitoids contains more TiO_2 (38.7 – 34.58 wt%), Al_2O_3 (1.27 – 2.20 wt%), FeO (0.68 – 1.26 wt%) and F (0.11 – 1.04 wt%) relative to titanite from MMEs (with TiO_2 values of 36.88 to 37.61 wt%, Al_2O_3 1.15 to 1.79 wt%, FeO 0.73 to 1.08 wt%, F 0.12 to 0.60 wt%). Both granitoids and enclaves titanites display negative correlation on Al+Fe^{3+} versus Ti diagram (Fig. 4C), which reflects the common substitution of Al and Fe for Ti in the octahedral site (Cao et al., 2015). According to the titanite chemistry descriptions mentioned above and using the fields defined by Kowallis et al. (1997), it is observed that all analyzed titanites fall between the fields suggested for magmatic and metamorphic titanites (Fig. 4D). This is

consistent with the petrographic observations, which indicate that titanite was crystallized early but had its initial composition subsequently re-equilibrated during post-magmatic processes.

4.2.5. Epidote

The composition of epidote has very restricted composition: SiO_2 35.8 – 38.0 wt%, Al_2O_3 20.4 – 24.5 wt%, FeO 10.2 – 14.2 wt%, CaO 22.4 – 23.3 wt% (Table 5). According to the criteria proposed by Tulloch (1979) and Evans & Vance (1987), epidote can be interpreted as magmatic in origin if it presents pistacite component (Ps = molar [Fe^{3+} / (Fe^{3+}+ Al)] x100) >25% and < 0.2 wt% TiO_2. Epidote from the Carmo stock have Ps contents varying between 23 and 33 mol% and TiO_2 contents are always < 0.2 wt%. A comparative study carried out by Pandit et al. (2014), between magmatic and hydrothermal epidotes, showed an overlap of the values obtained from the Ps content. Nevertheless, the importance of the petrography, texture and mineral assemblages was highlighted by these authors, allowing to discriminate both varieties of epidote. Thus, the textural evidence and the chemical composition of the analyzed epidotes clearly point to a magmatic origin.

Table 1 - Representative microprobe analyses of plagioclase from Carmo granitoids (BCAR) and MMEs (BCAR E). C – Center, R – Rim, <dl – below detection limits. Stand. at 5 cations and 8 oxygen.

Sample	BCAR56 -C3	BCAR56 -C3	BCAR56 -C5	BCAR56 -C5	BCAR57 -C2	BCAR57 -C2	BCAR60 -C2	BCAR60 -C2	BCAR20E -C1	BCAR20E -C2	BCAR20E -C3
Position	C	R	C	R	C	R	C	R	C	C	C
SiO_2	64.29	62.67	56.82	62.78	62.54	62.97	59.58	63.81	60.18	60.50	60.60
TiO_2	<dl	<dl	<dl	0.01	0.03	0.07	0.04	0.01	0.03	0.05	0.09
Al_2O_3	21.83	23.07	26.9	23.57	23.39	22.72	25.01	22.33	25.39	24.72	24.84
Cr_2O_3	<dl	<dl	0.07	0.01	0.01	0.03	0.04	0.06	<dl	0.03	0.05
FeO	0.03	0.02	0.12	0.23	0.15	0.08	0.01	0.09	0.09	0.02	0.03
MnO	<dl	<dl	0.01	<dl	<dl	<dl	<dl	0.05	<dl	<dl	<dl
MgO	0.01	0.02	0.02	<dl	0.03	0.01	0.01	<dl	0.00	<dl	0.01
CaO	3.55	4.30	8.27	4.35	4.05	3.4	6.84	4.45	6.70	6.46	6.99
Na_2O	9.68	8.28	6.61	9.36	9.17	9.7	7.6	9.16	7.16	7.63	7.24
K_2O	0.11	1.19	0.22	0.27	0.18	0.27	0.26	0.13	0.26	0.12	0.15
Total	99.50	99.55	99.13	100.58	99.55	99.25	99.39	100.09	99.81	99.52	99.99
Si	2.851	2.796	2.565	2.755	2.776	2.794	2.671	2.823	2.696	2.712	2.712
Ti	<dl	<dl	<dl	<dl	0.001	0.002	0.001	<dl	0.001	0.002	0.003
Al	1.141	1.213	1.436	1.219	1.223	1.188	1.321	1.164	1.341	1.306	1.310
Cr	<dl	<dl	0.002	<dl	<dl	0.001	0.001	0.002	<dl	0.001	0.002
Fe^{+3}	<dl	<dl	0.004	0.008	0.005	0.003	<dl	<dl	<dl	<dl	<dl
Fe^{+2}	0.001	0.001	<dl	<dl	<dl	<dl	<dl	0.003	0.004	0.001	0.001
Mn	<dl	<dl	<dl	<dl	<dl	<dl	<dl	0.002	<dl	<dl	<dl
Mg	0.001	0.001	0.001	<dl	0.002	0.001	0.001	<dl	<dl	<dl	0.001

Ca	0.169	0.206	0.400	0.205	0.192	0.161	0.329	0.211	0.322	0.310	0.335
Na	0.832	0.716	0.579	0.796	0.789	0.834	0.661	0.786	0.622	0.663	0.628
K	0.006	0.068	0.012	0.015	0.010	0.015	0.015	0.007	0.015	0.007	0.009
An	16.751	20.771	40.360	20.127	19.398	15.969	32.732	21.020	33.579	31.643	34.484
Ab	82.637	72.369	58.370	78.363	79.564	82.547	65.815	78.255	64.889	67.657	64.635
Or	0.613	6.860	1.261	1.510	1.039	1.484	1.453	0.725	1.533	0.700	0.881

Table 2 - Representative microprobe analyses of biotite from Carmo granitoids (BCAR) and MMEs (BCAR E). C – Center, R – Rim, <dl – below detection limits. Stand. at 22 oxygen.

Sample	BCAR56-C2	BCAR56-C2	BCAR56-C5	BCAR56-C5	BCAR56-C7	BCAR56-C7	BCAR60-C1	BCAR60-C3	BCAR20 E-C2	BCAR25 E-C1	BCAR25 E-C2
Position	C	R	C	R	C	R	C	C	C	R	C
SiO_2	35.62	35.58	35.61	35.87	35.92	36.02	36.11	37.16	37.68	36.73	36.01
TiO_2	2.47	2.95	1.84	2.08	2.37	1.96	2.43	1.97	3.00	2.12	1.88
Al_2O_3	15.60	15.14	15.63	15.72	15.69	15.96	16.05	15.10	14.80	16.11	16.40
FeO	21.92	22.92	21.88	21.12	21.86	21.88	20.84	21.90	20.57	20.06	20.29
MnO	0.38	0.34	0.18	0.27	0.33	0.26	0.36	0.36	0.27	0.29	0.31
MgO	8.56	8.63	8.56	8.18	9.00	9.27	9.12	9.49	9.08	9.85	10.14
CaO	<dl	<dl	<dl	<dl	8,998	<dl	<dl	<dl	<dl	<dl	<dl
Na_2O	0.04	0.09	0.15	0.13	0.15	0.10	0.14	0.04	0.10	0.11	0.12
K_2O	9.18	9.48	8.91	9.24	9.56	9.62	9.19	9.56	9.27	9.29	9.39
Cr_2O_3	0.02	<dl	0.06	0.06	0.03	0.04	<dl	0.03	0.00	0.04	0.05

NiO	<dl	<dl	<dl	0.01	8,998	0.02	<dl	0.02	0.07	0.00	0.08
F	0.54	0.26	0.32	0.44	0.29	0.25	0.47	0.10	0.15	0.47	0.36
Cl	0.01	<dl	0.03	0.02	0.01	0.02	0,01	0.01	<dl	0.02	0.01
Total	94.34	95.38	93.18	93.15	95.20	95.41	94.72	95.74	94.99	95.08	95.02
Si	5.549	5.507	5.592	5.623	5.529	5.526	5.546	5.631	5.693	5.577	5.503
Al^{IV}	2.451	2.493	2.408	2.377	2.471	2.474	2.454	2.369	2.307	2.423	2.497
Al^{VI}	0.413	0.268	0.486	0.527	0.376	0.411	0.452	0.328	0.329	0.460	0.456
Ti	0.289	0.343	0.217	0.246	0.275	0.226	0.281	0.225	0.341	0.242	0.216
Cr	0.003	<dl	0.008	0.007	0.004	0.005	<dl	0.004	<dl	0.005	0.006
Fe^{+3}	0.135	0.187	0.157	0.020	0.168	0.217	0.096	0.020	<dl	0.100	0.225
Fe^{+2}	2.738	2.801	2.735	2.773	2.673	2.617	2.603	2.792	2.631	2.473	2.391
Mn	0.050	0.045	0.024	0.035	0.043	0.034	0.046	0.046	0.035	0.038	0.040
Mg	1.988	1.992	2.005	1.912	2.065	2.120	2.089	2.143	2.044	2.228	2.310
Ni	<dl	<dl	<dl	0.002	<dl	0.003	<dl	0.003	0.009	<dl	0.009
Ca	<dl	<dl	<dl	<dl	<dl	<dl	<dl	<dl	<dl	<dl	<dl
Na	0.012	0.027	0.046	0.040	0.044	0.031	0.043	0.012	0.030	0.031	0.034
K	1.825	1.871	1.784	1.847	1.877	1.882	1.801	1.849	1.787	1.799	1.829
F	0.267	0.126	0.160	0.217	0.139	0.124	0.226	0.048	0.069	0.226	0.175
Cl	0.002	<dl	0.009	0.006	0.002	0.007	0.002	0.002	0.001	0.006	0.003
Fe/(Fe + Mg)	0.590	0.598	0.589	0.591	0.577	0.570	0.562	0.564	0.560	0.533	0.529
Mg/(Fe + Mg)	0.410	0.402	0.411	0.409	0.423	0.430	0.438	0.436	0.440	0.467	0.471

Table 3 - Representative microprobe analyses of amphibole from Carmo granitoids (BCAR) and MMEs (BCAR E). C – Center, R – Rim, <dl – below detection limits. Stand. at 23 oxygen.

Sample	BCAR56-C1	BCAR56-C1	BCAR56-C7	BCAR56-C7	BCAR57-C4	BCAR57-C4	BCAR60-C2	BCAR60-C2	BCAR20E-C2	BCAR25E-C1	BCAR25E-C1
Position	C	R	C	R	C	R	C	R	C	C	R
SiO_2	41.36	41.33	41.55	40.82	42.40	42.49	41.27	42.71	40.18	44.78	43.44
TiO_2	1.63	1.26	1.01	1.54	1.53	1.52	1.78	1.60	1.34	1.05	1.31
Al_2O_3	11.28	11.38	10.95	11.16	11.15	10.96	11.42	10.97	10.56	10.34	9.81
FeO	20.25	20.58	20.43	21.11	18.37	19.10	20.54	19.80	19.62	17.10	18.85
MnO	0.41	0.47	0.44	0.42	0.41	0.33	0.49	0.48	0.42	0.37	0.45
MgO	7.84	7.55	7.94	7.25	8.96	8.80	6.87	7.52	8.20	10.05	8.42
CaO	11.36	11.30	11.44	11.33	11.30	11.14	11.30	11.43	11.55	11.63	11.39
Na_2O	1.59	1.51	1.57	1.47	1.68	1.59	1.72	1.45	1.59	1.33	1.55
K_2O	1.40	1.54	1.25	1.35	1.10	1.14	1.52	1.33	1.32	0.93	1.31
Cr_2O_3	<dl	0.02	0.02	<dl	<dl	0.05	0.07	<dl	0.02	<dl	0.01
NiO	<dl	0.04	<dl	<dl	<dl	<dl	<dl	<dl	<dl	<dl	0.04
F	<dl	0.42	0.63	0.26	0.30	<dl	0.26	0.41	0.23	0.08	0.31
Cl	0.01	0.02	<dl	0.02	0.01	0.01	0.02	0.02	0.02	0.02	0.02
Total	97.14	97.39	97.23	96.72	97.23	97.12	97.26	97.72	95.03	97.68	96.90
Si	6.337	6.352	6.391	6.322	6.427	6.426	6.391	6.531	6.322	6.664	6.666
Al^{IV}	1.663	1.648	1.609	1.678	1.573	1.574	1.609	1.469	1.678	1.336	1.334
Al^{VI}	0.373	0.413	0.375	0.359	0.419	0.380	0.475	0.508	0.280	0.478	0.439
Ti	0.188	0.145	0.116	0.179	0.175	0.173	0.208	0.184	0.159	0.117	0.151
Cr	<dl	0.002	0.002	<dl	<dl	0.006	0.008	<dl	0.002	<dl	0.001

Fe^{+3}	0.440	0.471	0.513	0.493	0.426	0.548	0.147	0.161	0.438	0.353	0.129
Fe^{+2}	2.155	2.174	2.115	2.241	1.902	1.867	2.512	2.371	2.143	1.775	2.290
Mn	0.054	0.062	0.057	0.055	0.052	0.042	0.065	0.062	0.056	0.047	0.059
Mg	1.791	1.729	1.821	1.673	2.025	1.983	1.585	1.714	1.922	2.230	1.927
Ni	<dl	<dl	<dl	<dl	<dl	<dl	<dl	<dl	<dl	<dl	0.004
Ca	1.864	1.861	1.886	1.879	1.836	1.804	1.874	1.872	1.946	1.854	1.872
Na	0.472	0.449	0.469	0.443	0.495	0.466	0.516	0.430	0.484	0.385	0.461
K	0.274	0.301	0.245	0.266	0.212	0,220	0.300	0.260	0.264	0.177	0.257
F	<dl	0.202	0.307	0.127	0.145	<dl	0.129	0.200	0.112	0.038	0.148
Cl	0.003	0.005	<dl	0.004	0.003	0.003	0.005	0.005	0.006	0.004	0.005
$(Ca+N)_B$	2	2	2	2	2	2	2	2	2	2	2
Na_B	0.136	0.139	0.114	0.121	0.164	0.196	0.126	0.128	0.054	0.146	0.128

Table 4 - Representative microprobe analyses of titanite from Carmo granitoids (BCAR) and MMEs (BCAR E). C – Center, R – Rim, <dl – below detection limits. Stand. at 5 oxygen.

Sample	BCAR56-C3	BCAR56-C3	BCAR56-C5	BCAR56-C8	BCAR57-C3	BCAR57-C3	BCAR60-C5	BCAR60-C7	BCAR20E-C2	BCAR20E-C4	BCAR20E-C4.1
Position	C	R	R	C	C	R	R	C	C	C	C
SiO_2	30.18	30.13	29.69	28.45	29.56	29.45	29.91	29.49	28.92	29.33	29.23
TiO_2	35.64	36.43	36.80	36.50	38.72	38.66	34.58	36.94	37.61	37.17	36.88
Al_2O_3	2.20	2.19	1.53	1.50	1.44	1.49	2.10	1.27	1.48	1.79	1.77
FeO	1.26	1.24	0.97	0.87	0.68	0.87	1.24	0.84	0.81	1.04	1.08

MnO	0.02	0.01	0.10	0.12	0.07	0.12	0.11	0.08	0.11	0.14	0.11
MgO	0.02	0.01	<dl	<dl	0.03	0.03	0.01	<dl	<dl	<dl	0.01
CaO	28.08	28.04	27.76	27.45	27.60	27.36	28.14	27.53	28.17	27.90	27.69
Na_2O	0.03	0.04	0.02	0.08	0.02	<dl	0.06	<dl	<dl	0.02	0.01
K_2O	0.09	0.03	0.02	0.03	0.01	0.03	<dl	<dl	0.01	0.01	0.02
P_2O_5	0.46	0.26	0.11	0.07	0.11	0.11	0.02	0.06	0.01	0.03	0.03
Cr_2O_3	<dl	0.04	<dl	<dl	0.05	0.07	0.04	0.09	0.03	0.06	0.06
NiO	0.03	<dl	0.01	0.04	0.02	0.03	<dl	0.02	<dl	<dl	<dl
V_2O_3	0.37	0.31	0.39	0.34	0.44	0.40	0.37	0.41	0.24	0.38	0.33
F	0.72	0.12	1.04	<dl	0.17	<dl	0.33	0.60	0.60	0.12	0.45
Total	99.10	98.84	98.44	95.44	98.93	98.61	96.91	97.33	98.00	98.00	97.66
Si	0.994	0.996	0.987	0.978	0.977	0.977	1.011	0.991	0.968	0.981	0.981
Ti	0.884	0.906	0.920	0.944	0.963	0.965	0.879	0.934	0.947	0.935	0.931
Al	0.086	0.085	0.060	0.061	0.056	0.058	0.084	0.050	0.058	0.071	0.070
Fe	0.035	0.034	0.027	0.025	0.019	0.024	0.035	0.024	0.023	0.029	0.030
Mn	0.001	<dl	0.003	0.004	0.002	0.003	0.003	0.002	0.003	0.004	0.003
Mg	0.001	<dl	<dl	<dl	0.001	0.001	<dl	<dl	<dl	<dl	0.001
Ca	0.991	0.993	0.988	1.011	0.977	0.972	1.019	0.991	1.011	1.000	0.996
Na	0.002	0.003	0.002	0.005	0.001	<dl	0.004	<dl	<dl	0.001	0.001
K	0.004	0.001	0.001	0.001	<dl	0.001	<dl	<dl	0.001	<dl	0.001
P	0.013	0.007	0.003	0.002	0.003	0.003	0.001	0.002	<dl	0.001	0.001
Cr	<dl	0.001	<dl	<dl	0.001	0.002	0.001	0.002	0.001	0.001	0.002
Ni	0.001	<dl	<dl	0.001	0.001	0.001	<dl	<dl	<dl	<dl	<dl
V	0.010	0.008	0.010	0.009	0.012	0.011	0.010	0.011	0.006	0.010	0.009

F	0.075	0.012	0.109	<dl	0.017	<dl	0.035	0.063	0.064	0.013	0.047

Table 5 - Representative microprobe analyses of epidote from Carmo granitoids (BCAR) and MMEs (BCAR E). C – Center, R – Rim, <dl – below detection limits. Stand. at 12 oxygen.

Sample	BCAR56-C4	BCAR56-C4	BCAR56-C5	BCAR56-C5	BCAR56-C7	BCAR57-C4	BCAR57-C4	BCAR57-C5	BCAR60-C5	BCAR60-C5.1	BCAR60-C6	BCAR60-C6
Position	C	R	C	R	C	C	R	C	C	C	C	R
SiO_2	37.22	37.15	37.34	37.98	35.82	37.64	37.92	36.75	37.40	37.02	36.96	37.04
TiO_2	0.07	0.10	0.11	0.06	0.14	0.01	0.06	0.25	0.04	0.08	0.15	0.07
Al_2O_3	24.54	23.02	21.68	20.42	21.78	23.47	23.36	23.95	22..90	22.25	22.23	22.46
FeO	10.48	12.18	13.26	14.18	13.62	12.73	12.70	12.41	12.81	12.91	12.47	12.75
MnO	0.23	0.17	0.19	0.14	0.18	0.20	0.19	0.24	0.15	0.20	0.14	0.17
MgO	0.01	<dl	0.02	<dl	0.01	0.02	0.03	0.03	0.01	0.04	0.04	0.02
CaO	23.35	23.22	22.89	22.74	22.93	22.80	22.94	22.91	22.86	23.05	22.37	23.05
Na_2O	0.01	0.03	0.06	<dl	0.01	0,01	<dl	<dl	0.04	0.03	<dl	0.01
K_2O	0.02	0.02	0.02	0.01	<dl	<dl	<dl	0.02	<dl	0.01	0.02	<dl
Total	95.92	95.89	95.57	95.54	94.49	96.87	97.20	96.57	96.20	95.58	94.37	95.57
Si	2.976	2.987	3.019	3.074	2.942	2.989	3.000	2.930	2.995	2.992	3.015	2.991
Ti	0.004	0.006	0.006	0.004	0.009	0.001	<dl	0.020	0.002	0.005	0.009	0.004
Al	2.312	2.181	2.066	1.948	2.108	2.197	2.180	2.250	2.161	2.119	2.137	2.138
Fe^{+3}	0.701	0.819	0.897	0.960	0.936	0.845	0.840	0.830	0.858	0.873	0.851	0.861
Mn	0.016	0.012	0.013	0.009	0.012	0.014		0.020	0.010	0.014	0.010	0.011

Mg	0.001	<dl	0.003	<dl	0.001	0.003	0.010	<dl	0.001	0.004	0.004	0.003
Ca	2.000	2,000	1.983	1.972	2.018	1.940	<dl	1.960	1.962	1.997	1.955	1.995
Na	0.001	0.005	0.009	<dl	0.002	0.001	1.950	<dl	0.006	0.004	<dl	0.002
K	0.002	0.002	0.002	0.001	<dl	<dl	<dl	<dl	<dl	0.001	0.002	<dl
Ps	23.3	27.3	30.3	33.0	30.7	27.8	27.8	26.9	28.4	29.2	28.5	28.7

4.3. Magmatic physicochemical conditions

4.3.1. Al-in-hornblende geobarometry

Calcic amphibole is a common mineral in calc-alkalic granitic rocks. Its presence in this type of rock has been considered as a useful tool to estimate the thermobarometric conditions under which the magmas crystallized (Anderson, 1996; Anderson et al., 2008). Considering the linear relationship between amphibole aluminum content and pressure, Hammarstrom & Zen (1986) proposed an empirical barometer that has been discussed and recalibrated by several authors, using estimates from natural pluton (Hollister et al., 1987) or experimental studies (Johnson & Rutherford, 1989; Thomas & Ernst, 1990; Schmidt, 1992). These studies calibrated the geobarometer for pressures in the range of 2 – 14 kbar and a mineral assemblage that includes quartz + alkali feldspar + plagioclase + hornblende + biotite + Fe-Ti oxides + titanite + melt + fluid. Anderson & Smith (1995) assessed the sensitivity of the Al-in-hornblende barometer to variations in temperature and oxygen fugacity and recalibrated the previously proposed formulation. These authors used the experimental data of Johnson & Rutherford (1989) and Schmidt (1992) to incorporate the effect of temperature. They also limited the use of the barometer to amphiboles with $Fe_T/(Fe_T+Mg)$ ratios ranging from 0.40 to 0.65, in order to assess oxygen fugacity before applying the barometer. More recently, Mutch et al. (2016) proposed a calibration of the Al-in-hornblende barometer based on an experimental study of amphibole stability in granitic magmas. This study recognized a non-linear relationship at low pressures (< 2.5 kbar), which has not been explored by previous calibrations.

In order to constraint geobarometry of granitoids from the Carmo stock, we used calibrations of Schmidt (1992), Anderson & Smith (1995) and Mutch et al. (2016) and compare the values obtained according to their uncertainties. Results of the calculated crystallization pressures are presented in Table 6. The values calculated by the calibrations of Schmidt (1992) and Anderson & Smith (1995) are 6.4 – 7.4 kbar and 5.7 – 7.4 kbar, respectively. The differences between the two calibrations are within absolute errors (± 0.6 kbar for both). Estimates based on Mutch et al. (2016) yield consistently lower values (between 5.0 and 6.0 kbar; Table 6). Given that the relative uncertainty of the calibration by Mutch et al. (2016) is ± 16%, it fits well for typical granitic amphibole Al_T values (≤ 1.5 apfu). However, for unusual values (> 2.0 apfu), the relative uncertainty of Mutch et al. (2016) translates to an absolute uncertainty in the estimated pressure of > 0.8 kbar. All analyzed hornblende grains in this study have Al_T values > 1.9 apfu, therefore the calibration by Mutch et al. (2016) is inappropriate to estimate the unusual crystallization conditions of the Carmo stock. Thus, we use the pressures

obtained from Anderson & Smith (1995)'s calibration, which are in good agreement with pressure values previously calculated for mEp-bearing granitoids of the Transversal Zone Domain (Sial, 1986, 1990, 1993; Brasilino et al, 2011; Ferreira et al., 2011). Assuming an average crustal density of 2.7 g/cm^3 (Mutch et al., 2016), the amphibole crystallization depth calculated of the Carmo granitoids ranges from 22 to 27 km, which corresponds to the middle to lower crust depths.

Table 6 - Summary of the estimation of crystallization condition of the Carmo granitoids.

Sample	BCAR56		BCAR57		BCAR60			
Al-in-hornblende geobarometry								
Schmidt (1992)	6.7	6.8	7.1	6.4	6.9	6.4	7.2	7.4
Anderson & Smith (1995)	5.7	6.1	7.2	6.4	6.8	6.6	7.1	7.4
Mutch et al. (2016)	5.3	5.4	5.7	5.0	5.5	5.0	5.8	6.0
Depth (km)	22	23	27	24	26	25	27	28
Amphibole-plagioclase geothermometry								
Holland & Blundy (1994)	735	723	665	670	686	656	682	675
Zircon saturation geothermometry								
Watson & Harrison (1983)	781		779		763			
Shao et al. (2019)	769		767		749			
Oxygen fugacity								
Wones (1989)	-14.1	-14.7	-16.1	-15.7	-15.9	-17.1	-15.5	-15.8
Ridolfi et al. (2010)	-15.8	-16.1	-17.4	-17.2	-17.5	-18.0	-17.1	-17.3
ΔNNO	-0.72	-0.70	-0.55	-0.41	-1.18	-0.88	-0.69	-0.70
Water Content								
Putirka (2005)	5.4	5.4	6.3	6.8	5.2	6.5	6.5	6.9
Ridolfi et al. (2010)	6.7	6.8	7.3	6.6	6.9	7.5	7.1	7.7

4.3.2. Hornblende-plagioclase geothermometry

The geothermometer based on amphibole-plagioclase equilibria has often been used to estimate the crystallization temperature in calc-alkalic igneous rocks (Anderson, 1996; Anderson et al., 2008). Blundy & Holland (1990) developed a thermometer for silica-saturated rocks based on the reactions edenite+ 4quartz = tremolite + albite (reaction A) and pargasite + 4quartz = hornblende + albite (reaction B). Subsequently, Poli & Schmidt (1992) noted that this

thermometer produced erroneously high temperatures, which led Holland & Blundy (1994) to review the calibration for the reaction A and formulate a new calibration based on the equilibrium edenite + albite = richterite + anorthite. Anderson (1996) recommends the use of the edenite-richterite thermometer proposed by Holland & Blundy (1994), since it produces more reliable temperature values than other thermometers used to estimate magmatic temperatures. In this study, we used the formulation proposed by Holland & Blundy (1994) to calculate the crystallization temperature of the studied granitoid. The crystallization calculated temperatures range from 656 to 735°C (average = 689 °C; ± 27 °C). These temperatures estimated from the amphibole-plagioclase equilibrium are consistent with temperature close to the haplogranite solidus (725 ± 75 ° C; Mutch et al., 2016). These calculated temperatures decreased towards the center of pluton, an observation that correlates with decrease of the grain size from center towards the margins of pluton, and indicates slow cooling after magma emplacement.

4.3.3. Zircon saturation geothermometry

Through pressure/temperature experimental studies, Watson & Harrison (1983) observed that the crystallization and dissolution of zircon in magmatic systems are strongly dependent on the temperature and melt composition (M = (Na + K + 2Ca)/(Al.Si)). Their studies allowed to calibrate a thermometer for rocks of intermediate to felsic compositions (M = 0.9 to 1.9), which was later used in several petrological studies as an estimate of the magmatic temperatures near-liquidus (Hanchar & Watson, 2003; Anderson et al., 2008; Siegel et al., 2018). In the last decades, this thermometer has been revised and extended to peraluminous and peralkaline compositions (Boehnke et al., 2013; Gervasoni et al., 2016; Shao et al., 2019).

The temperatures of granitoids from the Carmo stock have been estimated using the zircon saturation geothermometer (T_{Zr}) based on the original work by Watson & Harrison (1983) and on the latest review developed by Shao et al. (2019). Samples with M values outside the calibration range (M > 1.9) were excluded from the calculations. Representative zircon saturation temperatures for Carmo granitoids are presented in Table 6. The $T_{Zr,}$ calculated using the geothermometer of Watson & Harrison (1983) range from 763 to 787 °C, and are slightly higher than the temperatures obtained from Shao et al. (2019)'s equation (749 – 776 °C).

Because zircon is an early phase during felsic magma crystallization, T_{Zr} are widely interpreted to represent the minimum liquidus temperature of magma, and to estimate partial

melting temperatures (e.g., Collins et al., 2016; Basak & Goswami, 2020). The thermometer originally proposed by Watson & Harrison (1983), however, contains certain limitations that denote some uncertainties. The method assumes that the bulk-rock composition is similar to the melt composition and that all zircons present in the rock are autocrysts. Nevertheless, fractional crystallization processes are common in granitic rocks, which can lead to an increase of Zr content and decrease of M, thereby raising T_{Zr} (n; Siegel et al., 2018). In addition, the presence of inherited or antecrystic zircon grains can result in overestimated values (Anderson et al., 2008; Siegel et al., 2018). The average T_{Zr} calculated for granitoids in the Carmo stock is ~ 769 ° C (ranging from 749 to 787 ° C; Table 6), which is consistent with the petrographic observations and temperatures determined by the amphibole-plagioclase geothermometer. These estimates are within the limit shown by Miller et al. (2003) for "cold" granitoids, and suggest that T_{Zr} can be considered maximum temperatures.

4.3.4. Oxygen fugacity

The redox state of magma plays an important role in controlling the stability field of some minerals. Its nature is a primary characteristic inherited from its source, although magmatic differentiation and assimilation processes can be locally important (Carmichael, 1991; Blevin, 2004). The oxygen fugacity (fO_2) is an intensive parameter that exerts an important control on the composition of minerals, controlling the abundance of Fe-Ti oxides, modal proportion of mafic minerals, and their Fe/Mg ratios (Anderson, 1996; Anderson et al. 2008). The equilibrium expression $\log fO_2 = -30930/T+14.98+0.142(P-1)/T$, proposed by Wones (1989), is widely applied to estimate fO_2 values in granitic rocks with mineral assemblage that include titanite + magnetite + quartz. The estimated fO_2 values for the Carmo stock using this equation show a small variation from -14.9 to -17.3, indicating that these granites crystallized under conditions above the fayalite-magnetite-quartz (FMQ) buffer (Fig. 5A). These values are consistent with moderate oxidation conditions during magma crystallization.

To better determine the fO_2 conditions during the crystallization of the Carmo granitoids, we also applied the formulation proposed by Ridolfi et al. (2010), for amphiboles in calc-alkalic magmas. The results calculated from this formulation vary from -15.8 to -18, suggesting crystallization conditions between the NNO (nickel-nickel-oxygen) and FMQ buffers (Fig. 5B), confirming moderately oxidized conditions.

Figure 5. (A) 10^3/T versus log fO_2 diagram to estimated redox conditions, showing the stability field of several mineral assemblages (Wones, 1989). (B) T versus log fO_2 diagram showing the formation temperature and fO_2 conditions calculated according to Ridolfi et al. (2010). (C) T versus P diagram displaying liquidus curves, which indicate the minimum water content that can be dissolved in granite systems (Holtz et al., 2001). (D) H_2O versus T diagram showing mafic phase stability fields, based on experiments of Naney (1983) in granodioritic compositions at 8 kbar. Note that the increase in the abundance of biotite and mEp towards the center of the pluton due to the decrease in hornblende is consistent with the amphibole reacts out before the magma reaches the solidus.

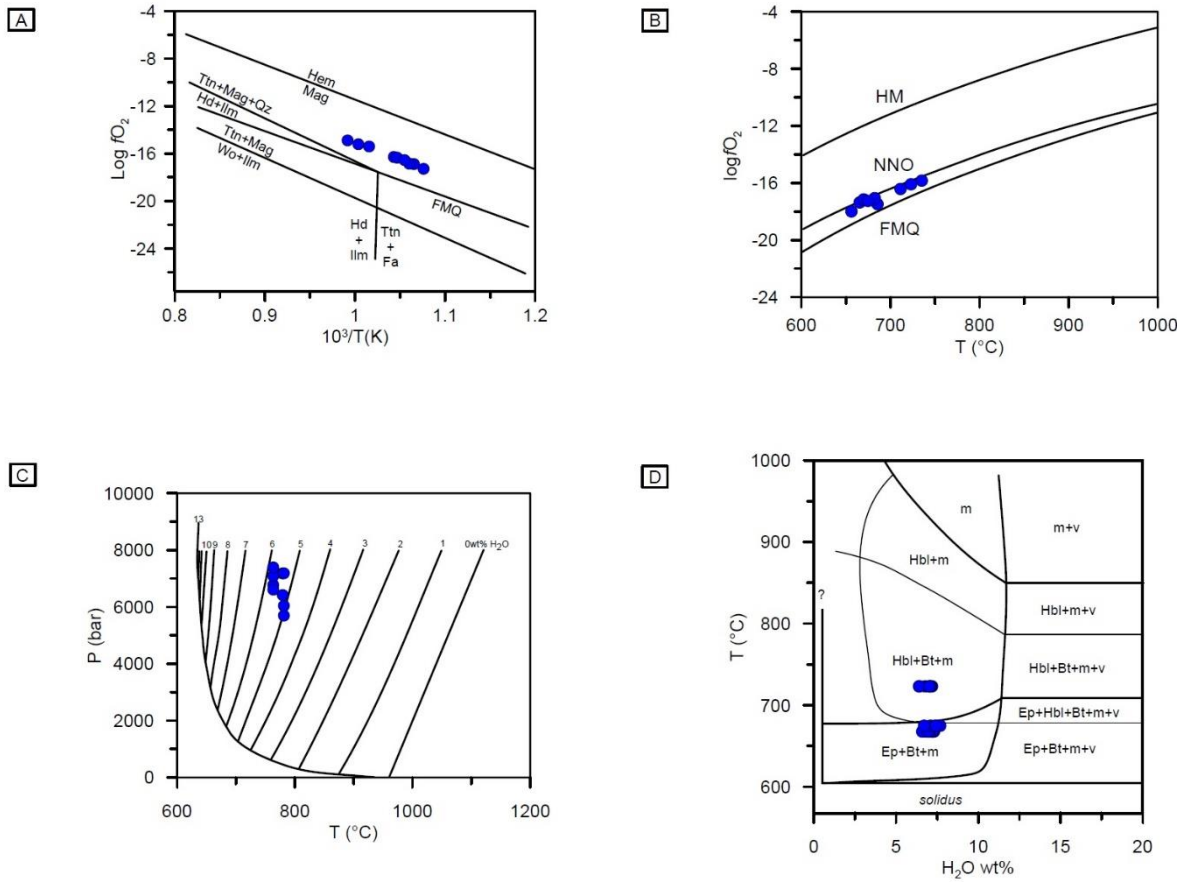

4.3.5. Estimation of water contents

Water is the main fluid component in silicic magmas and is responsible for the stabilization of the hydrated minerals, such as amphibole and biotite, which form part of the mineral assemblages of calc-alkalic granitoids (Holtz et al., 2001; Castro, 2013). Empirical and experimental studies have shown that water content is a primary feature of the magma and, although assimilation and magma mixing processes can change the content, it depends fundamentally on the initial water content in the system (e.g., Wyllie et al., 1976; Naney, 1983). Given that most of the water content of a magma is lost during the crystallization process,

consequently the initial water content in granitic magmas can only be estimated through indirect approaches (Castro, 2013).

The minimum water content to stabilize the system in its liquidus can be estimated following the methodology developed by Holtz et al. (2001), as a function of initial temperature and pressure. Therefore, using the pressure calculated based on the approach by Anderson & Smith (1995) and the zircon saturation temperatures (Watson & Harrison, 1983), as an estimate of the liquidus temperature, the minimum water content in Carmo granodiorites-monzogranites varies from ~ 5 to 6 wt% (Fig. 5C). Furthermore, we used the formulation proposed by Putirka (2005), based on plagioclase-melt compositions, for the calculation of the water content. According to this hygrometer the average water content in the studied granitoids is ~ 6.11 wt%. Finally, the water content estimated in the initial melt, using the equation by Ridolfi et al. (2010) ranges from 6.6 to 7.7 wt% (Table 6). These results are consistent with the presence of hydrated phases in the Carmo stock, such as hornblende and biotite, and agree with the typical values for calc-alkalic granitoids (ca. 4 – 6 wt% H_2O; Scaillet et al., 1998).

5. Discussion

5.1. Petrogenetic Implications

Different intensive parameters (e.g., temperature, pressure, fO_2) have been addressed in this work to allow the evaluation of the crystallization conditions that accompanied formation of mEp-granitoids from the Carmo stock. The calculated pressures (~ 6 – 7 kbar), from the Al_T content in hornblende, are within the range estimated for other mEp-bearing granitoids in the CSD (6 to 9 kbar; Sial, 1990, 1993) and close to that used in the experimental work of Naney (1983), where epidote was reported to be in equilibrium with melts of granitic-granodioritic composition at 6 – 8 kbar. On the other hand, more extensive experimental work carried out by Schmidt & Thompson (1996), showed that the minimum crystallization pressure of mEp depends on fO_2. In that study, epidote was a stable phase at temperatures above the water-saturated solidus and at pressures greater than 5 kbar, under conditions of fO_2 buffered to NNO. Nonetheless, experiments carried out under more oxidizing conditions (fO_2 buffered to hematite-magnetite (HM)) resulted in an increase of the stability field of epidote. Under these conditions, the minimum crystallization pressure of mEp occurs at about 3 kbar. The ΔNNO values, estimated for the studied granitoids, exhibit restricted variations from -1.2 to -0.4 (Table 6), which suggests moderately oxidized conditions buffered by NNO (Fig. 5B). Taken together,

our results reinforce the idea that the occurrence of mEp, when combined with oxybarometric data, provides additional information on the magma emplacement depth (Zen & Hammarstrom, 1984; Vyhnal et al., 1991; Sial et al., 2008; Ferreira et al., 2011). Independent constraints for estimate emplacement pressures include barometric calculations on appropriate mineral assemblages in contact metamorphic aureoles around igneous intrusions (Anderson et al., 2008; Mutch et al., 2016). Caby et al. (2009) described contact metamorphism aureoles in two plutons with mEp, located in the CSD, with mineral assemblage garnet, kyanite, staurolite, muscovite, biotite, plagioclase ± quartz, and interpreted this as additional evidence indicating high emplacement pressure for these intrusions.

As discussed above, T_{Zr} (749 – 787 °C) are relatively close to the temperatures estimated by Holland & Blundy's method (656 – 735 °C), probably suggesting that the hornblende was an early-crystallized phase. Experimental studies in acidic to intermediate calcic-alkalic systems have shown that under water-undersaturated conditions, pyroxene and plagioclase, instead of hornblende, are the first phases to crystallize, indicating that the liquidus temperature was higher than the upper limit of hornblende stability, which is around 900 – 950 °C (Dall'Agnol et al., 1999; Castro, 2013). Nonetheless, very high initial water contents, close to saturation, can reach the liquidus temperature values necessary to hornblende stability (Castro, 2013).

The estimates of the initial water content, from different approaches, of the Carmo granitoids show values > 5wt% (Fig. 5D), compatible with the minimum values required to stabilize hornblende as near-liquidus phase at 8 kbar (> 4.5 wt% H_2O; Naney, 1983). Furthermore, crystallization sequence deduced from textures of the studied granodiorites indicate that hornblende, and not plagioclase, is the near-liquidus phase (Fig. 2G). In this sense, the decrease in modal abundance of hornblende towards the center of the pluton, accompanied by the increase in biotite and epidote, could be reflecting the reaction that delimits the stability of epidote in tonalitic melts with excess H_2O (Ep + Bt + Qz + H_2O = Hbl + Pl + Mag + melt; Schmidt & Thompson, 1996).

Some mEp-bearing plutons, intruding low-grade metasedimentary rocks of the CSD, have also been reported for presenting clinopyroxene phenocrysts (Sial, 1993; Sial & Ferreira, 2016; Siqueira et al., 2018). Thus, given that all of these mEp-bearing plutons, in this domain, share similar mineralogical, geochemical and isotopic characteristics (Sial, 1990; Sial & Ferreira, 2016), the studied granitoids could also represent a residual melt that became colder and sufficiently rich in water, during magma crystallization, reaching the experimental

requirements to crystallize hornblende. This is viable with the anhydrous assemblage (clinopyroxene and plagioclase) being consumed through a peritectic reaction, leading to an increase in the water content of residual melt (Castro, 2013; Jiang & Zhu, 2018).

5.2. Nature of magma

The mineral chemistry of ferromagnesian minerals has become an effective tool to constraint the nature of magmas and potentially infer the tectonic environment in which granitic magmas were formed (Nachit et al., 1985; Zhou, 1986; Brimhall & Crerar, 1987; Abdel-Rahman, 1994). Here, chemical compositions of biotite and amphibole are used to infer the nature of the magma from which the Carmo granites crystallized. In the Al_2O_3-MgO-FeO ternary diagram (Fig. 6A; Abdel-Rahman,1994), all of the analyzed biotite flakes are moderately enriched in Mg, in relation to Al and Fe, plotting in the field of calc-alkalic orogenic suites. As shown in Figure 6B, the progressive increase of Fe^{2+} and the $Fe^{2+}/(Fe^{2+}+Mg)$ ratios in biotite structure defines a characteristic trend of I-type granitoids (Villaseca et al., 2017). In addition, biotite compositions plotted on the Al_T versus Fe# diagram (Fig. 6C; Anderson et al., 2008) indicate that the Carmo granitoids were generated under moderately oxidized fO_2 conditions, typical of calc-alkalic I-type granitoids (Chappell & White, 1974; Ishihara, 1977). Despite magnetite is lacking in rocks from the Carmo stock, several lines of evidence suggest that the studied granitoids correspond to relatively oxidized, magnetite-series I-type granitoids. This apparent contradiction was discussed in the experimental studies of Schmidt (1992) and Schmidt & Thompson (1996), who point out that magnetite is less abundant in epidote-bearing granitoid intrusions. This was also found by Sial et al. (1999) for Neoproterozoic plutons in NE Brazil, Early Palaeozoic granitoids in Argentina and Late Palaeozoic in Chile, and indicates that epidote is the main phase containing Fe^{3+} at pressures > 5 kbar. Instead, at low pressures and under fO_2 buffered to HM, Fe^{3+} is mainly associated with the magnetite structure (Schmidt & Poli, 2004).

Figure 6. (A) FeO-MgO-Al_2O_3 discrimination ternary diagram based on biotite composition (Abdel-Rahman, 1994). (B) $Fe^{2+}/(Fe^{2+}+Mg^{2+})$ versus Fe^{2+} classification diagram showing trends for I-type and S-type granites defined from biotite composition (Villaseca et al., 2017). (C) Al_T versus Fe/(Fe+Mg) diagram for biotite compositions, showing variations in ilmenite-series and magnetite-series granites, according to Anderson et al. (2008). (D) Ca-Fe_T-Mg ternary diagram for the amphibole showing interaction between juvenile and crustal components (Xie & Zhang, 1990). (E) MgO versus FeO/(FeO+MgO) diagram for biotite showing the components present in the magma source (Zhou, 1986). (F) log (X_{Mg}/X_{Fe}) versus log (X_F/X_{OH}) discrimination diagram for classification of magma type according to the biotite composition, field boundaries are from Brimhall & Crerar (1987).

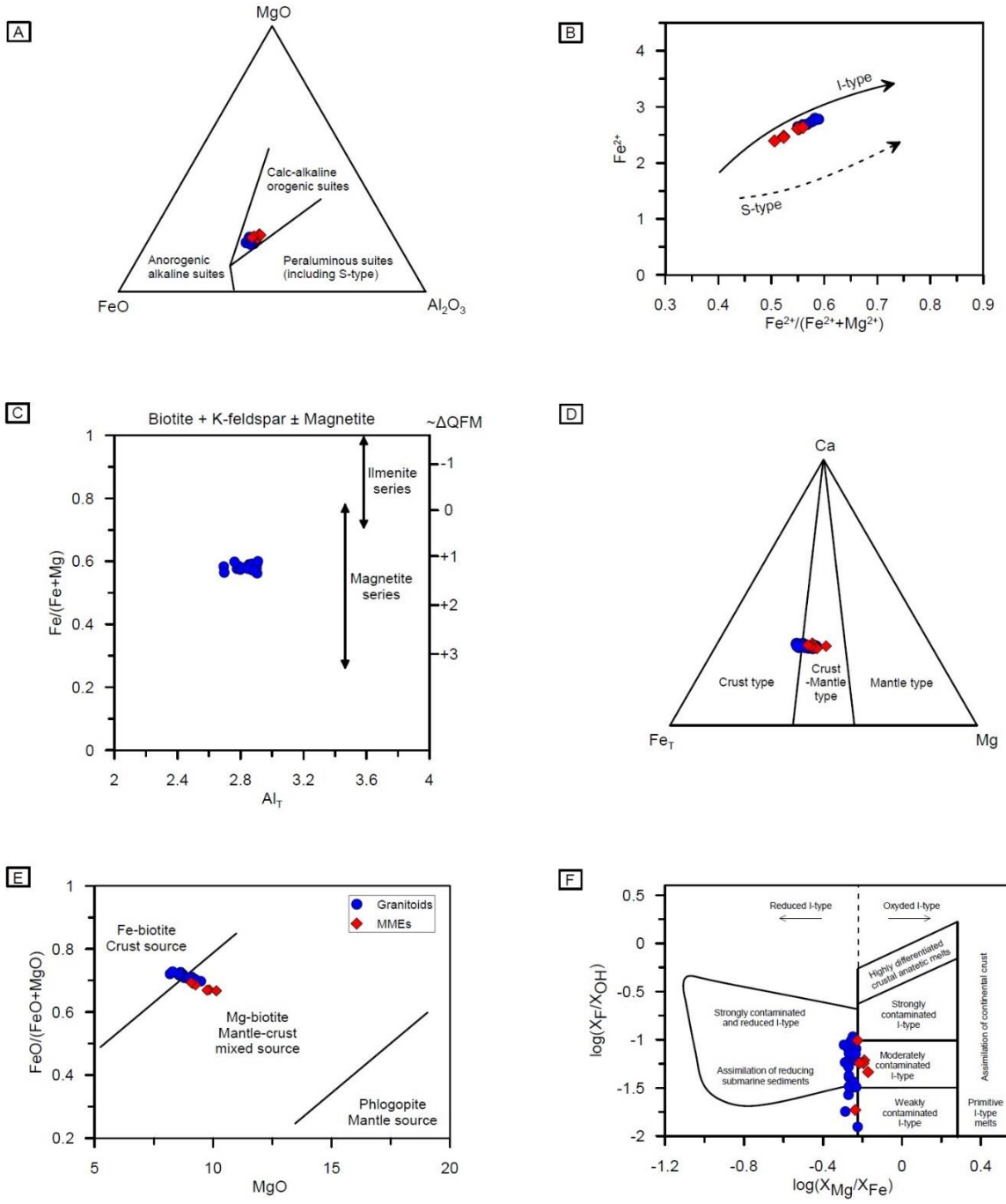

These results are in accord with whole-rock geochemical studies of mEp-bearing granitoids in the Transversal Zone Domain (Brasilino et al., 2011; Ferreira et al., 2011; Sial & Ferreira, 2016). These studies have indicated that these rocks are metaluminous and calc-alkalic in character, indicative of an I-type affinity for these granitoids (Sial & Ferreira, 2016; Lima & Ferreira, 2019). The source of these magmas, however, is debated. Petrogenetic studies carried out in several mEp-bearing plutons, in the Borborema Province, suggest the participation of a juvenile component in the genesis of these granitoids (Guimarães et al., 2004; Ferreira et al.,

2004; Silva et al., 2016). The Mesoproterozoic Nd model ages and the slightly negative εNd values support this interpretation (Guimarães et al., 2011; Ferreira et al., 2004).

The chemical composition of the amphibole and biotite of the Carmo granodiorites-monzogranites and their MMEs reflects an origin that involves interaction between juvenile and crustal components (Figs. 6D, 6E). This interaction is also evident in Figure 6F, where the variation in the Mg/Fe and F/OH ratios of biotite is used to examine the degree of contamination of primitive I-type melts with continental crust components (Brimhall & Crerar, 1987, Babazadeh et al., 2019). Biotite from the Carmo granitoids and related MMEs straddles the boundary between oxidized and reduced I-type granites with low to moderate degree of crustal contamination (Fig. 6F). In the works of Ague & Brimhall (1988a, 1988b), in granitic batholiths of California, the limit between reduced and oxidized granites separates rocks that contain mineralogical assemblages with muscovite, garnet and tourmaline, from those devoid of these phases. The chosen limit (log X_{Mg}/X_{Fe} = -0.21) was determined from the calculated fO_2 values based on a representative temperature of 800 °C (Zhang et al., 2016). However, the experimental work of Wones & Eugster (1965) showed that biotite crystallized at low temperatures (i.e., at 700 °C and buffered by NNO), with constant Fe/Mg ratios, represent more oxidizing conditions. Calculated temperatures for Carmo granitoids are lower than those estimated by Ague & Brimhall (1988b), and close to those reported by Wones & Eugster (1965). Accordingly, the values plotted in the strongly contaminated and reduced I-type granites field could represent oxidized I-type granites, and the line dividing the two fields could be lower than -0.21, as also stated by Zhang et al. (2016). Another explanation for what is observed in Figure 6F, is the participation of a reducing component such as submarine sediments in the magma source that formed the Carmo granitoids. This may explain the relatively higher X_{Mg}/X_{Fe} values presented in the biotite of MMEs, which plot outside the reduced I-type granites field. In any case, ferromagnesian minerals compositions together with bulk-rock geochemical and Nd-Sr isotopic data from previous studies (Sial & Ferreira, 2016 and references therein), clearly demonstrate that interaction between two end-member components occurred during the generation of the Carmo magma. Such interaction, however, could be explained by a variety of mechanisms such as partial melting, wall-rock assimilation and magma mixing.

Magma mixing/mingling is a model often invoked to account for the hybrid mantle-crust geochemical signatures that present certain igneous rocks and the most popular mechanism to explain the generation of MMEs (e.g., Didier, 1973; Barbarin & Didier, 1991; Perugini et al., 2003; Barbarin, 2005). In the Carmo stock, interaction between acid and basic

magmas is evidenced by a series of petrographic characteristics of MMEs and field relations with their host rocks. The spheroidal to ellipsoidal shape of MMEs, the presence of K-feldspar and plagioclase megacrysts and quartz grains partially included in MMEs, and micro-petrographic observations such as acicular apatite, ocelli quartz and plagioclase with oscillatory zoning suggest that the MMEs may represent globules of a hot mafic magma that was injected into the host felsic magma (e.g., Vernon, 1984; Barbarin & Didier, 1991; Hibbard, 1991; Baxter & Feely, 2002; Kocak et al., 2011). However, all of these characteristics are more likely to result from physical interaction (mingling or co-mingling) rather than from chemical interactions (magma mixing). Thus, the effect of these processes on the chemical composition of granodiorite-monzogranite magma was limited, at least without significant effect on the whole-rock and mineral chemical composition, probably due to the inefficient diffusion that granitic magmas have under sub-liquidus conditions (Ramos & Reid, 2005; McLeod et al., 2012).

The lack of partially disaggregated metasedimentary enclaves and resorbed contacts in the studied granitoids rule out assimilation processes (Kemp et al., 2007). Moreover, although local wall-rock assimilation may have occurred near the contacts with host rocks, this process does not explain the widespread hybrid features present in all plutons throughout the CSD. Therefore, assimilation of country rocks has probably only played a limited role, but could have occurred in the partial melting region. Assimilation at depth of a thick sequence of metasedimentary rocks by ascending calc-alkalic magma is a plausible scenario for this interpretation. This hypothesis has recently been proposed to interpret the atypical granodiorite-tonalite magmatism from Southern Iberia (Castro et al., 2020). Nonetheless, the melt resulting from this process is markedly peraluminous (A/CNK = 1.2; Castro et al., 2020), unlike epidote-bearing granitoids of the CSD that are typically metaluminous (Sial & Ferreira, 2016). On other hand, partial melting of recycled mature crustal materials (e.g., terrigenous sediments) and mantle-like sources would produce metaluminous granodioritic melts with geochemical signatures and Sr-Nd isotopic compositions that approaching those of the studied granitoid rocks (Castro et al., 2010; Errázuriz-Henao et al., 2019; Fu et al., 2019; Zhu et al., 2019). This hypothesis has recently been invoked in several Asian orogenic belts to explain syn-collisional felsic magmatism (Mo et al., 2008; Huang et al., 2014; Chen et al., 2017; Kong et al., 2020). We thus infer that the mEp-bearing Carmo granitoids were derived from mantle-like sources (e.g., basaltic oceanic crust derived from mantle) along with assimilation of terrigenous sediments in the source. This conclusion requires a geodynamic environment where interaction

between juvenile and crustal components may have occurred. Active continental margins are primary sites where such interaction can occur (Sen & Stern, 2021 and references therein), but the existence of a subduction zone in the Transversal Zone Domain of the Borborema Province during the Brasiliano Orogeny is not a consensus among geologists owing to the lack of robust evidence to support this model (Brito Neves et al., 2016; Sial & Ferreira, 2016; Neves, 2018; Caxito et al., 2020, 2021). Although there is evidence that argues in favor of Ediacaran subduction (see discussion in Caxito et al., 2020), it is still questioned whether this was of long standing and whether a continental magmatic arc was developed during this period (Neves, 2018).

Alternatively, the interaction between two end-member components may have also been generated in a syn-collisional setting (e.g., Mo et al., 2008; Fu et al., 2019), which is more consistent with regional geological features. In this scenario, the remaining oceanic crust (with mantle-like isotopic signature) along with terrigenous sediments are slowly underthrust below the overlying lithosphere during the early collisional stage. At this point, hydrated oceanic crust and sediments would melt when thermal equilibrium with the previously heated continental lithosphere is reached, evolving along a high T/P path (Mo et al., 2008; Niu et al., 2013). Another possibility invokes the slab break-off model (Davies & von Blanckenburg, 1995), which causes the asthenosphere upwelling and supplies the heat required to trigger the partial melting of the materials involved (oceanic crust and sediments) (e.g., Fu et al., 2019). In any case, testing any of these models is beyond the scope of this paper, and further research is needed to better constrain the tectonic setting of the Carmo magma generation.

6. Conclusions

The application of Al-in-hornblende geobarometer in the granitoids of the Carmo stock gave pressures of ~ 6-7 kbar, indicating that the crystallization of this phase occurred at depths of lower-middle crust (~ 22 – 27 km). The high pressures, together with the moderately oxidized conditions determined for the rocks of this pluton (fO_2 buffered to NNO), are consistent with the presence of mEp and demonstrates the importance of this phase as an effective tool to indirectly estimate pluton emplacement depth.

Zircon saturation thermometry provided temperatures between 749 and 776 ° C (Shao et al., 2019) and are interpreted as near-liquidus temperatures. The proximity between the temperatures determined by plagioclase-amphibole thermometry (656 – 735 ° C) and the T_{Zr},

the high initial water content (~ 5 – 6 wt%), and textural observations, suggest that hornblende was an early crystallized phase in the history of crystallization.

The chemical composition of primary biotite and amphibole are consistent with crystallization from calc-alkalic I-type magma and suggest interaction between two end-member components. Our new data, integrated with those from previous studies from CSD, suggest that mEp-bearing granitoids are best explained by partial melting of mantle-like sources (e.g., ocean crust derived from mantle) along with recycled terrigenous sediment, presumably in a syn-collisional setting.

Acknowledgements

We thank the Brazilian Council of Research (Conselho Nacional de Desenvolvimento Científico e Tecnológico - CNPq, process number 404472/2016 – 8) for funding this work. BTAL thank the Brazilian agency FACEPE (process number IBPG 0780 1.07/18) for the scholarship. This is the contribution n. 302 of the NEG-LABISE, Federal University of Pernambuco.

References

Abbott Jr, R.N, Clarke, D.B., 1979. Hypothetical liquidus relationships in the subsystem Al_2O_3-FeO-MgO projected from quartz, alkali feldspar and plagioclase for a (H_2O). Can. Min. J. 17, 549–560.

Abdel-rahman, A.F.M., 1994. Nature of biotites from alkaline, calc-alkaline, and peraluminous magmas. J. Petrol. 35, 525–541. https://doi.org/10.1093/petrology/35.2.525

Ague, J.J., Brimhall, G.H., 1988a. Regional variations in bulk chemistry, mineralogy, and the compositions of mafic and accessory minerals in the batholiths of California. Bull. Geol. Soc. Am. 100, 891–911. https://doi.org/10.1130/0016-7606(1988)100<0891:RVIBCM>2.3.CO;2

Ague, J.J., Brimhall, G.H., 1988b. Magmatic arc asymmetry and distribution of anomalous plutonic belts in the batholiths of California: Effects of assimilation, crustal thickness, and depth of crystallization. Bull. Geol. Soc. Am. 100, 912–927. https://doi.org/10.1130/0016-7606(1988)100<0912:MAAADO>2.3.CO;2

Almeida, F.F.M., Leonardos, O.H., Valença, J., 1967. Review on granitic rocks of northeast South America. International Union of Geological Sciences/UNESCO, 41.

Almeida, F.F.M., Hasuy, H., Brito Neves, B.B., Fuck, R.A., 1977. Províncias estruturais brasileiras. In: Simpósio de Geologia do Nordeste, Sociedade Brasileira de Geologia, Campina Grande, 363 – 391.

Almeida, F.F.M., Hasui, Y., de Brito Neves, B.B., Fuck, R.A., 1981. Brazilian structural provinces: An

introduction. Earth Sci. Rev. 17, 1–29. https://doi.org/10.1016/0012-8252(81)90003-9

Anderson, J.L., 1996. Status of thermobarometry in granitic batholiths. Spec. Pap. Geol. Soc. Am. 315, 125–138. https://doi.org/10.1130/0-8137-2315-9.125

Anderson, J.L., Barth, A.P., Wooden, J.L., Mazdab, F., 2008. Thermometers and thermobarometers in granitic systems. Rev. Mineral. Geochemistry 69, 121–142. https://doi.org/10.2138/rmg.2008.69.4

Anderson, J.L., Smith, D.R., 1995. The effects of temperature and fO_2 on the Al-in-hornblende barometer. American Mineralogist 80(5–6), 549–559. https://doi.org/10.2138/am-1995-5-614

Babazadeh, S., Furman, T., Cottle, J.M., Raeisi, D., Lima, I., 2019. Magma chamber evolution of the Ardestan pluton, Central Iran: evidence from mineral chemistry, zircon composition and crystal size distribution. Mineral. Mag. 83, 763–780. https://doi.org/10.1180/mgm.2019.44

Barbarin, B., 2005. Mafic magmatic enclaves and mafic rocks associated with some granitoids of the central Sierra Nevada batholith, California: Nature, origin, and relations with the hosts. Lithos 80, 155–177. https://doi.org/10.1016/j.lithos.2004.05.010

Barbarin, B., Didier, J., 1991. Review of the main hypothesis proposed for the genesis and evolution of mafic microgranular enclaves. In: Didier, J., Barbarin, B. (Eds.), Enclaves and granite petrology. Developments in Petrology, 13. Elsevier, Amsterdan, 367–373.

Basak, A., Goswami, B., 2020. The physico-chemical conditions of crystallization of the Grenvillian arfvedsonite granite of Dimra Pahar, Hazaribagh, India: constraints on possible source regions. Mineral. Petrol. 114, 329–356. https://doi.org/10.1007/s00710-020-00708-w

Baxter, S., Feely, M., 2002. Magma mixing and mingling textures in granitoids: examples from the Galway Granite, Connemara, Ireland. Mineral. Petrol. 76, 63–74. https://doi.org/10.1007/s007100200032

Blevin, P.L., 2004. Redox and compositional parameters for interpreting the granitoid metallogeny of eastern Australia: Implications for gold-rich ore systems. Resour. Geol. 54, 241–252. https://doi.org/10.1111/j.1751-3928.2004.tb00205.x

Blundy, J.D., Holland, T.J.B., 1990. Calcic amphibole equilibria and a new amphibole-plagioclase geothermometer. Contrib. to Mineral. Petrol. 104, 208–224. https://doi.org/10.1007/BF00306444

Boehnke, P., Watson, E.B., Trail, D., Harrison, T.M., Schmitt, A.K., 2013. Zircon saturation re-revisited. Chem. Geol. 351, 324–334. https://doi.org/10.1016/j.chemgeo.2013.05.028

Bittar, S. M. B., 1998. Faixa Piancó-Alto Brígida: Terrenos tectono-estratigráficos sob regimes metamórficos e deformacionais contrastantes. Ph.D. thesis. Universidade de São Paulo

Brandon, A.D., Creaser, R.A., Chacko, T., 1996. Constraints on rates of granitic magma transport from epidote dissolution kinetics. Science 271, 1845–1848. https://doi.org/10.1126/science.271.5257.1845

Brasilino, R.G., Sial, A.N., Ferreira, V.P., Pimentel, M.M., 2011. Bulk rock and mineral chemistries and ascent rates of high-K calc-alkalic epidote-bearing magmas, Northeastern Brazil. Lithos 127, 441–454. https://doi.org/10.1016/j.lithos.2011.09.017

Brimhall, G.H., Crerar, D.A., 1987. Ore fluids: magmatic to supergene. In: Carmichael, I., Eugster, H. (Eds.), Thermodynamic modeling of geological materials: Minerals, fluids and melts. Reviews in Mineralogy, 17. Mineralogical Society of America, Washington DC.

Brito Neves, B.B., 1975. Regionalização geotectônica do Pre-cambriano nordestino. Ph.D. thesis. Universidade de São Paulo, pp. 198.

Brito Neves, B.B., Santos, E.J., Van Schmus, W.R., 2000. Tectonic history of the Borborema Province, northeastern Brazil. In: Cordani, U., Milani, E.J., Thomaz Filho, A., Campos, D.A. (Eds.), Tectonic Evolution of South Ametica. 31 st International Geological Congress, Rio de Janeiro, Brazil, 151–182.

Brito Neves, B.B., Van Schmus, W.R., Fetter, A., 2002. North-western Africa-North-eastern Brazil. Major tectonic links and correlation problems. J. African Earth Sci. 34, 275–278. https://doi.org/10.1016/S0899-5362(02)00025-8

Brito Neves, B.B., Dos Santos, E.J., Fuck, R.A., Santos, L.C.M.L., 2016. A preserved early Ediacaran magmatic arc at the northernmost portion of the Transversal Zone central subprovince of the Borborema Province, Northeastern South America. Brazilian J. Geol. 46, 491–508. https://doi.org/10.1590/2317-4889201620160004

Brito Neves, B.B., Van Schmus, W.R., da Costa Campos Neto, M., 2018. Piancó-alto brígida branching system of orogens (PE-PB-CE), Tectonic regionalization and geochronology. Geol. USP - Ser. Cient. 18, 149–171. https://doi.org/10.11606/issn.2316-9095.v18-142182

Caby, R., Sial, A.N., Arthaud, A. Vauchez, A., 1990. Crustal evolution and the Brasiliano orogeny in northeast Brazil. In: Lecorché, J.P., Dallmeyer, R.D. (Eds.), The West African Orogens and Circum Atlantic Correlatives. Springer-Verlag, 373–397.

Caby, R., Sial, A.N., Ferreira, V.P., 2009. High-pressure thermal aureoles around two Neoproterozoic synorogenic magmatic epidote-bearing granitoids, Northeastern Brazil. J. South Am. Earth Sci. 27, 184–196. https://doi.org/10.1016/j.jsames.2008.09.005

Cao, M.J., Qin, K.Z., Li, G.M., Evans, N.J., Jin, L.Y., 2015. In situ LA-(MC)-ICP-MS trace element and Nd isotopic compositions and genesis of polygenetic titanite from the Baogutu reduced porphyry Cu deposit, Western Junggar, NW China. Ore Geol. Rev. 65, 940–954. https://doi.org/10.1016/j.oregeorev.2014.07.014

Carmichael, I.S.E., 1991. The redox states of basic and silicic magmas: A reflection of their source regions?. Contrib. Mineral. Petrol. 106, 129–141.

Castro, A., Gerya, T., García-Casco, A., Fernández, C., Díaz-Alvarado, J., Moreno-Ventas, I., Löw, I., 2010. Melting relations of MORB-sediment mélanges in underplated mantle wedge plumes; Implications for the origin of Cordilleran-type batholiths. Journal of Petrology 51, 1267–1295. https://doi.org/10.1093/petrology/egq019

Castro, A., 2013. Tonalite-granodiorite suites as cotectic systems: A review of experimental studies with applications to granitoid petrogenesis. Earth-Science Rev. 124, 68–95. https://doi.org/10.1016/j.earscirev.2013.05.006

Castro, A., Pereira, M.F., Rodríguez, C., Fernández, C., de la Rosa, J.D., 2020. Atypical peri-Gondwanan granodiorite–tonalite magmatism from Southern Iberia. Origin of magmas and implications. Lithos 372–373. https://doi.org/10.1016/j.lithos.2020.105684

Caxito, F. A., Santos, L.C.M.L., Ganade, C.E., Bendaoud, A., Fettous, E.H., Bouyo, M.H., 2020. Toward an integrated model of geological evolution for NE Brazil-NW Africa: The Borborema Province and its connections to the Trans-Saharan (Benino-Nigerian and Tuareg shields) and

Central African orogens. Brazilian Journal of Geology 50. https://doi.org/10.1590/2317-4889202020190122

Caxito, F.A., Basto, C.F., de Lira Santos, L.C.M., Dantas, E.L., de Medeiros, V.C., Dias, T.G., Barrote, V., Hagemann, S., Alkmim, A.R., Lana, C., 2021. Neoproterozoic magmatic arc volcanism in the Borborema Province, NE Brazil: possible flare-ups and lulls and implications for western Gondwana assembly. Gondwana Research. https://doi.org/10.1016/j.gr.2020.11.015

Chappell, B.W., White, A.J.R., 1974. Two contrasting granite types. Pac. Geol. 8, 173–174.

Chen, J., Wei, J., Fu, L., Li, H., Zhou, H., Zhao, X., Zhan, X., Tan, J., 2017. Multiple sources of the Early Mesozoic Gouli batholith, Eastern Kunlun Orogenic Belt, northern Tibetan Plateau: Linking continental crustal growth with oceanic subduction. Lithos 292–293, 161–178. https://doi.org/10.1016/j.lithos.2017.09.006

Collins, W.J., Huang, H.Q., Jiang, X., 2016. Water-fluxed crustal melting produces Cordilleran batholiths. Geology 44, 143–146. https://doi.org/10.1130/G37398.1

Czamanske, G.K., Wones, D.R., 1973. Oxidation during magmatic differentiation, Finnmarka complex, Oslo area, Norway: Part 2, the mafic silicates1. J. Petrol. 14, 349–380. https://doi.org/10.1093/petrology/14.3.349

Dall'Agnol, R., Scaillet, B., Pichavant, M., 1999. An experimental study of a Lower Proterozoic A-type granite from the Eastern Amazonian Craton, Brazil. J. Petrol. 40, 1673–1698. https://doi.org/10.1093/petroj/40.11.1673

Davies, J.H., von Blanckenburg, F., 1995. Slab breakoff: A model of lithosphere detachment and its test in the magmatism and deformation of collisional orogens. Earth and Planetary Science Letters 129, 85–102.

Deer, W.A., Howie, R.A., Zussman, J., 1992. An Introduction to the Rock Forming Minerals. Longman 2nd ed., London, pp.696.

Deer, W.A., Howie, R.A., Zussman, J., 2013. An Introduction to the Rock-forming Minerals, third ed. The Mineralogical Society 3rd ed., London, 248–251.

Didier, J., 1973. Granite and their Enclaves. Elsevier, London, 393.

Didier, D., Barbarin, B., 1991. Enclaves and Granite Petrology, Developments in Petrology. Elsevier Science Publications, Amsterdam, pp.1–625.

Errázuriz-Henao, C., Gómez-Tuena, A., Duque-Trujillo, J., Weber, M., 2019. The role of subducted sediments in the formation of intermediate mantle-derived magmas from the Northern Colombian Andes. Lithos 336–337, 151–168. https://doi.org/10.1016/j.lithos.2019.04.007

Evans, B.W., Vance, J.A., 1987. Epidote phenocrysts in dacitic dikes, Boulder County, Colorado. Contrib. to Mineral. Petrol. 96, 178–185. https://doi.org/10.1007/BF00375231

Ferreira, V.P., Valley, J.W., Sial, A.N., Spicuzza, M.J., 2003. Oxygen isotope compositions and magmatic epidote from two contrasting metaluminous granitoids, NE Brazil. Contrib. to Mineral. Petrol. 145, 205–216. https://doi.org/10.1007/s00410-003-0443-4

Ferreira, V.P., Sial, A.N., Pimentel, M.M., Moura, C.A.V., 2004. Intermediate to acidic magmatism and crustal evolution in the Transversal Zone, northeastern Brazil. In: Mantesso-Neto, V., Bartorelli, A., Carneiro, C.D.R., Brito Neves, B.B. (Eds.), Geologia do Continente Sul-Americano: Evolução

da Obra de Fernando Flávio Marques de Almeida. Beca Produções Cultura Ltda, São Paulo, Brasil, 189–201.

Ferreira, V.P., Sial, A.N., Pimentel, M.M., Armstrong, R., Spicuzza, M.J., Guimarães, I.P., da Silva Filho, A.F., 2011. Contrasting sources and P-T crystallization conditions of epidote-bearing granitic rocks, northeastern Brazil: O, Sr, and Nd isotopes. Lithos 121, 189–201. https://doi.org/10.1016/j.lithos.2010.11.002

Foster, M.D., 1960. Interpretation of the composition of trioctahedral micas. USGS Prof. Pap. 354, 11–48.

Fu, D., Kusky, T., Wilde, S.A., Polat, A., Huang, B., Zhou, Z., 2019. Early Paleozoic collision-related magmatism in the eastern North Qilian orogen, northern Tibet: A linkage between accretionary and collisional orogenesis. Bulletin of the Geological Society of America 131, 1031–1056. https://doi.org/10.1130/B35009.1

Gervasoni, F., Klemme, S., Rocha-Júnior, E.R.V., Berndt, J., 2016. Zircon saturation in silicate melts: a new and improved model for aluminous and alkaline melts. Contrib. to Mineral. Petrol. 171, 1–12. https://doi.org/10.1007/s00410-016-1227-y

Guimarães, I.P., Da Silva Filho, A.F., Almeida, C.N., Van Schmus, W.R., Araújo, J.M.M., Melo, S.C., Melo, E.B., 2004. Brasiliano (Pan-African) granitic magmatism in the Pajeú- Paraíba belt, Northeast Brazil: An isotopic and geochronological approach. Precambrian Res. 135, 23–53. https://doi.org/10.1016/j.precamres.2004.07.004

Guimarães, I.P., Silva Filho, A.F., Almeida, C.N., Macambira, M.B., Armstrong, R., 2011. U-Pb SHRIMP data constraints on calc-alkaline granitoids with 1.3-1.6 Ga Nd TDM model ages from the central domain of the Borborema province, NE Brazil. Journal of South American Earth Sciences 31, 383–396. https://doi.org/10.1016/j.jsames.2011.03.001

Hammarstrom, J.M., Zen, E., 1986. Aluminum in hornblende: an empirical igneous geobarometer. Am. Mineral. 71, 1297–1313.

Hanchar, J.M., Watson, E.B., 2003. Zircon saturation thermometry. Rev. Mineral. Geochem. 53 (1), 89. https://doi.org/10.2113/0530089

Harrison, T.M., Watson, E.B., Aikman, A.B., 2007. Temperature spectra of zircon crystallization in plutonic rocks. Geology 35, 635–638. https://doi.org/10.1130/G23505A.1

Hibbard, M.J, 1991. Zircon saturation thermometry. Textural anatomy of twelve magma-mixed granitoid systems. In: Didier, J., Barbarin, B. (Eds.), Enclaves and Granite Petrology. Elsevier, Amsterdam, pp. 431–444.

Holland, T., Blundy, J., 1994. Non-ideal interactions in calcic amphiboles and their bearing on amphibole-plagioclase thermometry. Contrib. to Mineral. Petrol. 116, 433–447. https://doi.org/10.1007/BF00310910

Hollister, L.S., Grissom, G.C., Peters, E.K., Stowell, H.H., Sisson, V.B., 1987. Confirmation of the empirical correlation of Al in hornblende with pressure of solidification of calc-alkaline plutons. Am. Mineral. 72, 231–239.

Holtz, F., Johannes, W., Tamic, N., Behrens, H., 2001. Maximum and minimum water contents of granitic melts generated in the crust: A reevaluation and implications. Lithos 56, 1–14. https://doi.org/10.1016/S0024-4937(00)00056-6

Huang, H., Niu, Y., Nowell, G., Zhao, Z., Yu, X., Zhu, D.C., Mo, X., Ding, S., 2014. Geochemical constraints on the petrogenesis of granitoids in the East Kunlun Orogenic belt, northern Tibetan Plateau: Implications for continental crust growth through syn-collisional felsic magmatism. Chemical Geology 370, 1–18. https://doi.org/10.1016/j.chemgeo.2014.01.010

Ishihara, S., 1977. The magnetite-series and ilmenite-series granitic rocks. Min. Geol. 27, 293–305. https://doi.org/10.11456/shigenchishitsu1951.27.293

Jardim de Sá, E.F., 1994. A Faixa Seridó (Província Borborema, NE do Brasil) e o seu significado geodinâmico na cadeia Brasiliana/Pan-Africana, Unpublished Ph.D. Thesis, Univ. Brasilia, p. 803

Jiang, J., Zhu, Y., 2018. Characterization of anhydrous to hydrous paragenetic sequence from pyroxene-bearing and pyroxene-absent variants of the late Carboniferous Baobei pluton in west Junggar of China. Gondwana Res. 63, 129–151. https://doi.org/10.1016/j.gr.2018.05.010

Johnson, M.C., Rutherford, M.J., 1989. Experimental calibration of the aluminum-in-hornblende geobarometer with application of Long Valley caldera (California) volcanic rocks. Geology 17, 837–841. https://doi.org/10.1130/0091-7613(1989)017<0837:ECOTAI>2.3.CO;2

Keyes, C.R., 1892. Epidote as a primary component of eruptive rocks. Geol. Soc. Am. Bull. 4, 305–312.

Kemp, A.I.S., Hawkesworth, C.J., Foster, G.L., Paterson, B.A., Woodhead, J.D., Hergt, J.M., Gray, C.M., Whitehouse, M.J., 2007. Magmatic and crustal differentiation history of granitic rocks from Hf-O isotopes in zircon. Science 315, 980–983. https://doi.org/10.1126/science.1136154

Kocak, K., Zedef, V., Kansun, G., 2011. Magma mixing/mingling in the Eocene Horoz (Nigde) granitoids, Central southern Turkey: Evidence from mafic microgranular enclaves. Mineral. Petrol. 103, 149–167. https://doi.org/10.1007/s00710-011-0165-7

Kong, J., Niu, Y., Hu, Y., Zhang, Y., Shao, F., 2020. Petrogenesis of the Triassic granitoids from the East Kunlun Orogenic Belt, NW China: Implications for continental crust growth from syn-collisional to post-collisional setting. Lithos 364–365. https://doi.org/10.1016/j.lithos.2020.105513

Kowallis, B.J., Christiansen, E.H., Griffen, D.T., 1997. Compositional variations in titanite. Geol. Soc. Am. Abst. with Prog. 29 (6), 402.

Kozuch, M., 2003. Isotopic and trace element geochemistry of early Neoproterozoic gneissic and metavolcanic rocks in the Cariris Velhos orogen of the Borborema Province, Brazil, and their bearing on tectonic setting. Ph.D. thesis. University of Kansas.

Leake, B.E., Wooley, A.R., Arps, C.E.S., Birch, W.D., Gilbert, M.C., Grice, J.D., Hawthorne, C. & Kato, A. 1997. Nomenclature of amphiboles: Report of the subcommittee on amphiboles of the International Mineralogical Association, Commission on new minerals and mineral names. American Mineralogist 82, 1019–1037.

Le Maitre, R.W., Streckeisen, A., Zanettin, B., Le Bas, M.J., Bonin, B. and Bateman, P., 2002, Igneous Rocks: A Classification and Glossary of Terms. Cambridge University Press, 1–236.

Li, X., Zhang, C., Behrens, H., Holtz, F., 2020. Calculating biotite formula from electron microprobe analysis data using a machine learning method based on principal components regression. Lithos 356–357. https://doi.org/10.1016/j.lithos.2020.105371

Lima, B.T.A., Ferreira, V.P., 2019. Granitos metaluminosos com epidoto magmático: O exemplo do

Pluton Carmo, no Terreno Cachoeirinha-Salgueiro, Domínio da Zona Transversal, Província Borborema, nordeste do Brasil. In: Abstracts, XVII Congresso Brasileiro de Geoquímica, Fortaleza, Brazil, pp. 153.

Locock, A.J., 2014. An Excel spreadsheet to classify chemical analyses of amphiboles following the IMA 2012 recommendations. Computers and Geosciences 62, 1–11. https://doi.org/10.1016/j.cageo.2013.09.011

Marulanda, C.O., 2013. Estudo da Proveniência em sequências supracrustais neoproterozoicas da Zona Transversal, Província Borborema. Dissertação de mestrado. Universidade de São Paulo. https://doi.org/10.11606/D.44.2013.tde-03062015-092058

Massawe, R., Lentz, D.R., 2020. Evaluation of crystallization and emplacement conditions of the McKenzie Gulch porphyry dykes using chemistry of rock-forming minerals: Implications for mineralization potential. Ore Geol. Rev. 116. https://doi.org/10.1016/j.oregeorev.2019.103256

McLeod, C.L., Davidson, J.P., Nowell, G.M., de Silva, S.L., 2012. Disequilibrium melting during crustal anatexis and implications for modeling open magmatic systems. Geology 40, 435–438. https://doi.org/10.1130/G33000.1

Medeiros, V.C., 2004. Evolução geodinâmica e condicionamento estrutural dos terrenos Piancó-Alto Brígida e Alto Pajeú, Domínio da Zona Transversal, NE do Brasil. Tese de doutorado. Universidade Federal do Rio Grande do Norte.

Miller, C.F., McDowell, S.M., Mapes, R.W., 2003. Hot and cold granites: Implications of zircon saturation temperatures and preservation of inheritance. Geology 31, 529–532. https://doi.org/10.1130/0091-7613(2003)031<0529:HACGIO>2.0.CO;2

Mo, X., Niu, Y., Dong, G., Zhao, Z., Hou, Z., Zhou, S., Ke, S., 2008. Contribution of syncollisional felsic magmatism to continental crust growth: A case study of the Paleogene Linzizong volcanic Succession in southern Tibet. Chemical Geology 250, 49–67. https://doi.org/10.1016/j.chemgeo.2008.02.003

Mutch, E.J.F., Blundy, J.D., Tattitch, B.C., Cooper, F.J., Brooker, R.A., 2016. An experimental study of amphibole stability in low-pressure granitic magmas and a revised Al-in-hornblende geobarometer. Contrib. to Mineral. Petrol. 171, 1–27. https://doi.org/10.1007/s00410-016-1298-9

Nachit, H., Razafimahefa, N., Stussi, J.M., Carron, J.P., 1985. Composition chimique des biotites et typologie magmatique des granitos. Comptes Rendus de l'Académie des sciences Paris 301, 810–818.

Naney, M.T., 1983. Phase equilibria of rock-forming ferromagnesian silicates in granitic systems. American Journal of Science 283, 993–1033.

Neves, S.P., Vauchez, A., Feraud, G., 2000. Tectono-thermal evolution, magma emplacement, and shear zone development in the Caruaru area (Borborema Province, NE Brazil). Precambrian Res. 99, 1–32. https://doi.org/10.1016/S0301-9268(99)00026-1

Neves, S.P., 2003. Proterozoic history of the Borborema province (NE Brazil): Correlations with neighboring cratons and Pan-African belts and implications for the evolution of western Gondwana. Tectonics 22. https://doi.org/10.1029/2001TC001352

Neves, S.P., 2015. Constraints from zircon geochronology on the tectonic evolution of the Borborema Province (NE Brazil): Widespread intracontinental Neoproterozoic reworking of a

Paleoproterozoic accretionary orogen. J. South Am. Earth Sci. 58, 150–164. https://doi.org/10.1016/j.jsames.2014.08.004

Neves, S.P., 2018. Comment on "A preserved early Ediacaran magmatic arc at the northernmost part of the transversal zone central domain of the Borborema Province, Northeast of South America", by B. B. de Brito Neves et al. (2016). Brazilian J. Geol. 48, 623–630. https://doi.org/10.1590/2317-4889201820180049

Niu, Y., Zhao, Z., Zhu, D.C., Mo, X., 2013. Continental collision zones are primary sites for net continental crust growth - A testable hypothesis. Earth-Science Reviews. https://doi.org/10.1016/j.earscirev.2013.09.004

Pandit, D., Panigrahi, M.K., Moriyama, T., 2014. Constrains from magmatic and hydrothermal epidotes on crystallization of granitic magma and sulfide mineralization in Paleoproterozoic Malanjkhand Granitoid, Central India. Chemie der Erde 74, 715–733. https://doi.org/10.1016/j.chemer.2014.04.008

Perugini, D., Poli, G., Christofides, G., Eleftheriadis, G., 2003. Magma mixing in the Sithonia Plutonic Complex, Greece: Evidence from mafic microgranular enclaves. Mineralogy and Petrology 78, 173–200. https://doi.org/10.1007/s00710-002-0225-0

Poli, S., Schmidt, M.W., 1992. Comment on "'Calcic amphibole equilibria and a new amphibole-plagioclase geothermometer'". Contrib. to Mineral. and Petrol. 111, 273–82.

Putirka, K.D., 2005. Igneous thermometers and barometers based on plagioclase + liquid equilibria: Tests of some existing models and new calibrations. Am. Mineral. 90, 336–346. https://doi.org/10.2138/am.2005.1449

Ramos, F.C., Reid, M.R., 2005. Distinguishing melting of heterogeneous mantle sources from crustal contamination: Insights from Sr isotopes at the Phenocryst Scale, Pisgah Crater, California. Journal of Petrology 46, 999–1012. https://doi.org/10.1093/petrology/egi008

Ridolfi, F., Renzulli, A., Puerini, M., 2010. Stability and chemical equilibrium of amphibole in calc-alkaline magmas: An overview, new thermobarometric formulations and application to subduction-related volcanoes. Contrib. to Mineral. Petrol. 160, 45–66. https://doi.org/10.1007/s00410-009-0465-7

Santos, E.J., Medeiros, V.C., 1999. Constraints From Granitic Plutonism on Proterozoic Crustal Growth of the Transverse Zone, Borborema Province, Ne Brazil. Rev. Bras. Geociências 29, 73–84. https://doi.org/10.25249/0375-7536.1999297384

Scaillet, B., Clemente, B., Evans, B.W., Pichavant, M., 1998. Redox control of sulfur degassing in silicic magmas. Journal of Geophysical Research Solid Earth 103, 23937–23949.

Schmidt, M.W., 1992. Amphibole composition in tonalite as a function of pressure: An experimental calibration of the AI-in-hornblende barometer. Contrib. to Mineral. Petrol. 110, 304–310.

Schmidt, M.W., Poli, S., 2004. Magmatic epidote. Reviews in Mineralogy and Geochemistry 56, 399–430. https://doi.org/10.2138/gsrmg.56.1.399

Schmidt, M.W., Thompson, A.B., 1996. Epidote in calc-alkaline magmas: An experimental study of stability, phase relationships, and the role of epidote in magmatic evolution. Am. Mineral. 81, 462–474. https://doi.org/10.2138/am-1996-3-420

Sen, G., Stern, R.J., 2021. Subduction Zone Magmas, in: Encyclopedia of Geology. Elsevier, pp. 33–51. https://doi.org/10.1016/b978-0-08-102908-4.00086-2

Shao, T., Xia, Y., Ding, X., Cai, Y., Song, M., 2019. Zircon saturation model in silicate melts: a review and update. Acta Geochim. 39, 387–403. https://doi.org/10.1007/s11631-019-00384-4

Sial, A.N., 1986. Granite-types in northeast Brazil: current knowledge. Rev. Bras. Geociencias 16, 54–72. https://doi.org/10.25249/0375-7536.19865472

Sial, A.N., 1990. Epidote-Bearing Calc-Alkalic Granitoids in Northeast Brazil. Rev. Bras. Geociências 20, 88–100. https://doi.org/10.25249/0375-7536.199088100

Sial, A.N., 1993. Contrasting metaluminous magmatic epidote-bearing granitic suites from two Precambrian Foldbelts in Northeast Brazil. Proc. Work. MAGMA 141–162.

Sial, A.N., Ferreira, V.P., Fallick, A.E., Jerônimo, M., 1998. Amphibole-rich clots in calc-alkalic granitoids in the Borborema province, northeastern Brazil. J. South Am. Earth Sci. 11, 457–471. https://doi.org/10.1016/S0895-9811(98)00034-0

Sial, A.N., Toselli, A.J., Saavedra, J., Parada, M.A., Ferreira, V.P., 1999. Emplacement, petrological and magnetic susceptibility characteristics of diverse magmatic epidote-bearing granitoid rocks in Brazil, Argentina and Chile. Lithos 46, 367–392. https://doi.org/10.1016/S0024-4937(98)00074-7

Sial, A.N., Vasconcelos, P.M., Ferreira, V.P., Pessoa, R.R., Brasilino, R.G., Morais Neto, J.M., 2008. Geochronological and mineralogical constraints on depth of emplacement and ascencion rates of epidote-bearing magmas from northeastern Brazil. Lithos 105, 225–238. https://doi.org/10.1016/j.lithos.2008.04.002

Sial, A.N., Ferreira, V.P., 2016. Magma associations in Ediacaran granitoids of the Cachoeirinha–Salgueiro and Alto Pajeú terranes, northeastern Brazil: Forty years of studies. J. South Am. Earth Sci. 68, 113–133. https://doi.org/10.1016/j.jsames.2015.10.005

Siégel, C., Bryan, S.E., Allen, C.M., Gust, D.A., 2018. Use and abuse of zircon-based thermometers: A critical review and a recommended approach to identify antecrystic zircons. Earth-Science Rev. 176, 87–116. https://doi.org/10.1016/j.earscirev.2017.08.011

Silva, T.R., Ferreira, V.P., Lima, M.M.C., Sial, A.N., 2016. Two stage mantle-derived granitic rocks and the onset of the Brasiliano orogeny: Evidence from Sr, Nd, and O isotopes. Lithos 264, 189–200. https://doi.org/10.1016/j.lithos.2016.08.030

Silva, T.R., Ferreira, V.P., de Lima, M.M.C., Sial, A.N., 2020. Rapid magma ascent and formation of the Águas Belas-Canindé granitic batholith, NE Brazil: Evidence of epidote dissolution and thermobarometry. Brazilian Journal of Geology 50. https://doi.org/10.1590/2317-4889202020190110

Siqueira, R., Sial, A., Ferreira, V., 2018. Granitos com epidoto magmático e clinopiroxênio: plútons Tamboril e Olho d'Água, Terreno Cachoeirinha−Salgueiro, Nordeste do Brasil. Geochim. Bras. 32, 20–39. https://doi.org/10.21715/gb2358-2812.2018321020

Streckeisen, A., 1976. To each plutonic rock its proper name. Earth Sci Rev 12, 1–33.

Thomas,W.M., Ernst,W.G., 1990. The aluminium content of hornblende in calc-alkaline granitic rocks: a mineralogic barometer calibrated experimentally to 12 kbar. In: Spencer, R.J., Shou, I-Ming (Eds.), Fluid Mineral Interactions: A Tribute to H.P. Eugster, vol. 2. Geochemical Society, pp. 59–

63. special publication.

Tulloch, A.,1979. Secondary Ca Al silicates as low-grade alteration products of granitoid biotite. Contributions to Mineralogy and Petrology 69, 105–117.

Usma, C.D., Sial, A.N., Ferreira, V.P., Gaucher, C., Frei, R., 2021. Ediacaran banded iron formations and carbonates of the Cachoeirinha Group of NE Brazil: Paleoenvironment and paleoredox conditions. Journal of South American Earth Sciences 109. https://doi.org/10.1016/j.jsames.2021.103282

Van Schmus, W.R., de Brito Neves, B.B., Hackspacher, P., Babinski, M., 1995. U Pb and Sm Nd geochronologic studies of the eastern Borborema Province, Northeastern Brazil: initial conclusions. J. South Am. Earth Sci. 8, 267–288. https://doi.org/10.1016/0895-9811(95)00013-6

Van Schmus, W.R., Kozuch, M., de Brito Neves, B.B., 2011. Precambrian history of the Zona Transversal of the Borborema Province, NE Brazil: Insights from Sm-Nd and U-Pb geochronology. J. South Am. Earth Sci. 31, 227–252. https://doi.org/10.1016/j.jsames.2011.02.010

Vauchez, A., Neves, S., Caby, R., Corsini, M., Egydio-Silva, M., Arthaud, M., Amaro, V., 1995. The Borborema shear zone system, NE Brazil. J. South Am. Earth Sci. 8, 247–266. https://doi.org/10.1016/0895-9811(95)00012-5

Vernon, R.H., 1984. Microgranitoid enclaves in granites - Globules of hybrid magma quenched in a plutonic environment. Nature 309, 438–439. https://doi.org/10.1038/309438a0

Villaseca, C., Ruiz-Martínez, V.C., Pérez-Soba, C., 2017. Magnetic susceptibility of Variscan granite-types of the Spanish central system and the redox state of magma. Geol. Acta 15, 379–394. https://doi.org/10.1344/GeologicaActa2017.15.4.8

Vyhnal, C.R., Mcsween, H.Y., Speer, J.A., 1991. Aluminum Hornblende Thermobarometry and Magmatic Epidote Stability. Am. Mineral. 76, 176–188.

Watson, E.B., Harrison, T.M., 1983. Zircon saturation revisited: temperature and composition effects in a variety of crustal magma types. Earth Planet. Sci. Lett. 64, 295–304. https://doi.org/10.1016/0012-821X(83)90211-X

Whitney, D.L., Evans, B.W., 2010. Abreviations for names of rock-forming minerals. Am. Mineral. 95, 185–187. https://doi.org/10.2138/am.2010.3371

Wyllie, P.J., Huang, W.L., Stern, C.R., Maaloe, S., 1976. Granitic magmas: possible and impossible sources, water contents, and crystallization sequences. Canadian Journal of Earth Sciences 13, 1007–1019.

Wones, D.R., 1989. Significance of the assemblage titanite + magnetite + quartz in granitic rocks. Am. Mineral. 74, 744–749.

Wones, D.R., Eugster, H.P., 1965. Stability of biotite: experiment, theory, and applications. Am. Mineral. 50, 1228–1272.

Xie, Y.W., Zhang, Y.Q., 1990. Peculiarities and genetic significance of hornblende from granite in the Hengduanshan region. Acta Mineral 10 (1), 35–45.

Yavuz, F., 2003. Evaluating micas in petrologic and metallogenic aspect: I-definitions and structure of the computer program MICA+. Computers and Geosciences 29, 1203–1213.

https://doi.org/10.1016/S0098-3004(03)00142-0

Yousefi, F., Sadeghian, M., Wanhainen, C., Ghasemi, H., Lambrini, P., Bark, G., Rezaei-Kahkhaei, M., Koroneos, A., 2017. Mineral chemistry and P-T conditions of the adakitic rocks from Torud–Ahmad Abad magmatic belt, S-SE Shahrood, NE Iran. J. Geochemical Explor. 182, 110–120. https://doi.org/10.1016/j.gexplo.2017.09.006

Zen, E.A., Hammarstrom, J.M., 1984. Magmatic epidote and its petrologic significance. Geology 12, 515–518. https://doi.org/10.1130/0091-7613(1984)12<515:MEAIPS>2.0.CO;2

Zhang, W., Lentz, D.R., Thorne, K.G., McFarlane, C., 2016. Geochemical characteristics of biotite from felsic intrusive rocks around the Sisson Brook W-Mo-Cu deposit, west-central New Brunswick: An indicator of halogen and oxygen fugacity of magmatic systems. Ore Geol. Rev. 77, 82–96. https://doi.org/10.1016/j.oregeorev.2016.02.004

Zhou Z.X., 1986. The origin of intrusive mass in Fengshandong, Hubei province. Acta Petrologica Sinica 2, 59–70.

Zhu, R.Z., Lai, S.C., Qin, J.F., Zhao, S.W., Santosh, M., 2019. Petrogenesis of high-K calc-alkaline granodiorite and its enclaves from the SE Lhasa block, Tibet (SW China): Implications for recycled subducted sediments. Bulletin of the Geological Society of America 131, 1224–1238. https://doi.org/10.1130/B1841.1

4 ARTIGO 2 – Petrogenesis of the Late Neoproterozoic Carmo stock, northeastern Brazil: Implications for partial melting of oceanic crust and sediments in a syn-collisional setting

Bianca T.A. Lima*, Valderez P. Ferreira, Diego H. Ardila, Alcides N. Sial and Charles H.F.S. Neves

NEG–LABISE, Department of Geology, Federal Univ. of Pernambuco, Recife, PE, 50740-530, Brazil

Abstract

Granitic magmatism is undoubtedly the main geological feature of the Brasiliano Orogeny in the Borborema Province, northeastern Brazil. However, the petrogenesis and tectonic setting of the oldest magmatic pulse (640 – 620 Ma; Conceição-type granites) in the Central Subprovince is still hotly debated. The Carmo stock consists of calc-alkalic magmatic epidote-bearing Conceição-type porphyritic granodiorite and monzogranites that carry abundant mafic microgranular enclaves (MMEs). LA-ICP-MS zircon U–Pb data indicate crystallization around 615 Ma for these granitoids. Granitoids and MMEs exhibit similar chemical characteristics, both of which show high-K calc-alkalic, metaluminous and magnesian compositions. All studied rocks are enriched in large-ion lithophile elements (LILE) and light rare-earth elements (LREE), and depleted in high-field-strength elements (HFSE) and heavy rare-earth elements (HREE). Host granitoids are characterized by high initial $^{87}Sr/^{86}Sr$ ratios (0.707863 – 0.709677), weakly negative $\varepsilon Nd(t)$ values (-2.1 to -3.1), and T_{DM} model ages of 1.31 – 1.36 Ga. These geochemical and isotopic signatures, together with the low Ba/Th and Sm/La ratios and high La/Sm and Th/La ratios, suggest that granodiorites and monzogranites were generated from the partial melting of altered oceanic crust and subducted sediments. The MMEs have Sr-Nd isotopic compositions almost indistinguishable from their host granitoids, with initial $^{87}Sr/^{86}Sr$ ratios of 0.708895, $\varepsilon Nd(t)$ values of -2.8 and T_{DM} model ages of 1.40 Ga. The similarity in isotopic compositions and the petrographic evidence indicate that magma mixing and mingling played an important role in the formation of MMEs. Based on the new geochemical and isotopic data, together with regional geological features, we infer that the Carmo stock rocks, as well as Conceição-type granites, were most likely formed in a syn-collisional tectonic setting following the early break-off of a relatively weak oceanic slab.

Keywords: Syn-collisional magmatism, Slab melting, Sediment contribution, Mafic microgranular enclave, I-type granitoids, Borborema Province

__Corresponding author__: biancathalitalima@gmail.com

1. Introduction

The oceanic crust is a fundamental piece in the typical geodynamic processes that drive plate tectonics. It is constantly formed at mid-ocean ridges by partial melting of the mantle and is recycled in an altered form into the deep mantle at subduction zones (White and Klein, 2014). Partial melting of oceanic crust can occur at active continental margins and is a mechanism often invoked to explain the geochemical features (e.g., high Sr/Y and La/Yb ratios) shown by adakites (Defant and Drummond, 1990; Martin, 1999). This process is restricted to hot subduction systems, where the subducted lithosphere is young, or where the slab subduction has recently initiated (Peacock et al., 1994; Martin, 1999), both resulting in geothermal gradients high enough to partially melt the oceanic slab. However, in modern subduction zones, due to the lower thermal gradient, oceanic crust dehydrates before reaching the temperatures required to melt (Syracuse et al., 2010; Hernández-Uribe et al., 2020), so the magmatism generated in these environments is most likely derived from the melting of the mantle wedge via lowering the peridotite solidus. Subducted sediments can also participate in the melting processes and their role in influencing the geochemical and isotopic variations of subduction-related magmas has been widely debated through experimental and natural studies (e.g., Patiño Douce, 1995, 1999; McCarthy and Patiño Douce, 1997; Tatsumi, 2001; Hermann and Spandler, 2008; Castro et al., 2010; Behn et al., 2011; Zhu et al., 2019; Errázuriz-Henao et al., 2019; Zang et al., 2020; Wang et al., 2021).

There is increasing evidence indicating that partial melting of subducted oceanic crust and sediments can also take place during continental collision (Mo et al., 2008; Niu et al., 2013; Huang et al., 2014; Zhang et al., 2016; Shao et al., 2017; Chen et al., 2017, 2018; Fu et al., 2019; Kong et al., 2020). In this scenario, when the collision begins, altered oceanic crust along with terrigenous sediments are slowly underthrust beneath/against the overlying lithosphere. When the thermal equilibrium with previously heated continental arc lithosphere is attained, the hydrated oceanic crust and sediments evolve along a high T/P path capable of reaching the hydrous basaltic/granitic solidus (Mo et al., 2008; Niu et al., 2013).

Voluminous granitic magmatism is the most significant tectonic expression of the Brasiliano/Pan-African Orogeny in the Borborema Province (Fig. 1A) (Almeida et al., 1981; Brito Neves et al., 2000; Van Schmus et al., 2011). In the last decades, systematic geochronological studies in the Central Subprovince have allowed to establish that this magmatism occurred in different time intervals, at the successive stages of the orogeny evolution (Ferreira et al., 2004; Guimarães et al., 2004; Sial and Ferreira, 2016; Caxito et al., 2020; Neves et al., 2020). The oldest pulse (640 – 620 Ma) in this region is represented by I-type granitoids with geochemical features that resemble the magmatic rocks generated under subduction environments. Indeed, some workers have interpreted these granitic and granodioritic plutons as developed within a continental magmatic arc setting (Brito Neves et al., 2016; Santos et al., 2019, 2020; Caxito et al., 2021). Such a long-lived subduction episode, however, remains controversial because of the lack of robust geological evidence to support its existence (Neves, 2018). The latter author suggested that these calc-alkaline plutons more likely represent syn-collisional magmatism. The tectonic setting and petrogenesis of these granitoids is, therefore, in question and open for debate. In this paper, we conducted a detailed study of the Carmo stock using field observations and petrographic, whole-rock geochemical, isotopic (Rb-Sr and Sm-Nd) and geochronological (zircon U-Pb) data, to constrain the petrogenesis of these granitoids and to assess the role of partial melting of the subducted oceanic crust and sediments. From the new data and those available in the literature, we evaluate the possible tectonic scenarios involved in the generation of this magmatism.

Figure 1. (A) Simplified geological map of the Borborema Province showing the main domains and distribution of Brasiliano granitic plutons (modified from Medeiros, 2004); (B) Geological sketch-map of some domains of the Central Subprovince: SJCD = São José do Caiano Domain; CSD = Cachoeirinha-Salgueiro Domain; RGD = Riacho Gravatá subdomain; APD = Alto Pajeú Domain; AMD = Alto Moxotó Domain, and their main magma association (modified from Sial and Ferreira, 2016). Also shown are U-Pb ages of some calc-alkaline granitoids from the oldest magmatic pulse (640 – 620 Ma) in the Central Subprovince. The studied area is highlighted by the black rectangle; (C) Detailed geological map showing facies distribution of the Carmo stock and U-Pb dating sample locations.

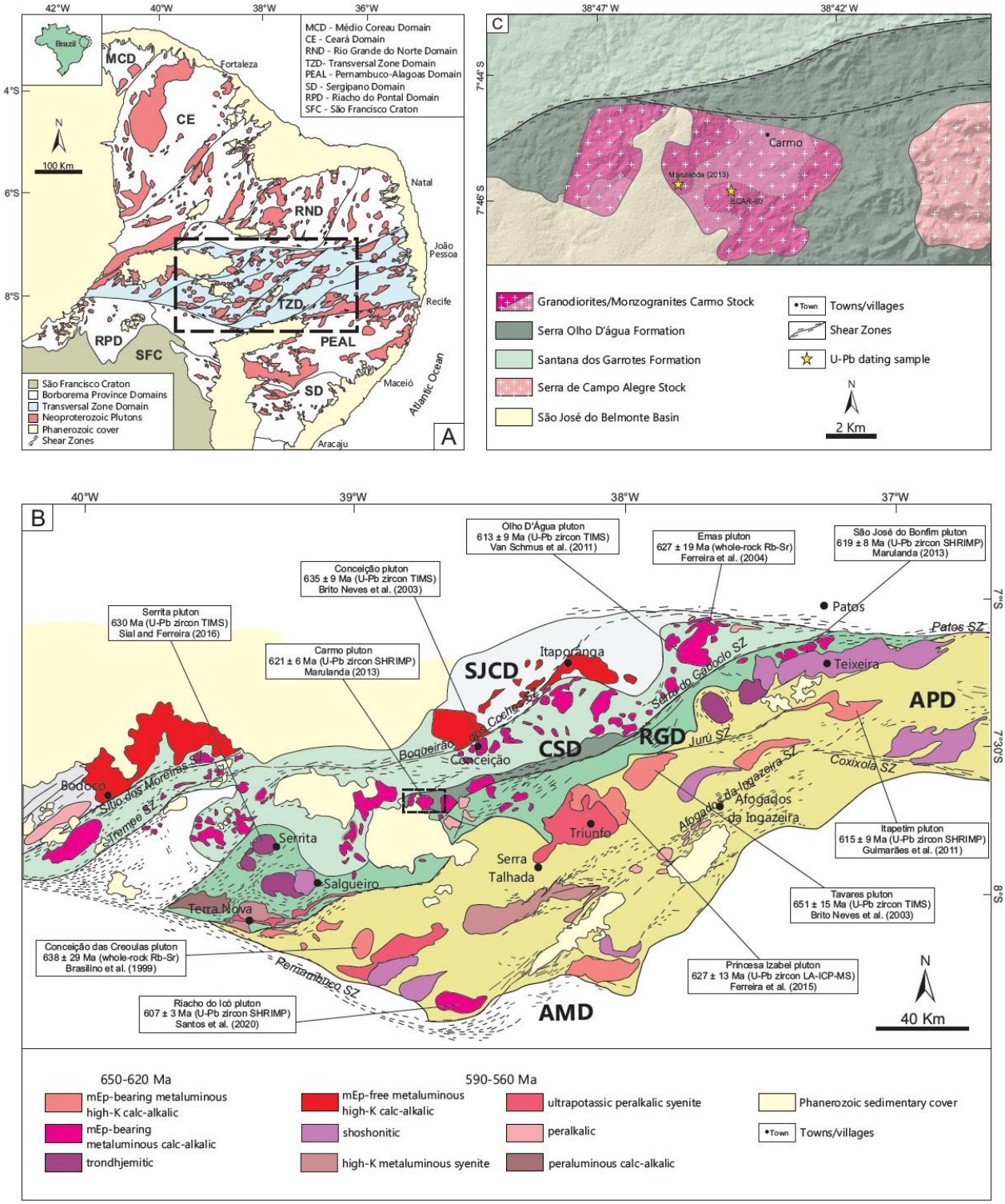

2. Geological background and petrography

The Borborema Province located in the northeast Brazil (Fig. 1A), involves a system of orogens characterized by several deformational, metamorphic and magmatic events, whose final structural framework was developed in the Brasiliano/Pan-African Orogeny (Neves, 2015;

Caxito et al., 2020, and references therein). Large E-W trending dextral shear zones, resulting from the transpressive tectonics developed during the late stages of Brasiliano Orogeny, are currently the basis for dividing the Borborema Province into the Northern, Central and Southern subprovinces (Vauchez et al. 1995; Brito Neves et al., 2000; Neves, 2003; Van Schmus et al., 2011). The Central Subprovince (also called Transversal Zone; Ebert, 1970; Jardim de Sá, 1994) is composed of Paleoproterozoic gneissic basement rocks, Early Neoproterozoic supracrustal sequences and rare Archean nuclei, that were later reworked and intruded by numerous plutons and batholiths during the Late Neoproterozoic (Van Schmus et al., 2011; Neves, 2015). A complex system of NE-SW-striking sinistral shear zones, connected to the main dextral shear zones, cut the basement of the Central Subprovince subdividing it into the following domains or terranes: São José do Caiano, Cachoeirinha-Salgueiro (Piancó-Alto Brígida belt in the sense of Brito Neves, 1975), Alto Pajeú, Alto Moxotó and Rio Capibaribe (Fig. 1B) (Santos et al., 2010; Van Schmus et al., 2011).

The Serra do Caboclo and Boqueirão dos Cochos sigmoidal shear zones separate the Cachoeirinha-Salgueiro Domain (CSD) from the Tonian orthogneisses and supracrustal rocks of the Alto Pajeú Domain (APD) to the east, and the Paleoproterozoic basement of the São Jose do Caiano Domain to the west, respectively (Fig. 1B) (Brito Neves and Campos Neto, 2016; Brito Neves et al., 2018). The CSD consists of a sequence of low-grade metavolcano-sedimentary rocks (Cachoeirinha Group; Kozuch, 2003; Medeiros and Jardim de Sá, 2009; Brito Neves et al., 2018), which is thought to represent an old coastal marine sedimentation basin that later suffered accretion and collision during the Cryogenian-Ediacaran (Brito Neves et al., 2018). The Cachoeirinha Group can be divided into at least two lithostratigraphic units, the Santana dos Garrotes Formation and the Serra do Olho D'Água Formation (Bittar, 1998; Medeiros, 2004; Medeiros and Jardim de Sá, 2009; Brito Neves et al., 2018). The stratigraphic relationship between them, however, has been a matter of debate. (see discussion in Marulanda, 2013). The youngest detrital zircon population in the Santana dos Garrotes Formation yielded an age range of 690 – 620 Ma (Van Schmus et al., 2011; Marulanda, 2013; Brito Neves et al., 2018) whereas in the Serra do Olho D'Água Formation the range varies from 1080 to 950 Ma (Marulanda, 2013), suggesting that the deposition of the Serra do Olho D'Água Formation probably preceded that of the Santana dos Garrotes Formation. The Santana dos Garrotes Formation is composed of metapelites and metapsammites with local occurrences of carbonates, banded iron formations and metavolcanics rocks, while the Serra do Olho D'Água

Formation consists dominantly of metaconglomerates and minor metapelites (Bittar, 1998; Medeiros, 2004; Marulanda, 2013; Brito Neves et al., 2018; Usma et al., 2021).

Numerous granitoid plutons intruded the CSD metasedimentary rocks as small stocks from ca. 640 to 620 Ma (Fig. 1B) (Sial, 1990, 1993; Brito Neves et al., 2003, 2016; Sial and Ferreira, 2016). Magmatism in this time interval is mainly composed of magmatic epidote-bearing calc-alkaline and high-K calc-alkaline tonalites and granodiorites (Sial and Ferreira, 2016). Granitoids with similar geochemical and isotopic features intruded into the APD, although to a lesser extent, in the same time interval and therefore are often considered as a single group (Conceição-type plutons; Almeida et al., 1967; Sial, 1986), whereby the petrogenetic and tectonic implications are generally the same for both (e.g., Sial and Ferreira, 2016). Nevertheless, as will be discussed below, granitoids from the CSD show certain petrographic and geochemical differences with those intrusive from the APD. Moreover, it is worth noting that despite the apparent large number of studies on this group of granitoids, the ages of the plutons intruded in the two domains (Cachoeirinha-Salgueiro and Alto Pajeú domains) are still poorly constrained.

The Carmo stock, located between the western branch of the Juru-Belém shear zone and the São José do Belmonte basin (Fig. 1C), intrudes metasedimentary rocks of the Serra do Olho D'Água Formation and is mainly composed of coarse-grained porphyritic monzogranites and granodiorites, with plagioclase megacrysts up to 11 cm in length (Figs. 2A–2F). The rocks consist of plagioclase (40 – 32 vol%), quartz (36 – 22 vol%), alkali feldspar (11 – 28 vol%), biotite (9 – 14 vol%), amphibole (< 3 vol%), and titanite, primary epidote, apatite, zircon and allanite as accessory phases (Figs. 2F, 2G). Fine-grained mafic microgranular enclaves (MMEs) and amphibole-rich clots are common and are randomly distributed within the pluton (Figs. 2B–2D). MMEs are spheroidal to ellipsoidal in shape and ranging from 5 cm to 1 m in size. In general, MMEs show irregular boundaries and gradual contacts with the host granitoids. They are quartz monzodiorite in composition and consist predominantly of plagioclase (37 – 45 vol%), amphibole (21 – 29 vol%), biotite (12 – 14 vol%), quartz (~ 12 vol%), alkali feldspar (8 – 10 vol%), and accessory minerals including titanite, epidote, apatite, zircon and rare opaque minerals. Quartz ocelli and acicular apatite are petrographic features present in all MME samples (Figs. 2H, 2I), which suggests magma mixing processes in their genesis (Vernon, 1990, 2014; Hibbard, 1991; Baxter and Feely, 2002). The amphibole-rich clots are a few centimeters in size (up to 8 cm) and have angular shapes (Fig. 2D). The contact relationships between granitoids and amphibole-rich clots are mostly sharp. Angular quartz lumps are also observed

included in both MMEs and host granitoids (Fig. 2E), and appear to be a common feature of the so-called Conceição-type granites (Sial et al., 1998; Guimarães et al., 2011).

Figure 2. (A) Contact between host granitoid and mafic enclave; (B) Rounded plagioclase phenocrysts and quartz xenocrysts within the enclave; (C) Plagioclase megacryst with corroded margin in the contact between the enclave and host granitoid; (D) Amphibole-rich clot into the granodiorite, showing their sharp boundaries; (E) Quartz lump of 7 cm in length within the host rock; (F-G) Typical mineral assemblage of the host granodiorite-monzogranite containing plagioclase (Pl), quartz (Qz), alkali feldspar (Kfs), biotite (Bt), amphibole (Amp), epidote (Ep); (H) Quartz xenocryst ('ocelli') with amphibole-rich rim in a mafic enclave; (I) Mafic clots predominantly composed of amphibole and apatite with acicular shape in the MME, evidencing magma mixing. Mineral abbreviations from Whitney and Evans (2010).

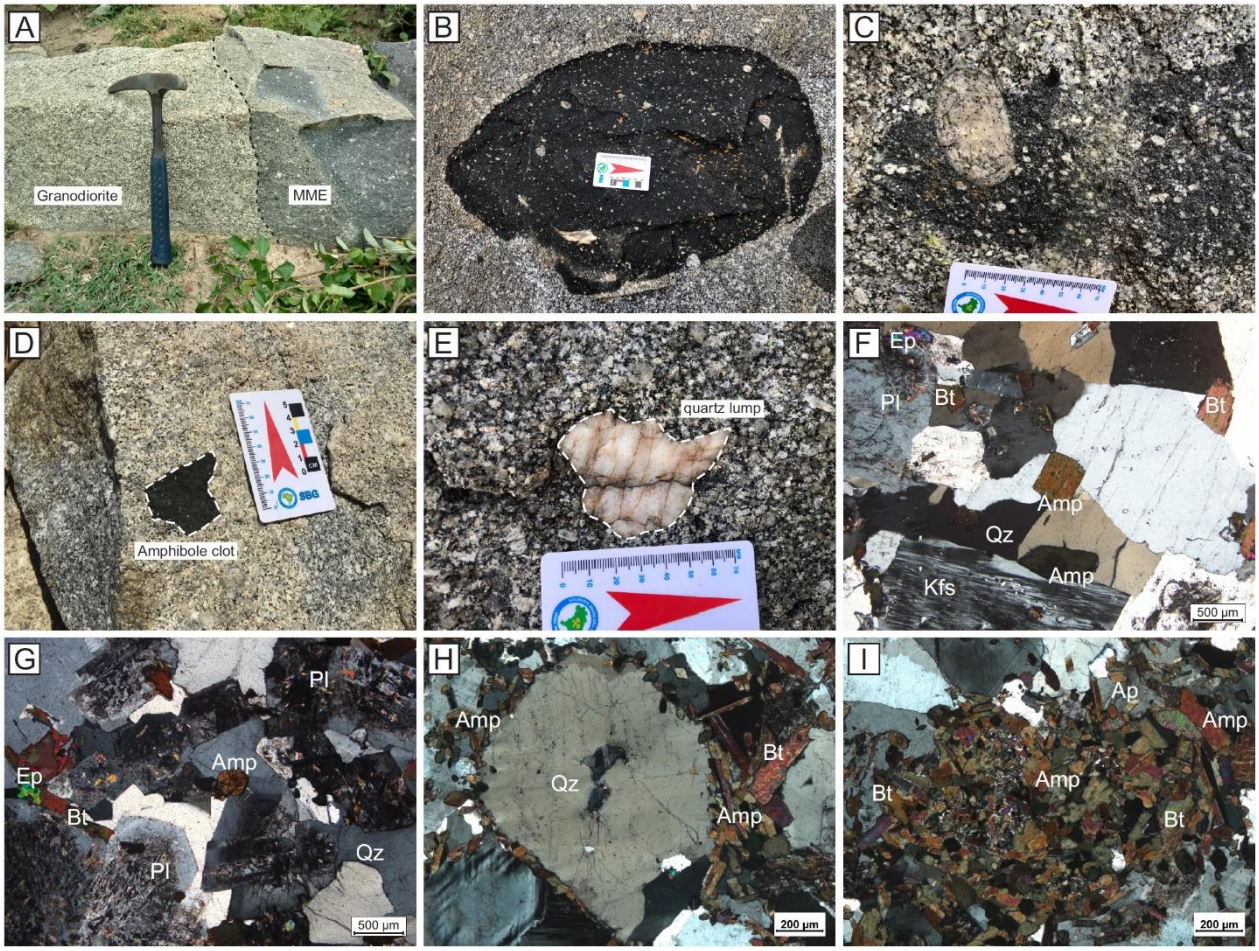

3. Analytical methods

In this study, fresh samples from the Carmo stock were selected for whole-rock major and trace element analyses. All samples were crushed in a jaw crusher and then powdered through a 200-mesh screen using a tungsten carbide ring mill. Whole-rock major element chemical analyses were determined on fused discs of samples mixed with lithium tetraborate

flux using a fully automated X-ray fluorescence spectrometer (Rigaku ZSX Primus II), by the method of calibration curves, at the Laboratory for Geochemical Studies, Department of Geology, Federal University of Pernambuco, Brazil. The calibration curves were prepared using international reference materials (AC-E, AL-I, AN-G, BE-N, IF-G, and MA-N from the International Working Group (IWG), DR-N, FK-N and UB-N from the *Association Nationale de la Recherche et de la Technologie* (ANRT), GA, GH, MICA-MG, PM-S and WS-E from the *Centre de Recherches Pétrographiques et Géochimiques* (CRPG). Trace element concentrations were analyzed by ICP-MS at the SGS Geosol laboratories, Belo Horizonte, Brazil. The analytical protocol at the SGS Geosol laboratories included the analysis of standard STD SG-142 e GRE-04 and of three sample duplicates. Representative whole-rock chemical analyses for the Carmo stock are listed in Table 2.

Conventional techniques were used to separate the zircon crystals, such as crushing, sieving and magnetic and heavy liquid separation. Zircon concentrates were cleaned using concentrated hydrofluoric acid (HF) and subsequently sulfuric acid (H_2SO_4), at the Stable Isotope Laboratory (LABISE) of the Federal University of Pernambuco, Brazil. The zircon grains were selected by handpicking under a binocular microscope and mounted in epoxy resin disks and then polished with 3 µm and 1 µm diamond paste to give a scratch-free surface. In order to examine the internal structure of individual zircon grains, images were taken by cathodoluminescence (CL). Zircon U-Pb isotope analyzes were performed at the Geochronological Research Center (CPGeo), University of São Paulo (USP), using a NEPTUNE inductively coupled plasma-mass spectrometer (ICP-MS) and an excimer laser ablation (LA) system.

The procedures used for LA-ICP-MS zircon U–Pb analyses were described by Sato et al. (2012) and Souza et al. (2017). The laser parameters used during the analysis were: 6 Hz frequency, 9.98 J/cm^2 fluence, ablating during approximate a minute and 32 µm spot size. The U-Pb analysis was performed in the following order: two blanks, two 612 NIST standard glasses, three external standards, 13 unknown samples, two external standards, and two blanks. The ^{235}U isotope signal was not measured, but obtained mathematically by dividing the ^{238}U signal by the relative abundance ^{238}U/^{235}U = 137.88. The ^{204}Hg interference on ^{204}Pb was corrected using ^{202}Hg. The ^{206}Pb/^{204}Pb, ^{207}Pb/^{204}Pb, and ^{208}Pb/^{204}Pb relative abundances were calculated and corrected for common Pb fraction using the partially corrected ^{207}Pb/^{206}Pb ratio. Analyzes of the GJ-1 standard (Jackson et al., 2004) were performed periodically, in order to correct the uncertainties and/or variations introduced by laser-induced fractionation of elements

and mass instrumental discrimination. The complete procedures follow those outlined in Kosler and Sylvester (2003). The statistical assessments were calculated using IsoplotR (Vermeesch, 2018). The zircon isotope data for single spot analyses are listed in Table 1. The uncertainties in the isotopic ratios and the ages are reported at the 1σ level.

Whole-rock Sr-Nd isotopic data were obtained using a Triton thermal ionization mass spectrometer (TIMS), at the Geochronological Research Center (CPGeo), University of São Paulo, Brazil. Sr and Nd isotopes were obtained using procedures similar to that described by Kawashita (1972) and Sato et al. (1995), respectively. The Sr isotopic ratios were normalized to the values of $^{86}Sr/^{88}Sr = 0.1194$ and the Nd isotopic ratios were normalized to $^{146}Nd/^{144}Nd = 0.7219$. International reference materials (NBS-987 and JNdi-1) were used to assess the stability of the equipment during the analysis of the samples. The average measured ratios of the standards were $^{87}Sr/^{86}Sr = 0.710257 \pm 0.000020$ for NBS-987 and $^{143}Nd/^{144}Nd = 0.512106$ for JNdi-1. Diagrams constructed using isotopic and whole-rock geochemistry data were performed with Grapher 12 software.

4. Results

a. Zircon U-Pb ages

One host granitoid sample (BCAR-60) was selected for LA-ICP-MS zircon U-Pb dating. CL images of representative zircon grains and U-Pb concordia diagrams are shown in Figure 3A. Most zircon grains are euhedral to subhedral prismatic of 150 – 300 μm in length and length/width ratios of 2:1–3:1. They show oscillatory zoning and have Th/U ratios ranging from 0.1 to 0.6, typical of magmatic origin (e.g., Williams and Claesson, 1987; Hoskin and Schaltegger, 2003).

A total of 17 spots were analyzed in the selected sample (Table 1). Five analyzes give a cluster of data, defining a concordia age of 615.3 ± 1.7 Ma (MSWD = 1.2). Among the 17 analyzes, four grains yield older relatively concordant $^{206}Pb/^{238}U$ ages (673, 697, 709 and 1355 Ma), which could represent inherited zircons, whereas the 8 remaining zircon grains define a discordia line with an upper intercept age of 622.4 ± 14.3 Ma (MSWD = 0.2). The two calculated ages are similar, however, the analyses of the discordant zircon grains show elevated common Pb content (5.1 – 9.4 %; Table 1). Thus, concordia age of 615 Ma is interpreted as the magma crystallization age of the granitoids from the Carmo stock. This age is identical (within

the error) to the SHRIMP U-Pb zircon age of 620 ± 5.5 Ma (MSWD = 1.2) previously determined by Marulanda (2013) for a granodiorite from the Carmo stock (Fig. 3B).

Figure 3. (A) Representative cathodoluminescence images of selected zircon crystals with indication of analyzed spots and U-Pb concordia diagram for the sample BCAR60; (B) U-Pb concordia diagram for the analyzed zircon grains from the Carmo stock by Marulanda (2013).

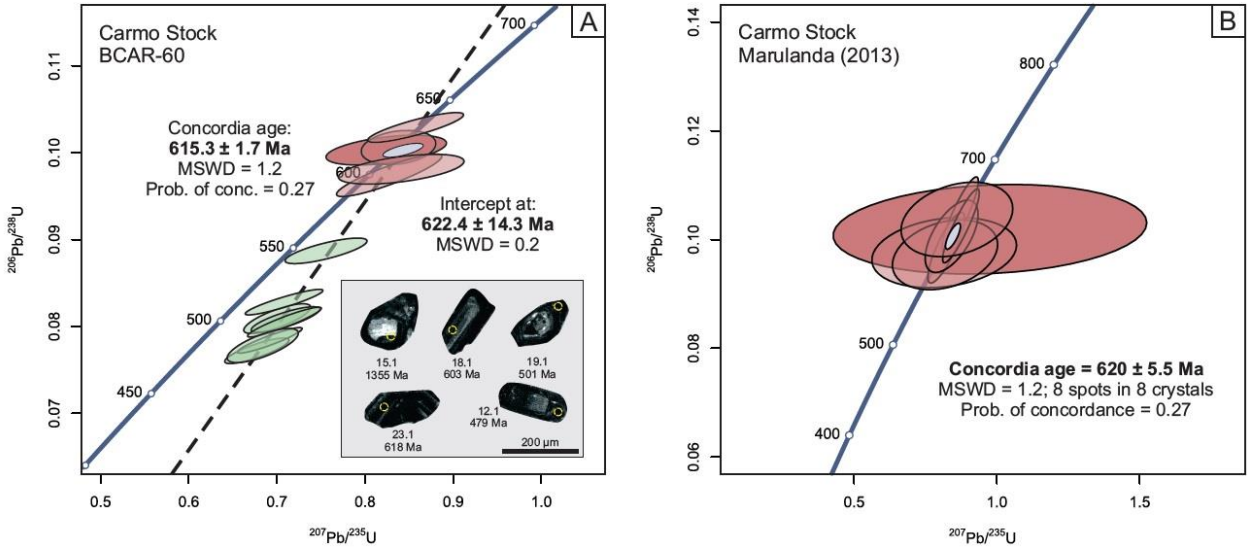

b. Major and trace elements geochemistry

Whole-rock major and trace elements chemical analyses of the host granitoids and their associated MMEs from the Carmo stock are given in Table 2. Granodiorites and monzogranites exhibit narrow variations in SiO_2 (62.63 – 66.44 wt%) and relatively high K_2O content (3.63 – 4.90 wt%), and plot in the field of high-K calc-alkaline series (Fig. 4A). They also plot in the calc-alkalic to alkali-calcic series on the (Na_2O+K_2O-CaO) vs. SiO_2 diagram (Fig. 4B). The rocks have moderate Na_2O (3.32 – 4.03 wt%), CaO (2.27 – 3.48 wt%), MgO (1.13 – 1.70 wt%), Fe_2O_{3T} (3.29 – 4.82 wt%), and Mg# values from 38.61 to 45.68. The Al_2O_3 contents (14.35 – 15.37 wt%) with A/CNK (molar Al_2O_3/[CaO + Na_2O + K_2O]) ratios of 0.73 – 0.91, denote a metaluminous affinity (Fig. 4C). Additionally, granitoid samples have low Fe# ratios ranging from 0.68 to 0.74, indicative of a magnesian character (Fig. 4D). In the Harker variation diagrams, the samples studied display a negative correlation trend with SiO_2 for most of the major oxides (Figs. 5A–5F), except for Na_2O, K_2O and Al_2O_3 (Figs. 5G–5I), which exhibit relatively constant contents and not well-defined correlation with SiO_2. These characteristics likely reflect the fractionation of ferromagnesian phases, such as biotite and amphibole, during magma evolution.

Figure 4. (A) K_2O versus SiO_2 diagram with fields after Peccerillo and Taylor (1976); (B) Modified alkali-lime index (Na_2O+K_2O-CaO) versus SiO_2 diagram (Frost et al., 2001); (C) A/NK (molar $Al_2O_3/[CaO + Na_2O + K_2O]$) versus A/CNK (molar $Al_2O_3/[Na_2O + K_2O]$) diagram (Shand, 1947; Maniar and Picolli, 1989); (D) $FeO_T/(FeO_T + MgO)$ versus SiO_2 diagram (Frost et al., 2001). Published data of granitoids in the CSD and APD are shown from: Sial (1986), Cunha (1994), Medeiros (1995), Pessoa (2001), Brasilino (2003), Guimarães et al. (2004), Siqueira (2017), Fonseca (2019).

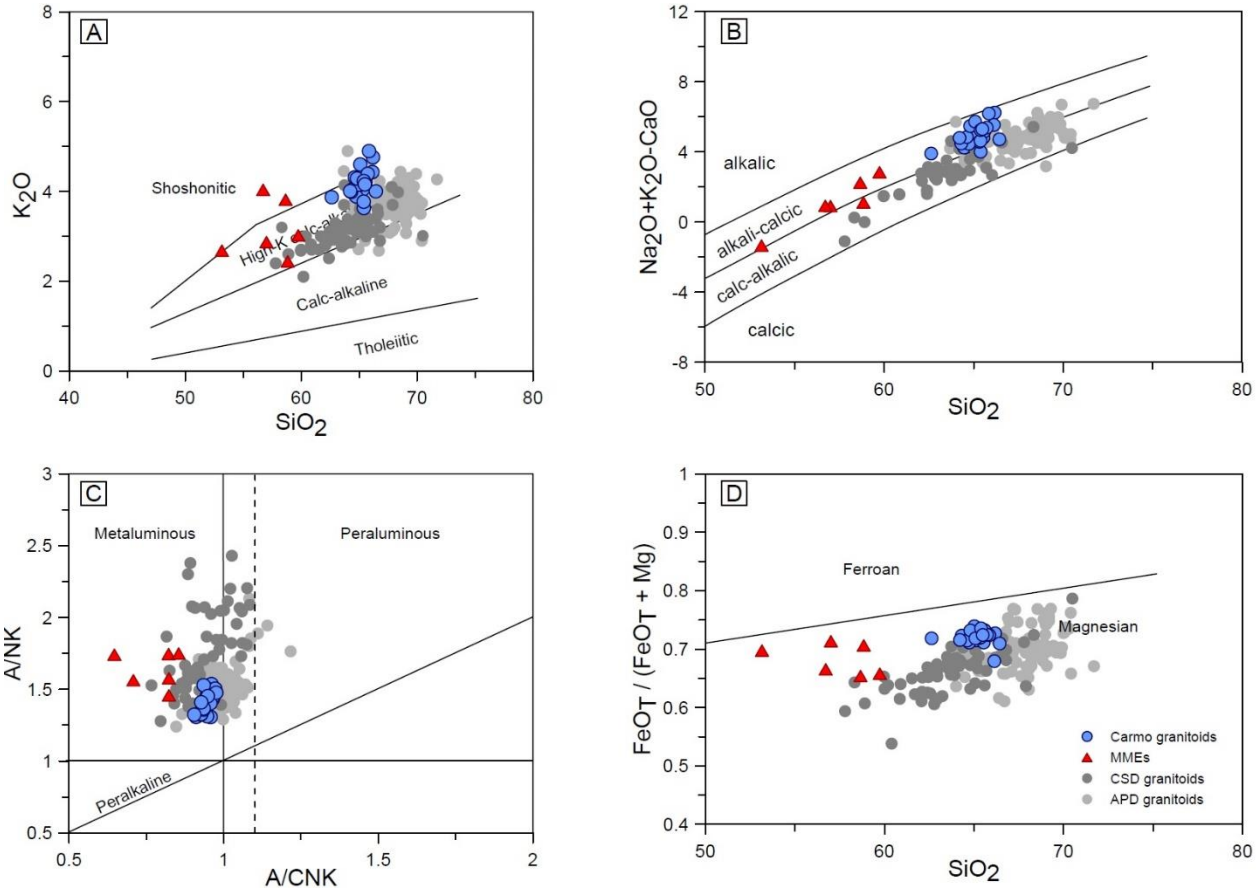

Figure 5. Harker variation diagrams of major oxide versus SiO_2 for samples from the Carmo stock. Data sources for comparison with CSD and APD plutons are the same as in Fig. 4.

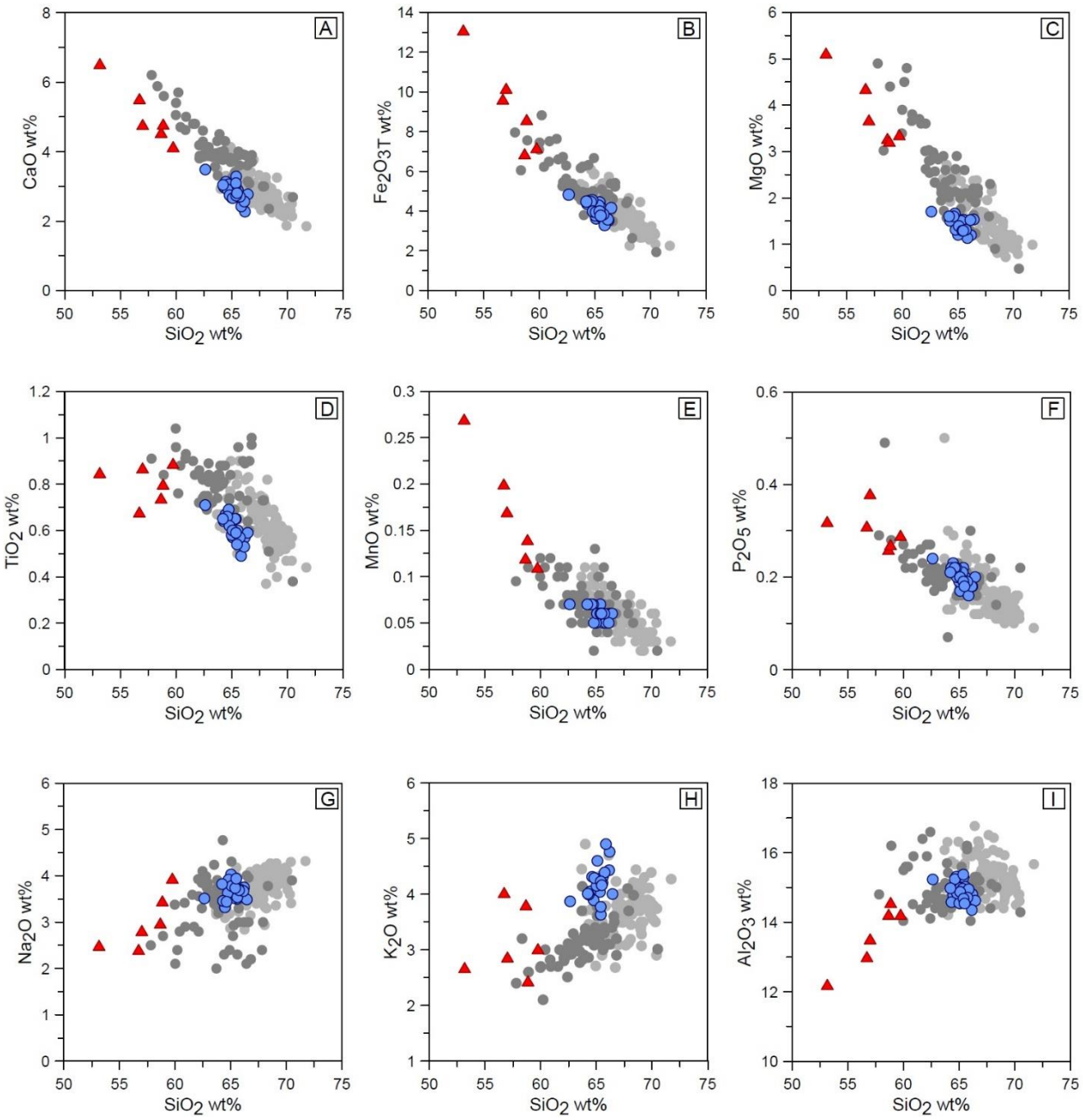

According to the chondrite-normalized rare earth element (REE) patterns (Fig. 6A), the host rock samples are enriched in ligth REE (LREE) and depleted in heavy REE (HREE), with $(La/Sm)_N$ = 3.47 – 4.29 and $(Gd/Yb)_N$ = 2.95 – 3.83. They have moderately fractionated REE patterns ($[La/Yb]_N$ = 17.36 – 25.82), with weak negative Eu anomalies (Eu/Eu* = 0.78 – 0.84). On the primitive mantle-normalized multi-element diagram (Fig. 6B), the granitoid samples show enrichment in large ion lithophile elements (LILE) and depletions in high field strength

elements (HFSE), with notable positive anomalies of U and K and negative anomalies of Nb, P, Ti.

Figure 6. (A) Chondrite-normalized rare earth element patterns, and (B) Primitive mantle-normalized multi-element diagrams for host granitoids and MME of the Carmo stock; (C) Chondrite-normalized rare earth element patterns from the Carmo stock and CSD and APD plutons; (D) Primitive mantle-normalized multi-element diagrams from the Carmo stock and CSD and APD plutons. The orange lines indicate patterns for experimental glasses of granodiorite compositions in equilibrium with Grt and in a Grt-free assemblage from the experimental work by Castro et al. (2010). Published data of granitoids in the CSD and APD are shown from: Cunha, (1994), Medeiros (1995), Brasilino (2003), Guimarães et al. (2004), Siqueira (2017).

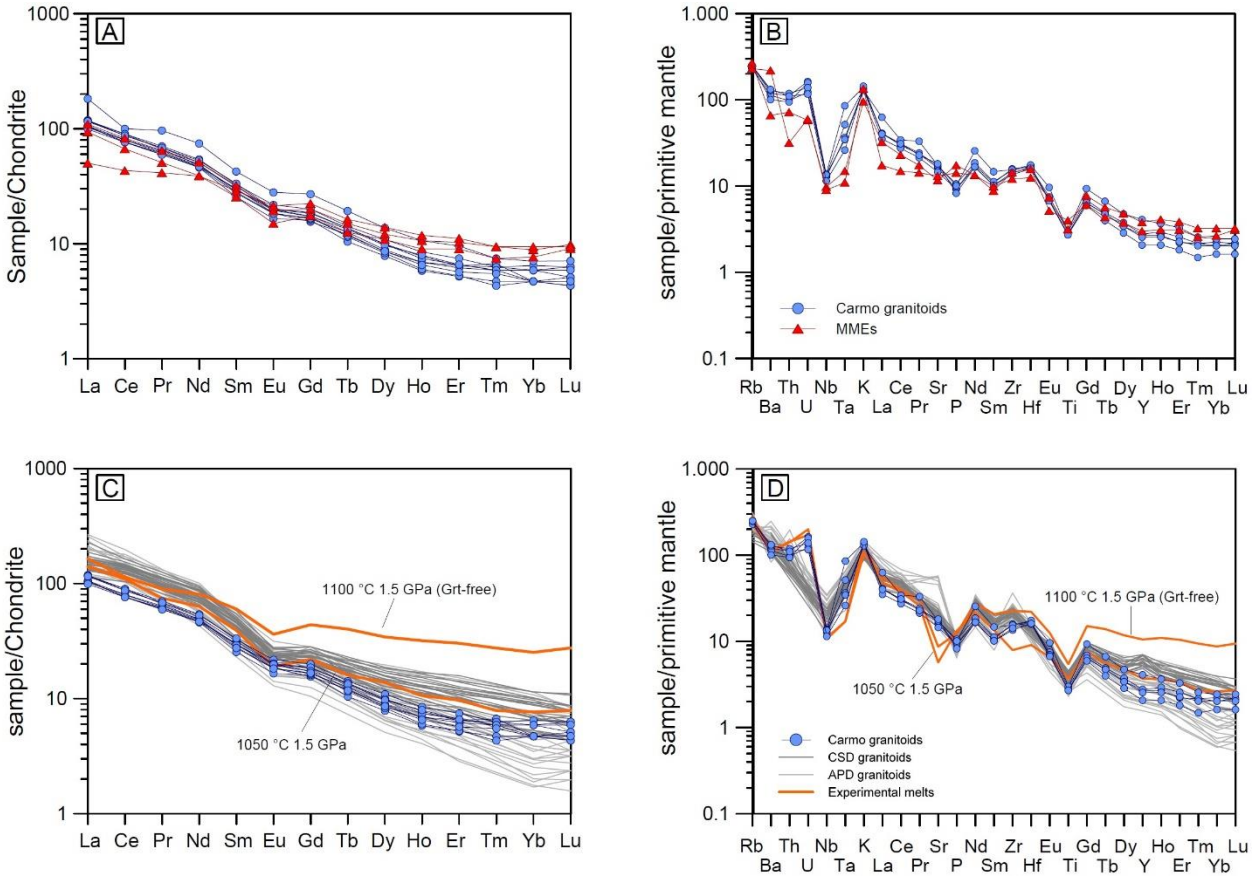

Compared with the host granites, the MME samples are characterized by lower SiO_2 (53.16 – 59.75 wt%), Al_2O_3 (12.21 – 14.57 wt%), Na_2O (2.41 – 3.95 wt%) and K_2O (2.44 – 4.03 wt%) and variable Fe_2O_3 (6.88 – 13.12 wt%) contents. They have higher CaO (4.14 – 6.53 wt%), MgO (3.22 – 5.12 wt%), Mg# (41.73 – 48.57) than the host granitoid (Table 2) and plot in the field of high-K calc-alkaline series (Fig. 4A). These rocks show metaluminous and magnesian affinity (Figs. 4C, 4D), with A/CNK ratios of 0.65 – 0.89 and Fe# = 0.65 – 0.71. The ΣREE (79 – 124 ppm) contents of the MMEs are lower than the host granitoids (111 – 170 ppm) and exhibit more flat REE patterns ($[La/Yb]_N$ = 5. 33– 12.39) (Fig. 6A), which is consistent with their higher modal proportion of hornblende. The primitive mantle-normalized

multi-element diagram (Fig. 6B) shows positive Ba, K and slight P anomalies, and depletions in Nb and Ti.

c. Whole-rock Sr-Nd isotopes

Whole-rock Rb-Sr and Sm-Nd isotopic compositions of the host granitoids and quartz monzodiorite enclaves are given in Table 3 and plotted in the diagram of $\varepsilon_{Nd}(t)$ versus initial $^{87}Sr/^{86}Sr$ (Fig. 8A). Initial $^{87}Sr/^{86}Sr$ and ε_{Nd} values were calculated using the crystallization age of 615 Ma (LA-ICP-MS zircon U-Pb), obtained from the granodiorite of the Carmo stock. The host granitoids (samples BCAR-1, BCAR-12, BCAR-24, and BCAR-39) have high initial $^{87}Sr/^{86}Sr$ ratios ranging from 0.707863 to 0.709677, weakly negative $\varepsilon_{Nd}(t)$ values ranging from –2.1 to –3.1, and T_{DM} values of 1.31 – 1.36 Ga. The Sr-Nd isotope compositions of the MME (sample BCAR-20E) overlap those of the host granitoids, with initial $^{87}Sr/^{86}Sr$ ratios of 0.708895, $\varepsilon_{Nd}(t)$ values of -2.8 and T_{DM} of 1.40 Ga.

Table 1 - LA-ICP-MS zircon U-Pb data for the sample BCAR60 from the Carmo stock.

Grain spot	Pb* (%)	Th (ppm)	U (ppm)	Th/U	$^{207}Pb/^{206}Pb$	± (1σ)	$^{207}Pb/^{235}U$	± (1σ)	$^{206}Pb/^{238}U$	± (1σ)	Rho	Apparent age (Ma)				Conc. (%)
												$^{206}Pb/^{238}U$	± (1σ)	$^{207}Pb/^{235}U$	± (1σ)	
24.1	0.4	62.1	125.5	0.5	0.0596	0.0023	0.8240	0.0279	0.1003	0.0007	0.47	616	4	610	16	100
23.1	0.0	131.4	221.9	0.6	0.0604	0.0015	0.8379	0.0173	0.1006	0.0008	0.23	618	5	618	10	99
17.1	2.5	22.4	295.7	0.1	0.0604	0.0015	0.8573	0.0222	0.1029	0.0007	0.85	632	4	629	12	100
4.1	1.0	26.8	184.1	0.1	0.0616	0.0020	0.8273	0.0244	0.0974	0.0010	0.89	599	6	612	14	97
18.1	0.0	87.4	155.5	0.6	0.0622	0.0021	0.8410	0.0291	0.0981	0.0007	0.53	603	4	620	16	97
12.1	9.4	21.9	382.7	0.1	0.0636	0.0016	0.6773	0.0149	0.0772	0.0006	0.83	479	4	525	9	91
21.1	7.5	127.6	304.0	0.4	0.0628	0.0014	0.7003	0.0155	0.0809	0.0007	0.77	501	4	539	9	93
19.1	9.2	56.6	304.8	0.2	0.0637	0.0014	0.7097	0.0159	0.0808	0.0006	0.81	501	4	545	9	91
16.1	6.2	70.6	319.9	0.2	0.0620	0.0015	0.7081	0.0180	0.0828	0.0006	0.91	513	4	544	10	94
9.1	5.5	29.5	334.4	0.1	0.0618	0.0017	0.7557	0.0190	0.0887	0.0006	0.77	548	4	572	11	95
10.1	5.1	32.5	337.3	0.1	0.0640	0.0015	0.6919	0.0150	0.0784	0.0006	0.92	486	3	534	9	91
3.1	9.4	88.6	371.5	0.2	0.0638	0.0017	0.7085	0.0171	0.0805	0.0007	0.93	499	4	544	10	91
6.1	7.2	49.1	365.9	0.1	0.0638	0.0015	0.6839	0.0165	0.0778	0.0008	0.73	483	5	529	10	91
20.1	2.9	194.9	379.3	0.5	0.0659	0.0013	1.0562	0.0233	0.1162	0.0008	0.94	709	5	732	11	96
13.1	0.0	17.2	48.5	0.4	0.0647	0.0036	0.9825	0.0403	0.1101	0.0016	0.47	673	10	695	22	96
14.1	0.6	33.0	112.8	0.3	0.0663	0.0020	1.0449	0.0304	0.1142	0.0011	0.66	697	6	726	15	95
15.1	0.8	33.3	332.6	0.1	0.1183	0.0023	3.8152	0.0755	0.2339	0.0018	0.98	1355	9	1596	15	84

Table 2 - Representative whole-rock major (wt%) and trace elements (ppm) chemical analyses of the Carmo granitoids (BCAR) and MMEs (BCAR E).

Sample	BCAR-1	BCAR-12	BCAR-14	BCAR-16	BCAR-17	BCAR-19	BCAR-20	BCAR-25	BCAR-39	BCAR-13E	BCAR-16E	BCAR-25E
SiO_2	65.16	66.19	65.55	64.47	66.44	64.74	65.60	62.63	65.39	57.01	53.16	56.72
Al_2O_3	15.17	14.80	15.02	14.77	14.62	15.31	14.73	15.23	15.37	13.52	12.21	13.01
MgO	1.40	1.19	1.52	1.56	1.53	1.66	1.21	1.70	1.13	3.69	5.12	4.36
MnO	0.06	0.06	0.06	0.07	0.06	0.07	0.05	0.07	0.05	0.17	0.27	0.20
CaO	2.88	2.27	2.89	3.13	2.77	3.06	2.69	3.48	3.09	4.78	6.53	5.52
Na_2O	3.60	3.75	3.50	3.32	3.49	3.63	3.54	3.51	3.95	2.82	2.50	2.41
K_2O	4.17	4.76	4.20	4.05	4.00	3.89	4.32	3.87	3.77	2.87	2.68	4.03
TiO_2	0.59	0.57	0.60	0.67	0.59	0.69	0.56	0.71	0.57	0.87	0.85	0.68
P_2O_5	0.19	0.18	0.20	0.23	0.20	0.22	0.18	0.24	0.19	0.38	0.32	0.31
Fe_2O_{3T}	3.90	3.52	4.16	4.50	4.15	4.54	3.68	4.82	3.75	10.18	13.12	9.63
P.F.	1.72	2.25	1.58	2.52	1.31	1.35	1.62	1.29	1.14	1.85	1.69	2.55
Total	98.84	99.54	99.28	99.29	99.16	99.16	98.18	97.55	98.59	98.13	98.45	99.42
A/NK	1.45	1.31	1.46	1.50	1.45	1.50	1.40	1.53	1.45	1.75	1.74	1.56
A/CNK	0.97	0.96	0.97	0.95	0.97	0.97	0.96	0.93	0.95	0.82	0.65	0.71
Fe#	71.48	72.69	71.12	72.19	70.94	71.11	73.24	71.84	72.03	71.34	69.75	66.53
Mg#	41.56	40.11	41.99	40.71	42.20	42	39.44	41.13	40.90	41.72	43.60	47.28
Ba			836	788	703	899	922			462		1532
Rb			160.10	146.30	157.90	158	159.40			170.40		145.70
Sr			344	359	307	366	382			245		275
Zr			177	171	152	173	160			162		135

Y	10.94	10.29	12.30	12.63	11.63	18.62	9.41	10.72	13.62	17.27
Nb			9.83	9.47	9.05	9.56	8.16		6.97	6.40
Ni			22	26	32	30	21		44	73
La	25	24.60	28	28	24.2	43.20	27.60	23.5	22.20	11.90
Ce	46.70	46.90	53.10	55	48.80	61.10	55	46.70	40.80	26.40
Pr	5.83	5.68	6.47	6.67	5.89	9.14	6.32	5.65	4.82	3.94
Nd	21.90	21.50	23.80	25.20	22.40	34.70	22.60	21.80	18.20	18.10
Sm	4.60	3.90	4.80	5	4.50	6.50	4.50	4.20	3.90	4.40
Eu	1.07	0.96	1.15	1.26	1.17	1.62	1.13	1.06	0.87	1.24
Gd	3.19	3.29	3.78	4.10	3.83	5.55	3.54	3.44	3.59	4.60
Tb	0.45	0.39	0.51	0.53	0.51	0.72	0.43	0.44	0.47	0.61
Dy	2.17	1.99	2.53	2.77	2.51	3.49	2.11	2.18	2.76	3.53
Ho	0.39	0.33	0.44	0.48	0.42	0.66	0.34	0.37	0.51	0.67
Er	1.07	0.86	1.06	1.23	1.09	1.58	0.87	0.94	1.49	1.84
Tm	0.17	0.12	0.16	0.16	0.15	0.19	0.11	0.14	0.19	0.24
Yb	0.80	0.80	1	1.10	1	1.2	0.8	0.80	1.3	1.60
Lu	0.13	0.11	0.16	0.16	0.15	0.18	0.12	0.12	0.23	0.24
Hf			5.20	5.06	4.92	5.42	4.98		4.86	5.20
Th	7.40	7.60	9.50	8.30	8	10.10	9.40	7.20	6.10	2.70
U	2.64	3.72	3.43	2.59	3.31	2.90	2.44	2.56	1.22	1.26
Ta			3.5	2.12	1.50	1.42	1.07		0.61	0.45
Ga			22.20	21	21.80	25.30	23.50		27.8	22.5
V			61	68	68	77	53		141	126

Co			11.20	12	11.30	12.90	9.80			24.9	24.40
Cs			9.80	7.21	8.59	9.34	9.88			13.41	7.39
Cu			7	9	5	46	38			92	54
Zn			104	94	84	220	94			178	163
Sn			2.80	2.30	2.10	2.90	2.30			4.30	4.30
Eu/Eu*	0.81	0.80	0.80	0.83	0.84	0.80	0.84	0.83		0.70	0.84
$(La/Yb)_N$	22.42	22.06	20.08	18.26	17.36	25.82	24.75	21.07		12.25	5.33
$(La/Sm)_N$	3.51	4.07	3.77	3.62	3.47	4.29	3.96	3.61		3.67	1.75
$(Gd/Yb)_N$	3.30	3.40	3.13	3.08	3.17	3.83	3.66	3.56		2.28	2.38

Table 3 - Rb-Sr and Sm-Nd isotopic analyses for samples from the Carmo granitoids (BCAR) and MMEs (BCAR E).

Sample	Rb (ppm)	Sr (ppm)	$(^{87}Sr/^{86}Sr)$ measured	$(^{87}Rb/^{86}Sr)$	$(^{87}Sr/^{86}Sr)_i$	εSr(t)	Sm (ppm)	Nd (ppm)	$(^{147}Sm/^{144}Nd)$ measured	$(^{143}Nd/^{144}Nd)$ measured	εNd(t)	T_{DM} (Ga)
BCAR1	158	457	0.717370	1.001246	0.708732	70.44	4.10	21.23	0.1167	0.512208	-2.10	1.31
BCAR12	194	397	0.721892	1.415808	0.709677	83.87	4.21	22.02	0.1156	0.512178	-2.59	1.34
BCAR24	140	439	0.716301	0.923459	0.708334	64.79	4.60	24.45	0.1137	0.512146	-3.08	1.36
BCAR39	116	507	0.713577	0.662350	0.707863	58.09	4.08	21.34	0.1156	0.512202	-2.12	1.30
BCAR20E	149	494	0.716431	0.873411	0.708895	72.76	4.64	22.84	0.1228	0.512199	-2.76	1.40

5. Discussion

a. Petrogenesis of the Carmo stock

i. Origin of enclaves

MMEs occur in many granitoid plutons worldwide, regardless of the nature and tectonic setting from which their host rocks were formed (Didier, 1973; Vernon, 1984; Didier and Barbarin, 1991; Barbarin, 2005; Clemens et al., 2017; Wu et al., 2020). They are almost ubiquitous in I-type calc-alkalic granites, but occurrences in other types of granitoids, such as A- and S-type granites, have also been reported and studied (e.g., Schödlbauer et al. 1997; Chappell and Wyborn, 2012; Hari et al., 2018). The origin of MMEs has long been a matter of debate and four main hypotheses have been proposed to explain their formation: (1) xenoliths of country rocks (e.g., Vernon, 1983), (2) residual phase assemblages from source rocks (restite model) (e.g., Chappell et al., 1987; Chappell and White, 1991; White et al. 1999; Chappell and Wyborn, 2012; Huang et al., 2018), (3) segregation of early-formed magmatic crystals from the host magma (cumulate/autolith) (e.g., Dahlquist, 2002; Donaire et al., 2005; Chen et al., 2015, 2016), (4) magma mixing or mingling (e.g., Vernon, 1984; Castro et al., 1990; Barbarin and Didier, 1991; Hibbard, 1991; Baxter and Feely, 2002; Barbarin, 2005; Kocak et al., 2011; Kumar, 2020).

The MMEs from the Carmo stock are spheroidal to ellipsoidal in shape (Figs. 2B, 2C), without evidence of solid-state deformation. They are finer-grained than their host rocks and show a clearly magmatic fabric. These characteristics rule out the possibility that MMEs represent xenoliths entrained during the magma ascent. In addition, the initial $^{87}Sr/^{86}Sr$ ratios and ε_{Nd} values of the MMEs are indistinguishable from their host granitoids (Table 3), reinforcing that the Carmo MMEs are not xenoliths. The MMEs with restite origins should show metamorphic microstructures and refractory mineral assemblages as residual products after partial melting (Chappell et al., 1987; Chappell and White, 1991; Vernon, 2014), which are not observed in the Carmo enclaves. Thus, restite model can also be excluded.

Despite the mixing of mafic and felsic magmas has always been the most popular petrogenetic process to explain the generation of MMEs, the cogenetic cumulate hypothesis has been widely invoked in recent years as a potential mechanism, mainly in syn-collisional settings where the participation of mantle-derived magmas is questioned (e.g., Niu et al., 2013; Huang et al., 2014; Chen et al., 2015, 2016, 2018; Zhang et al., 2016; Shao et al., 2017; Kong et al., 2020). Such autolithic origin is favored by these authors based on the following textural and

chemical observations that usually present MMEs: (1) cumulate textures, (2) similar crystallization ages and whole-rock $^{87}Sr/^{86}Sr$ and $\varepsilon_{Nd}(t)$ values to the host granitoids (3) identical mineral assemblage and mineral compositions in MMEs and host rocks, (4) linear geochemical trends for the enclaves and host granitoids in the Harker diagrams, (5) parallel REE patterns between the MMEs and the hosts, and (6) Rb-Sr data of enclaves and granitoids showing excellent co-linearity along Rb-Sr isochrons.

Nonetheless, these observations are not exclusive to a cognate origin, and many of them are also used as evidence to argue in favor of the classic model of magma mixing and mingling. Although some of the observations mentioned above are found in MMEs from Carmo stock and other plutons in the CSD (e.g., Sial, 1993; Sial et al., 1998), several lines of evidence argue against this model. The apparently linear correlation trends of CaO, Fe_2O_{3T}, MgO, TiO_2, MnO with SiO_2, between MMEs and hosts (Figs. 5A–5E), could be interpreted as reflecting cumulate nature. However, a detailed individual observation of the diagrams shows that actually granitoids and enclaves exhibit parallel trends, which is inconsistent with MMEs and host granites being generated from the same magma.

On the other hand, the mafic phases vary not only in modal abundance, but also in chemical composition. For example, Lima et al. (2021) found that biotite in MMEs from the Carmo stock has Fe/(Fe+Mg) ratios ranging from 0.53 – 0.56, while host rock biotite ranges from 0.56 – 0.60. Amphibole crystals in the Carmo MMEs have Mg# up to 56, while the host rocks contain amphibole with Mg# ranging from 39 to 52, whereby amphibole in granitoids is mostly hastingsite whereas in MMEs it ranges from edenite to pargasite (see Fig. 4B in Lima et al., 2021). Furthermore, magmatic epidote has long been recognized as an important phase in these granitoids (Conceição-type granites) (Sial, 1990; Sial et al., 2008; Ferreira et al., 2003, 2011; Brasilino et al., 2011; Sial and Ferreira, 2016). The role of this phase during intermediate magma crystallization has been studied experimentally and from natural intrusive rocks (e.g., Naney, 1983; Zen and Hammarstrom, 1984; Schmidt and Thompson, 1996; Sial et al., 1999; Ferreira et al., 2011). These studies suggest that epidote appears before or is coeval with biotite, but always after hornblende (Schmidt and Poli, 2004, and references therein), a fact that has also been observed in the Carmo stock and other magmatic epidote-bearing granitoids in the CSD (e.g., Sial, 1990, 1993; Lima et al., 2021). Thus, given that the epidote is not an early-crystallized phase, therefore, its occurrence in the MMEs from the Carmo stock is hard to reconcile with the cumulate model.

As shown above, Carmo granitoids and enclaves have relatively uniform Nd-Sr isotopic compositions and relatively parallel REE and incompatible element patterns (Fig. 6A, 6B), but this does not necessarily indicate a genetic connection between them. Experimental and natural studies of enclaves (e.g., Baker, 1989; Lesher, 1990, 1994; Elburg, 1996; Holden et al., 1991; Poli et al., 1996; Tepper and Kuehner, 2004) have indicated that during magma mixing processes significant chemical changes take place in basic magmas. These studies also showed that isotopic diffusion is at least three times faster than chemical diffusion (Baker, 1989; Lesher, 1990), indicating that isotopic re-equilibrium is theoretically feasible while the diffusive exchange of major elements is limited and slower. Accordingly, the Sr-Nd isotopic signatures in the Carmo MMEs are most likely the result of diffusion and homogenization processes during magma mixing rather than evidence of cumulate or autolith origin. This conclusion is further supported by the following field evidence and petrographic observations found in the MMEs from the Carmo stock. Feldspar megacrysts in MMEs, sometimes cross-cutting the contact between MME and host granitoid (Fig. 2A–2C), are often interpreted as derived from their host magmas via mechanical interaction (Baxter and Feely, 2002; Slaby et al., 2008). Moreover, chilled margins and acicular morphology of the apatite (Fig. 2I) imply thermal quenching during the injection of a hotter mafic magma into a cooler granitic magma (Hibbard, 1991). Quartz ocelli (Fig. 2H), which is interpreted as quartz xenocrysts reacting with the enclosing mafic magma (Vernon, 1990), is another evidence of the interaction between contrasting magmas. Consequently, we conclude that the available evidence is consistent with the interpretation that MMEs represent mafic magma blobs injected into an evolving felsic magma chamber.

In contrast, the magma sources of the MMEs is difficult to establish, as the Sr-Nd isotopic composition may have been significantly modified, or even entirely overprinted by those of their host rocks. However, as pointed out previously, chemical diffusion coefficients are much lower than isotopes during the interaction of a basic magma with an acid magma, so elemental interdiffusion is less likely (Poli et al., 1996). Thus, assessing the major and trace element chemical compositions of the MMEs is key to constraint the magma sources.

The Carmo MMEs have relatively lower SiO_2 (53.2 – 59.8 wt%) and higher MgO (3.2 – 5.1 wt%) and Fe_2O_3 (6.9 – 13.1 wt%) contents than the bulk continental crust (SiO_2 = 60.6 wt%, MgO = 4.7 wt% and Fe_2O_3 = 7.4 wt%) (Rudnick and Gao, 2014), indicating that a mantle-like magmatic component was involved. Juvenile lower crust could be a possible source, however, the SiO_2 and Mg# (42 to 49) in the MMEs studied are significantly different (Fig. 7C)

to the values found in experimental melts derived from basaltic lower crust (SiO_2 > 53 wt% and Mg# < 40) (e.g., Beard and Lofgren, 1991; Patiño Douce and Johnston, 1991; Rapp and Watson, 1995; Patiño Douce and Beard, 1995; Sisson et al., 2005), thus excluding this possibility. Therefore, mantle-derived magmas are required to explain their generation. Nevertheless, the MMEs have lower Cr (274 – 342 ppm) and Ni (44 – 73 ppm) contents and Nb/Ta (11.4 – 14.2) ratios than primary-mantle-derived melts (Cr > 1000 ppm, Ni > 400 ppm and Nb/Ta ~ 15) (Wilson, 1989; Stern and Kilian, 1996; Salters and Stracke, 2004; Karsli et al., 2007), suggesting that MMEs do not represent the parental magmas. Furthermore, on the SiO2 vs. Mg# diagram (Fig. 7C), data for MMEs plot outside the field of mantle melts and apparently follow the crustal assimilation and fractional crystallization (AFC) curve. This assumption is also supported by the linear correlation trends that show the MME samples (Fig. 5), which indicates that the enclave magmas may have been modified by fractional crystallization. In summary, based on the above interpretations, we propose that the Carmo MMEs were generated from a relatively evolved mantle-derived melt and are thermally quenched magma globules into the host felsic magma.

Figure 7. (A) K_2O versus SiO_2, (B) Na_2O versus SiO_2, and (C) Mg# versus SiO_2 diagrams. The fields of partial melts determined in experimental studies are from Beard and Lofgren (1991) (amphibolites; 1, 3, 6, 9 kbar; 800–1000 °C), Patiño Douce and Johnston (1991) (pelitic rocks at 7–13 kbar and 825–950 °C); Rapp and Watson (1995) (metabasalt; 8–32 kbar; 1000–1125 °C), Patiño Douce and Beard (1995) (quartz amphibolites; 3–15 kbar; 850–930 °C and biotite gneiss; 3–15 kbar; 850–930 °C), and Sisson et al. (2005) (medium- to high-K basaltic rocks; 7 kbar; 825–975 °C). Field of adakites derived by partial melting of subducting oceanic crust and crustal AFC curve are Stern and Kilian (1996). (D) $(La/Yb)_N$ versus $(Yb)_N$ diagram (Defant and Drummond, 1990). Data sources of the CSD and APD plutons are the same as in Fig. 4.

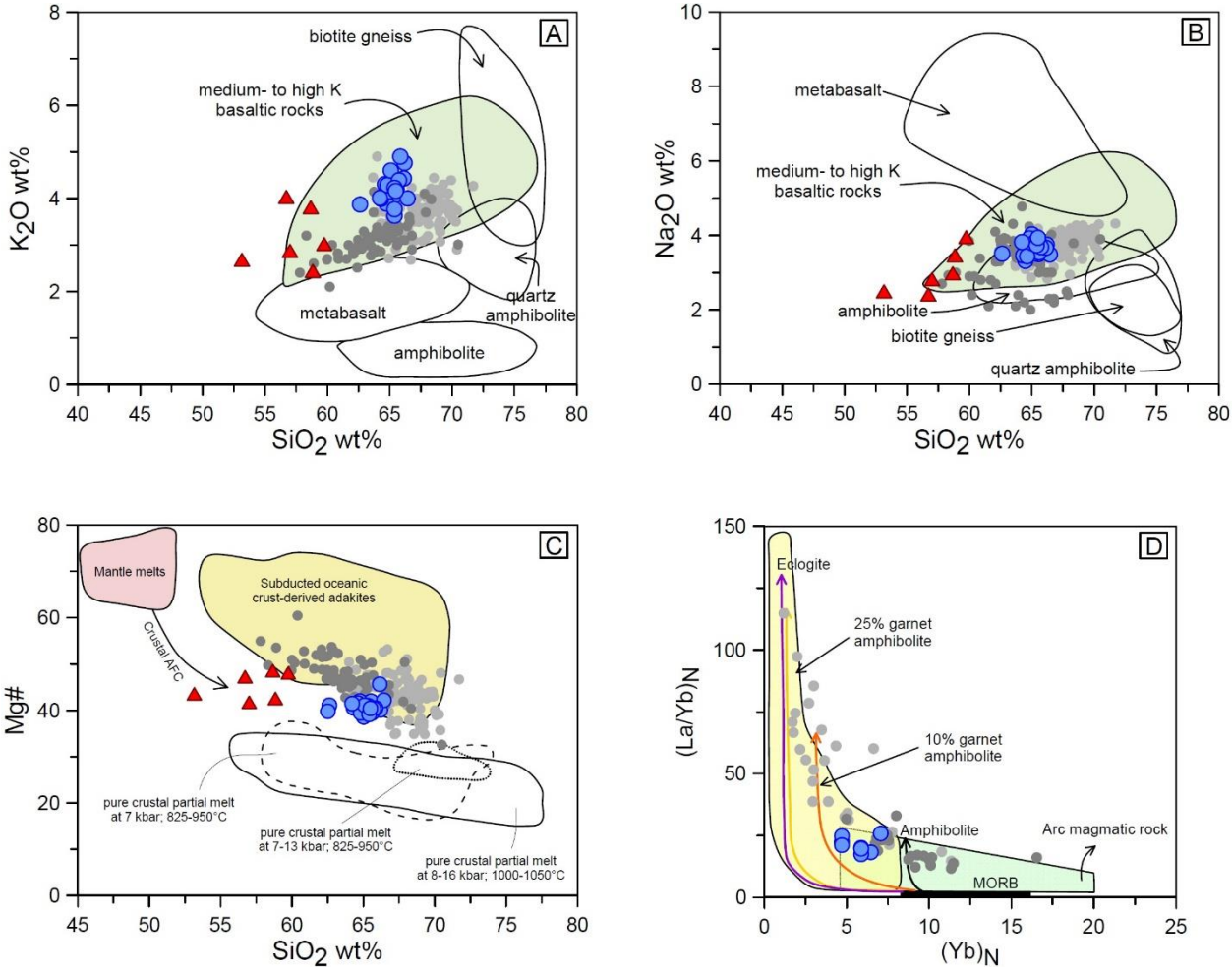

ii. Generation of the Carmo granitoids: Assessing the model of partial melting of oceanic crust and sediments

The Sr-Nd isotopic composition of the granodiorites and monzogranites from the Carmo stock is very similar to that of the granitoids that intruded the Cachoeirinha-Salgueiro and Alto Pajeú domains during the 640 – 620 Ma time interval (see review in Sial and Ferreira, 2016). Indeed, based on these isotopic similarities, both groups of granitoids (from both CSD and

APD) are interpreted as a single group and the inferences about the source rocks and the tectonic environment are generally the same (Guimarães et al., 2004; Brito Neves et al., 2016; Sial and Ferreira, 2016). Nonetheless, at this point, it is worth noting that CSD granitoids show indisputable differences with those that intruded APD. Granitoids from CSD are mainly tonalites to granodiorites and, to a lesser extent, monzogranites (as in the Carmo stock), while those from APD are mostly monzogranites. Although both groups of granitoids are porphyritic in texture, the megacrysts in CSD granodiorites are plagioclase, while in APD monzogranites they are microcline. Unusual magmatic and flow structures, such as ladder dikes, snail structures, mushroom-shaped blobs, and pillow-like structures, are common in granitoids that intrude APD (Weinberg et al., 2001), but are rare or absent in granitoids from the CSD.

Remarkable differences are also evident in the whole-rock chemical composition (Figs. 4–7). Overall, CSD granitoids are less silicic than APD granitoids, but there is some degree of overlap (Figs. 4 and 5). In the Harker correlation diagrams, data from both groups of granitoids form parallel trends (Figs. 5A–5F) rather than continuous linear trends, which would be expected in rocks that share a genetic link. In addition, APD granites have more fractionated HREE patterns (Fig. 6C) (average $[Gd/Yb]_N$ of 5.5) and higher $(La/Yb)_N$ ratios (Fig. 7D) than CSD granitoids (average $[Gd/Yb]_N$ of 3.3). In the spider diagrams, APD monzogranites are also relatively more depleted in HFSE than CSD granodiorites (Fig. 6D). Available geochronological data for both groups of granitoids are scarce (Fig. 1B), and although the plutons intruding the APD are apparently older than the CSD intrusions, this assumption is poorly supported as the current data are not very robust. Therefore, care must be taken when interpreting these two types of granitoids as being generated from a common source or under the same tectonic setting.

Despite intensive research, the petrogenesis of the 640 – 620 Ma granitoids has been enigmatic and several source rock candidates, such as Tonian crustal rocks (Guimarães and Silva Filho, 2000; Guimarães et al., 2004, 2011), mixture of mantle-derived and crustal magmas (Ferreira et al., 2004), and subducted oceanic basaltic crust (Ferreira et al., 2011; Sial and Ferreira, 2016; Santos et al., 2020), have been proposed. Most of these models have in common that they invoke a mantle-like juvenile component to explain the dominantly Mesoproterozoic Nd model ages, which are unknown in this region of the Borborema Province. However, they differ in the relative contribution of a crustal component (metasedimentary and/or igneous) and in the tectonic context associated with the generation of the granitoid magmas.

Partial melting of Tonian crustal rocks (metagraywackes) (Guimarães and Silva Filho, 2000; Guimarães et al., 2004) or even a hybrid source consisting of metagraywackes and mafic rocks (Guimarães et al., 2011) are possible sources that would explain some of the geochemical features present in the Carmo stock. For example, a mafic source is suggested by the K_2O and Na_2O versus SiO_2 contents of the rocks (Figs. 7A, 7B), which approximate the composition of experimental melts derived from medium- to high-K basaltic rocks (Sisson et al., 2005). Nevertheless, the Mg# values of the Carmo granitoids, and those intruding CSD, are higher than expected for pure crustal melts (Fig. 7C). Furthermore, Tonian supracrustal rocks in the Central Subprovince have slightly older Nd model ages (T_{DM} from 1.4 to 1.8 Ga; Santos et al., 2010) than those of the granitoids studied ($T_{DM} \leq 1.4$ Ga; Table 3 and Fig. 8B), so again a juvenile component is required.

A mixture of mantle-derived and crustal magmas is perhaps the most immediate explanation because it can justify the radiogenic Sr and slightly radiogenic Nd values. However, other lines of evidence question this model. In the ε_{Nd} vs. $^{87}Sr/^{86}Sr$ diagram, melts derived from such a mixture would exhibit a curvilinear trend towards lower crust composition (Fig. 8A). Instead, the isotopic compositions of the Carmo samples show nearly constant ε_{Nd} values and variable $^{87}Sr/^{86}Sr$ ratios, a typical feature of basaltic oceanic crust that interacted with seawater (Staudigel, 2003; Hauff et al., 2003). On the other hand, the $\delta^{18}O$ isotopic compositions of the Carmo granodiorite-monzogranite (whole-rock $\delta^{18}O \sim 12‰$; Sial, 1990, 1993) and other CSD plutons (zircon $\delta^{18}O$ up to 10‰; Sial and Ferreira, 2016), are different from mantle wedge-derived magmas (zircon $\delta^{18}O$ of 5.3 ± 0.3 ‰; Valley et al., 2005). Even considering a mixture of mantle (^{18}O-poor) and crustal (^{18}O-rich) magmas, the resulting melts could balance and produce a $\delta^{18}O$ value lower than that of the CSD granitoids (Bindeman et al., 2005). Based on these anomalously high $\delta^{18}O$ characteristics, some authors have proposed hydrothermally altered oceanic slab as the magma source for these granitoids (Sial, 1993; Ferreira et al., 2011; Sial and Ferreira, 2016). In fact, melts derived from a hydrothermally altered basaltic crust would have chemical and isotopic compositions similar to those of the Carmo granitoids, including the high $^{87}Sr/^{86}Sr$ ratios generated by the interaction with seawater. Nonetheless, as discussed above, the ε_{Nd} values and the Nd model ages suggest the participation of a radiogenic component (Figs. 8A, 8B). Moreover, it is known that slab melting produces adakite-type melts with high Sr/Y and La/Yb ratios, features that are absent in the studied granitoids. Hence, hydrothermally altered oceanic crust may be important in the generation of the Carmo stock

granitoids, but it cannot be the only component involved in creating the chemical and isotopic compositions observed in these granites.

Figure 8. (A) $\varepsilon_{Nd(t)}$ versus $(^{87}Sr/^{86}Sr)_i$ diagram for the granodiorite and monzogranite samples of the Carmo stock and CSD granitoids; (B) ε_{Nd} (620 Ma) versus T_{DM} (Ga) diagram for the host granitoids studied. Isotopic data from the CSD granitoids, Olho D'Água Formation and Riacho Gravatá Complex are plotted for comparision (see discussion in the text). The isotopic compositions for GL-08B sample (Lages and Dantas, 2006), global subducted sediments (GLOSS) (Plank and Langmuir, 2014), altered oceanic crust (AOC) (Gale et al., 2013), lower continental crust (LCC) (Rudnick and Gao, 2014) were recalculated to 620 Ma. Sr-Nd isotopic data of the CSD and APD lithologies are from the following references: Van Schmus et al. (2011), Marulanda (2013), Siqueira (2017), Brito Neves et al. (2005).

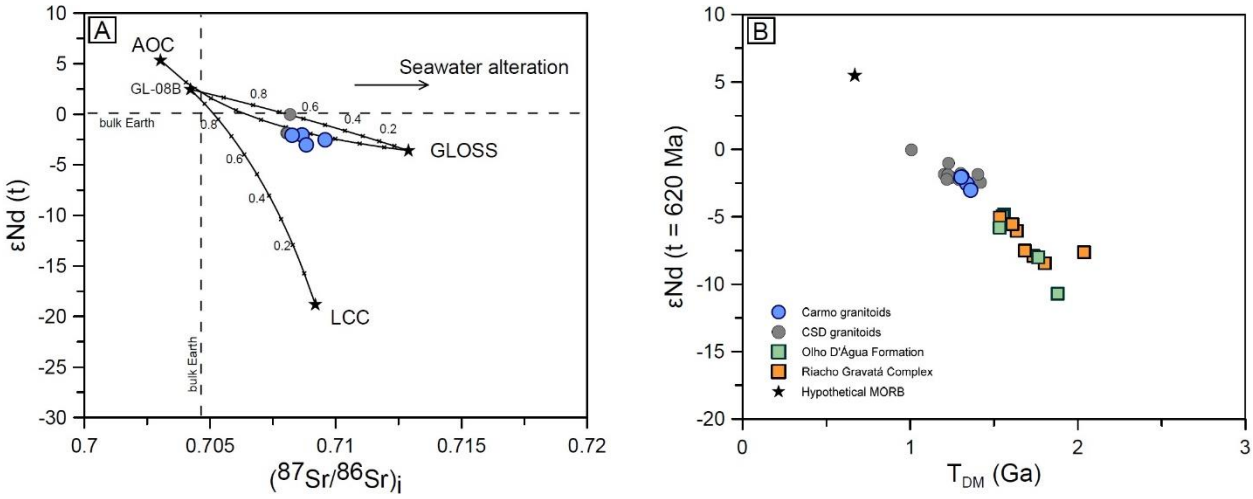

There is increasing evidence suggesting that melts derived from oceanic crust and sediments play an important role in the generation of granodiorite magmas, regardless of geodynamic context (e.g., Castro et al., 2010; Niu et al., 2013; Zang et al., 2020). The Th/La and Ba/Th ratios are often used to explore the participation of sediments in the genesis of intermediate magmas (e.g., Zhang et al., 2019). Subducted sediments have higher Th/La and lower Sm/La ratios than mantle-derived magmas (Plank, 2014), which makes this trace element ratio useful for tracing the involvement of sediment-derived melt. Carmo stock samples have low Ba/Th and Sm/La and high La/Sm and Th/La (Figs. 9A, 9B), similar to values of modern marine sediments and global subducting sediments (GLOSS), indicating the incorporation of sediment melt in the magma source. This conclusion is further evidenced by the inherited zircon cores found in the Carmo granitoids (Fig. 3A and Table 1).

Figure 9. (A) Th/La versus Sm/La diagram (Plank, 2014); (B) Ba/Th versus $(La/Sm)_N$ diagram (after Tatsumi, 2006). Data for MORB are from Niu and Baltzar (1997), marine sediments and global subducting sediment (GLOSS) are from Plank and Langmuir (1998). Data sources of the CSD and APD plutons are the same as in Fig. 6.

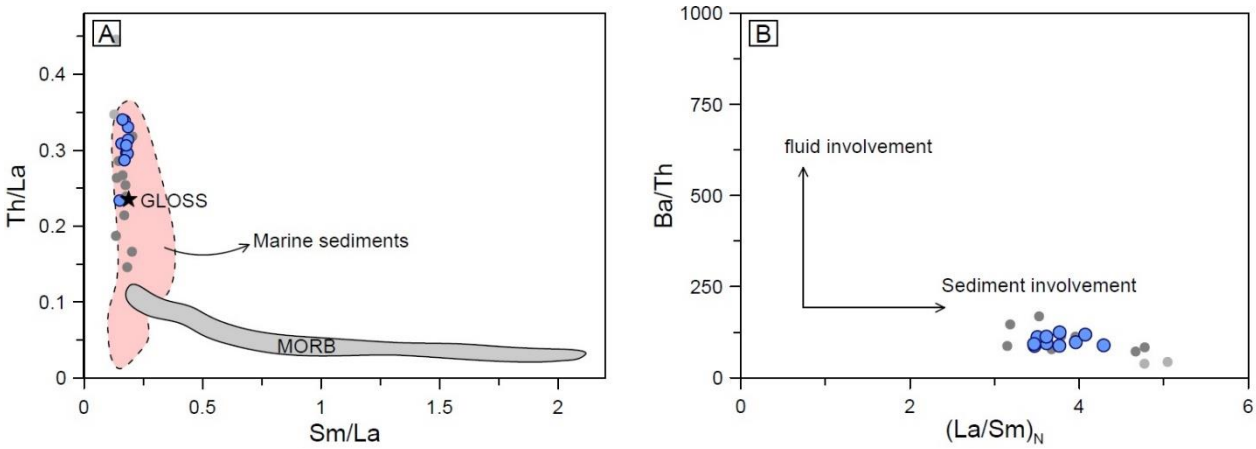

The above observations indicate that partial melting of basaltic oceanic crust along with subducted sediments should be an appropriate model for the generation of the Carmo granodiorites. Experimental data (Hermann and Splander, 2008; Castro et al., 2010; Zang et al., 2020) and geochemical evidence (e.g., Zhu et al., 2019; Chen et al., 2017; Errázuriz-Henao et al., 2019; Wang et al., 2021) show that partial melting of a mixture of subducted oceanic basalts and sediments can produce granodiorite melts with hybrid isotopic signatures that resemble those in the Carmo granodiorites. In addition, the $(La/Yb)_N$ ratios and Yb_N contents of the granodiorite can be well modelled by the partial melting of MORB with residues of amphibolite (Fig. 7D). This is consistent with the hypothesis that amphibole-rich clots found in the CSD plutons likely represent fragments or restites from melting of the source rocks (Sial et al., 1998; Ferreira et al., 2003). The relatively high $(La/Yb)_N$ ratio could be explained by less than 10% residual garnet, which is always a peritectic phase in partial melting experiments on basalt-sediment mixtures at pressures ≥ 1 GPa (Castro et al., 2010; Zang et al., 2020). This conclusion is also supported by the fact that all the samples from the Carmo stock show REE and incompatible elements patterns almost identical to those of experimental glasses in equilibrium with garnet from the experimental work by Castro et al. (2010) (Fig. 6C, 6D). Other geochemical features present in Carmo granodiorites, such as enrichment in LILE (e.g., K, Rb, Ba, Th and U) and depletion in HFSE (e.g., Nb, Ta, Ti) (Fig. 6B), are also supported by the combined effect of ilmenite as a residual phase and the addition of sediments (Hermann and Splander, 2008; Mo et al., 2008; Zang et al., 2020).

To evaluate the relative contribution of the components (ocean crust and subducted sediments) involved in the magma source, we conducted a simple binary simulation using the whole rock Sr-Nd isotopic compositions (Fig. 8A). The selected end-members are represented by the mean compositions of oceanic ridge basalts (considering Sr enrichment for seawater alteration; Gale et al., 2013) and global subducted sediments (Plank, 2014). An amphibolite

garnet sample (GL-08B), interpreted as a possible remnant of a Neoproterozoic oceanic crust (Lages and Dantas, 2016), was also chosen as the mafic end-member. According to the simulated results the Carmo granodiorites could have formed from a mixture of ~ 70 – 50% altered oceanic crust and ~ 50 – 30% subducted sediments. Nevertheless, the lack of Rb-Sr data from the lithologies assumed as sources of the subducted sediments (Riacho Gravatá Complex and/or Olho D'Água Formation) (Fig. 8B), makes a more robust calculation impossible. Thus, it is worth noting that the proportion of sedimentary component involved in the mixture could be overestimated. Finally, quartz lumps present in the ~ 640 – 620 Ma plutons from the CSD and APD is a feature that has not been studied so far and could be key to understanding the petrogenesis of these granitoids. We speculate that the quartz lumps may be remaining from the partial melting of silica-rich sediments (cherts?) but this assumption must be evaluated from more detailed studies, that could include Si and O isotope analysis which are used to unravel the contribution of sedimentary components, such as pelites and cherts, to granitoid magmas (e.g., Deng et al., 2019). In summary, the evidence discussed here suggests that the petrographic observations and the geochemical and Sr-Nd-O isotope compositions of the Carmo stock granitoids are best explained by a model involving partial melting of hydrothermally altered oceanic crust and subducted sediments.

iii. Geodynamic implications: Syn-collisional or subduction-related magmatism?

The tectonic setting from which the ~ 640 – 620 Ma plutons from the CSD and APD were generated is debated, with previous studies proposing a continental magmatic arc setting (Medeiros, 2004; Caby et al., 2009; Sial and Ferreira, 2016; Brito Neves et al., 2016; Brito Neves and Campos Neto, 2016; Santos et al., 2019, 2020; Caxito et al., 2021) or a syn-collisional setting (Guimaraes et al., 2004, 2011; Neves, 2018). The debate stems from insufficient petrogenetic and geochronological constraints on the Conceição-type granitoids, as well as the scarce of robust evidence to argue in favor of subduction, such as accretionary complexes and/or high-pressure metamorphic rocks.

Most models advocating a magmatic arc setting suggest a southeast-dipping subduction zone. The main lines of evidence for this model are: (1) occurrence of mafic and ultramafic rock lenses near the southwestern boundary of the CSD, interpreted as retroeclogites (Beurlen et al., 1992; Lages and Dantas, 2016), (2) arc-like geochemical signature of Conceição-type

granitoids, (3) Sr-Nd isotopic compositions indicative of the participation of a juvenile component, and (4) presence of multiple mafic enclaves suggesting interaction processes between contrasting magmas, which is common in continental magmatic arcs. The first evidence is consistent with high-pressure metamorphism in the CSD. All other evidence is common in magmatic arc rocks, but is not unique to this environment. Thus, oceanic crust in this region of Borborema Province was probably developed, but the development of a continental magmatic arc is still questioned.

Santos et al. (2020), proposed a continental magmatic arc setting to explain the genesis of the Riacho do Icó stock, a granitoid pluton intruding APD. Based on the geochemical data, the authors suggested that Riacho do Icó magma could have resulted from the partial melting of an oceanic slab. Nonetheless, although the samples from the Riacho do Icó stock have features of adakitic rocks (high Sr/Y), the MgO (0.6 – 1.2 wt%) and Mg# (38 – 44) values of these granitoids are lower than the subducted oceanic crust-derived adakites (1 – 6 wt% MgO and Mg# > 50; e.g., Martin et al., 2005; Wang et al., 2006). These features together with the high K_2O/Na_2O ratios (0.8 to 1.0), relative to typical adakites (~ 0.4; Martin et al., 2005), indicate that these rocks most likely correspond to continental adakites, presumably generated from melting of a thick lower crust (Moyen, 2009). SHRIMP U-Pb zircon dating for this granitoid gave an age of 607 ± 3 Ma, which is in the assumed time interval for the peak of the Central Subprovince regional metamorphism (610 – 595 Ma; e.g., Van Schmus et al., 2011), thus reinforcing the hypothesis that these adakite-like rocks could be derived from a thick continental crust and not from a subduction-related oceanic slab.

More recently, Caxito et al. (2021) proposed a tectonic model that invokes a northwest-dipping subduction zone. According to this model, the Alto Pajeú and Cachoeirinha-Salgueiro domains constitute the upper plate, while the Alto Moxotó Domain corresponds to the lower plate. This interpretation is based on the nappe-like structures found in the Serra de Jabitacá shear zone, which indicate that the APD thrusts the Alto Moxotó Domain, on the interpretations of geophysical data that suggest that this structure (Serra de Jabitacá nappes system) corresponds to an ancient suture zone, as well as the occurrence of mafic-ultramafic rocks along the boundary of the Alto Pajeú and Alto Moxotó domains, interpreted as ophiolite remnants in the Gurjão region (Lages et al., 2017) and as retroeclogites in the Floresta region (Lages and Dantas, 2016). All these characteristics are undoubtedly evidence of accretionary processes between the Alto Pajeú and Alto Moxotó domains, however the age of this event is not yet very restricted, so the inference of an Ediacaran age is speculative. Indeed, mafic-ultramafic rock

lenses, with petrographic and geochemical features similar to those found by Lages et al. (2017), have been described further southeastern of the Gurjão region and dated at 1870 ± 27 Ma (Almeida et al., 2005, 2009).

In the model by Caxito et al. (2021), the granitoids intruding the APD represent the central belt of the arc system, while the Santana dos Garrotes formation would have been deposited in a continental back-arc basin. In this context, the CSD granodiorites (including the Carmo stock) would have been generated in an arc extensional environment. This model would well explain the similarities between the younger detrital zircon populations in the Santana dos Garrotes Formation and the crystallization ages of the Conceição-type plutons (Cawood et al., 2012), as well as the nature of the sequence (turbidite deposit; Brito Neves et al., 2018), but it is not consistent with the geochemical characteristics of the granitoids intruding the Cachoeirinha-Salgueiro and Alto Pajeú domains. For example, the central belt of an Andean-type arc system (the APD plutons in the model by Caxito et al., 2021) should comprise a complete suite of calc-alkaline rocks, including important volumes of mafic and intermediate rocks (50 – 80 wt% SiO_2; e.g., Stern, 2002). Nevertheless, the plutons intruding the APD are all granitic in composition (63.7 – 71.7 wt% SiO_2; Figs. 4 and 5). In turn, volcanism in the back-arc zones is often bimodal (e.g., Shinjo and Kato, 2000), and plutons developed in this setting generally have characteristics of intraplate granites (e.g., Zhang and Zhang, 2014; Zhu et al., 2017; Lee et al., 2019), evidence which is lacking in the CSD plutons and their volcanic equivalents. Furthermore, the volume of rock produced usually decreases towards the back-arc region while high-K calcic-alkaline rocks increase (Frisch et al., 2011). An opposite situation occurs in the Alto Pajeú and Cachoeirinha-Salgueiro domains, where the K_2O contents are relatively lower in the CSD granodiorites (Fig. 5H) and the intrusive volume decreases into the APD (Fig. 1B). On the other hand, if the CSD granitoids were generated in the back-arc basin they would have crystallization ages younger than those in the central belt of the arc system, assuming that the development of a back-arc basin always succeeds to arc formation. Nonetheless, geochronological data for both groups of plutons are almost indistinguishable (Fig. 1B).

Our geochemical and isotopic data from Carmo granodiorite suggest that melting of altered oceanic crust along with sediments are possible source rocks for these granitoids. This conclusion requires a geodynamic context where such lithologies are available to melting. The immediately intuitive alternative is a subduction zone, where partial melting of oceanic crust and sediments could occur along a hot slab-top geotherm (e.g., Hernández-Uribe et al., 2020).

However, as discussed above, there is still no robust evidence to support the subduction model. In addition, oceanic crust-derived melts plus sediment below a subduction zone are expected to interact with the mantle wedge. Such an interaction between slab melts and the peridotitic mantle would produce high-Mg andesites (e.g., Tatsumi et al., 2006) or low-silica adakites (Martin et al., 2005). These features are absent in our studied granitoids. Consequently, it is unlikely that the melting of oceanic crust plus sediment invoked in this paper had been generated in a continental arc configuration.

Alternatively, the Conceição-type granites could be the record of syn-collisional magmatism (Neves, 2018). Recent studies on syn-collisional granitoids from several orogenic belts suggest that melting of oceanic crust and sediment may occur during the onset of a continental collision (e.g., Mo et al., 2008; Huang et al., 2014; Chen et al., 2017; Fu et al., 2019; Kong et al., 2020). In general, two models are proposed to explain the syn-collisional oceanic crust melting. In the first model (Mo et al., 2008; Niu et al., 2013), when the collision begins, the remaining oceanic crust (and sediments) is slowly underthrust beneath the warmer continental lithosphere. This causes the subducted slab to evolve along a high T/P path, trying to reach thermal equilibrium with the continental lithosphere. This model, however, requires the development of an active continental margin prior to the collision event (see Fig. 7 in Mo et al., 2008). The other model proposes that the partial melting of the involved lithologies (altered oceanic crust and sediments) was in response to slab break-off and asthenospheric upwelling (e.g., Fu et al., 2019).

In the geological context of the study area, a continental lithosphere previously heated by a protracted subduction event is unlikely, as a long-lived subduction zone probably never existed in this region of Borborema Province (see discussion in Neves, 2018). Nonetheless, an extensional event prior to the Brasiliano Orogeny (Neves, 2021) may have contributed the heat required for the oceanic slab to evolve along a high T/P path. A similar model is proposed by Neves et al. (2020) to explain the generation of magmatism in the eastern region of the Pernambuco-Alagoas Domain, during the early stages of the Brasiliano Orogeny. This model would theoretically justify the generation of granodiorite magmas, but it fails to explain the formation of enclave magmas, which require contribution from the mantle. Conversely, a local slab break-off model is plausible for the generation of the Carmo granitoids. Numerical modeling (Hunen and Allen, 2011) demonstrated that the viability and style of the slab break-off is mainly controlled by the strength and age of the previously subducted oceanic plate. This study also concludes that when the oceanic plate is relatively weak (and young in age), it cannot

drag down the buoyant continent to great depths and therefore would lead to an earlier and shallower break-off. The implication is that the continental crust would not reach the depths necessary to form high- and ultrahigh-pressure rocks and/or to promote the onset of arc magmatism.

Similar to other supracrustal sequences in the Borborema Province, the Santana dos Garrotes Formation, which is interpreted as an ancient coastal marine sedimentation basin, contains detrital zircon populations younger than ca. 690 Ma (Marulanda et al., 2013), so oceanic crust may have formed in the CSD only after this age. By analogy with other places where continental rifting evolved to oceanic basin formation (e.g., the Red Sea), it is possible to assume that oceanic crust occurs approximately 20–30 Ma after the initial rift (Bosworth, 2015; Stern and Johnson, 2019). If this is true, and assuming that the beginning of the contractional deformation in the Central Subprovince took place at ca. 640 – 630 Ma (Neves et al., 2015, 2020), so the oceanic crust developed at CSD would be sufficiently young and weak to break-off early and avoid the generation of high-pressure rocks and the formation of a magmatic arc. This is further supported by a study of the metamorphic facies of mafic-ultramafic rocks from the Bodocó region (Silva et al., 2019), which suggests that these rocks actually reached the blueschist facies and not the eclogite facies.

We propose, therefore, the following scenario to explain the tectonic evolution of this region of the Borborema Province and the generation of the Carmo granodiorites and all Conceição-type granites in the CSD. During the Cryogenian, extensional tectonics generated the opening of small basins that may have evolved later to a proto-oceanic stage. At ca. 640 – 630 Ma, the tectonic regime shifted to a compressional setting. With the onset of convergence, the weak oceanic crust subducted beneath the continental lithosphere, but this ephemeral subduction did not generate any magmatism. Afterwards, due to the low strength of the oceanic crust, slab break-off might have taken place, causing rising of the asthenosphere. During this process, asthenospheric mantle-derived magma supplied both the heat needed to melt the underthrusting oceanic crust and sediments, and the mantle material required to generate the enclave magmas. The melting of the altered oceanic crust along with sediments (probably derived from APD) produced the granodiorite magmas from the Carmo stock.

6. Conclusions

LA-ICP-MS zircon U-Pb geochronology indicates that the granitoids from the Carmo stock were formed at ca. 615.3 – 622.4 Ma. Whole-rock geochemical data and Sr-Nd-O isotopic compositions suggest that granodiorite-monzogranites were produced by melting of altered oceanic crust and sediments, while quartz monzodiorite MMEs most likely represent a relatively evolved mantle-derived melt. Magma mixing and mingling played an important role in the generation of the MMEs, as indicated by field and petrographic observations and chemical analyses. The petrological, geochronological and geochemical data combined with the regional data available so far point out that the Carmo stock and Conceição-type granites were generated in a syn-collision setting following the early break-off of a relatively weak oceanic slab.

Acknowledgements

We thank the National Council for Scientific and Technological Development (Conselho Nacional de Desenvolvimento Científico e Tecnológico – CNPq, process number 404472/2016 – 8) for funding this work. B.T.A. Lima thank the Brazilian agency FACEPE (process number IBPG 0780 1.07/18) for the scholarship. This is the scientific contribution n. 304 of the NEG-LABISE, Federal University of Pernambuco.

References

Almeida, F.F., Leonardos Jr., O.H., Valença, J., 1967. Review on granitic rocks of Northeast South America, Proceedings of the Symposium on Northeastern South America Granites, Recife, IUGS/UNESCO, 41.

Almeida, F.F.M., Hasui, Y., de Brito Neves, B.B., Fuck, R.A., 1981. Brazilian structural provinces: An introduction. Earth Science Reviews 17, 1–29. https://doi.org/10.1016/0012-8252(81)90003-9

Almeida, C.N., Guimarães, I.P., Beurlen, H., Topitsch, 2005. Evidências para uma zona de sutura Transamazônica na Província Borborema, Nordeste do Brasil: Os retroeclogitos da Faixa de Dobramentos Pajeú-Paraíba. XXI Simpósio de Geologia do Nordeste, Abstract, Recife, 47–51.

Almeida, C.N., Guimarães, I.P., Beurlen, H., Topitsch, W.M., Ferrer, D.M.M., 2009. Evidências de metamorfismo de alta pressão na faixa de dobramentos Pajeú-Paraíba, Província Borborema, nordeste do Brasil: petrografia e química mineral de rochas metamáficas. Revista Brasileira de Geociências 39 (3), 421–434.

Baker, D.R., 1989. Tracer versus trace element diffusion: Diffusional decoupling of Sr concentration from Sr isotope composition, Geochimca et Cosmochimica Acta, 53(11), 3015–3023. https://doi.org/10.1016/0016-7037(89)90177-4

Barbarin, B., Didier, J., 1991. Review of the main hypothesis proposed for the genesis and evolution of mafic microgranular enclaves. In: Didier, J., Barbarin, B. (Eds.), Enclaves and granite petrology. Developments in Petrology, 13. Elsevier, Amsterdan, 367–373.

Baxter, S., Feely, M., 2002. Magma mixing and mingling textures in granitoids: examples from the Galway Granite, Connemara. Mineralogy and Petrology 76, 63–74. https://doi.org/10.1007/s00710-001-0178-8

Beard, J.S., Lofgren, G.E., 1991. Dehydration Melting and Water-Saturated Melting of Basaltic and Andesitic Greenstones and Amphibolites at 1, 3, and 6-9 kb. Journal of Petrology, 32(2), 365–401. https://doi.org/10.1093/petrology/32.2.365

Behn, M.D., Kelemen, P.B., Hirth, G., Hacker, B.R., Massonne, H.J., 2011. Diapirs as the source of the sediment signature in arc lavas. Nature Geoscience 4, 641–646. https://doi.org/10.1038/ngeo1214

Beurlen, H., Silva Filho, A., Guimarães, I.P., Brito, S.B., 1992. Proterozoic c-type eclogites hosting unusual Ti-Fe±Cr±Cu mineralization in northeastern Brazil. Precambrian Research, 58(1-4), 195–214. https://doi.org/10.1016/0301-9268(92)90119-9

Bindeman, I.N., Eiler, J.M., Yogodzinski, G.M., Tatsumi, Y., Stern, C.R., Grove, T.L., Portnyagin, M., Hoernle, K., Danyushevsky, L. v., 2005. Oxygen isotope evidence for slab melting in modern and ancient subduction zones. Earth and Planetary Science Letters 235, 480–496. https://doi.org/10.1016/j.epsl.2005.04.014

Bittar, S.M.B., 1998. Faixa Piancó-Alto Brígida: Terrenos tectono-estratigráficos sob regimes metamórficos e deformacionais contrastantes. Ph.D. thesis. Universidade de São Paulo.

Bosworth, W., 2015. Geological Evolution of the Red Sea: Historical Background, Review, and Synthesis. Springer Earth System Sciences, 45–78. https://doi.org/10.1007/978-3-662-45201-1_3

Brasiliano, R. G., Sial, A.N., Lafon, J.M., 1999. Magmatic epidote, hornblende barometric estimates and emplacement of the Conceição das Creoulas pluton, Alto Pajeú Terrane, NE Brazil. An. Academia Brasileira de Ciências 7, 3 – 16.

Brasilino, R.G., 2003. Estudo petrológico e estrutural dos plutons graníticos cálcio-alcalinos de alto potássio de Conceição das Creoulas, Caldeirão Encantado, Murici e Boqueirão, Terreno Alto Pajeú, Pernambuco, NE do Brasil. Ph.D. thesis. Universidade Federal de Pernambuco.

Brasilino, R.G., Sial, A.N., Ferreira, V.P., Pimentel, M.M., 2011. Bulk rock and mineral chemistries and ascent rates of high-K calc-alkalic epidote-bearing magmas, Northeastern Brazil. Lithos 127, 441–454. https://doi.org/10.1016/j.lithos.2011.09.017

Brito Neves, B.B., 1975. Regionalização geotectônica do Pre-cambriano nordestino. Ph.D. thesis. Universidade de São Paulo.

Brito Neves, B.B., Santos, E.J., Van Schmus, W.R., 2000. Tectonic history of the Borborema Province, northeastern Brazil. In: Cordani, U., Milani, E.J., Thomaz Filho, A., Campos, D.A. (Eds.), Tectonic Evolution of South Ametica. 31 st International Geological Congress, Rio de Janeiro, Brazil, 151–182.

Brito Neves, B.B., Basei, M.A.S., Passarelli, C.R., Santos, E.J., 2003. Idades U-Pb em zircão de alguns granitos clássicos da Província Borborema. Geologia USP Série Científica 3, 25 – 38.

Brito Neves, B.B., Santos, E.J., Fuck, R.A., Santos, L.C.M.L., 2016. A preserved early Ediacaran magmatic arc at the northernmost portion of the Transversal Zone central subprovince of the Borborema Province, Northeastern South America. Brazilian Journal of Geology 46, 491–508. https://doi.org/10.1590/2317-48892016201600047

Brito Neves, B.B., Campos Neto, M.C., 2016. A faixa de dobramentos do Rio Salgado, norte-noroeste da Zona Transversal-Província Borborema (PB-CE). Geologia USP Série Científica 16 (3), 3 – 17.

Brito Neves, B.B., Van Schmus, W.R., Campos Neto, M.C., 2018. Piancó-Alto Brígida branching system of orogens (PE-PB-CE), Tectonic regionalization and geochronology. Geologia USP - Serie Cientifica 18, 149–171. https://doi.org/10.11606/issn.2316-9095.v18-142182

Caby, R., Sial, A.N., Ferreira, V.P., 2009. High-pressure thermal aureoles around two Neoproterozoic synorogenic magmatic epidote-bearing granitoids, Northeastern Brazil. Journal of South American Earth Sciences 27, 184–196. https://doi.org/10.1016/j.jsames.2008.09.005

Castro, A., Moreno-Ventas, I., La Rosa, J. D., 1990. Microgranular enclaves as indicators of hybridization processes in granitoid rocks, Hercynian Belt, Spain. Geological Journal, 25(3-4), 391–404. https://doi.org/10.1002/gj.3350250321

Castro, A., Gerya, T., García-Casco, A., Fernández, C., Díaz-Alvarado, J., Moreno-Ventas, I., Löw, I., 2010. Melting relations of MORB-sediment mélanges in underplated mantle wedge plumes; Implications for the origin of Cordilleran-type batholiths. Journal of Petrology 51, 1267–1295. https://doi.org/10.1093/petrology/egq019

Caxito, F.A., Santos, L.C.M.L., Ganade, C.E., Bendaoud, A., Fettous, E.H., Bouyo, M.H., 2020. Toward an integrated model of geological evolution for NE Brazil-NW Africa: The Borborema Province and its connections to the Trans-Saharan (Benino-Nigerian and Tuareg shields) and Central African orogens. Brazilian Journal of Geology 50. https://doi.org/10.1590/2317-4889202020190122

Caxito, F.A., Basto, C.F., Santos, L.C.M.L., Dantas, E.L., Medeiros, V.C., Dias, T.G., Barrote, V., Hagemann, S., Alkmim, A.R., Lana, C., 2021. Neoproterozoic magmatic arc volcanism in the Borborema Province, NE Brazil: possible flare-ups and lulls and implications for western Gondwana assembly. Gondwana Research 92, 1–25. https://doi.org/10.1016/j.gr.2020.11.015

Cawood, P.A., Hawkesworth, C.J., Dhuime, B., 2012. Detrital zircon record and tectonic setting. Geology 40, 875–878. https://doi.org/10.1130/G32945.1

Chappell, B.W., White, A.J.R., Wyborn, A.D., 1987. The Importance of Residual Source Material (Restite) in Granite Petrogenesis, Joitmal of Petrology 28(6), 1111–1138. https://doi.org/10.1093/petrology/28.6.1111

Chappell, B.W., White, A.J.R., 1991. Restite enclaves and the restite model. In: Didier, J., Barbarin, B. (Eds.), Enclaves and Granite Petrology. Elsevier, Amsterdam, pp. 375–381.

Chappell, B.W., Wyborn, D., 2012. Origin of enclaves in S-type granites of the Lachlan Fold Belt. Lithos, 154, 235–247. https://doi.org/10.1016/j.lithos.2012.07.012

Chen, S., Niu, Y., Sun, W., Zhang, Y., Li, J., Guo, P., Sun, P., 2015. On the origin of mafic magmatic enclaves (MMEs) in syn-collisional granitoids: evidence from the Baojishan pluton in the North Qilian Orogen, China. Mineralogy and Petrology 109, 577–596. https://doi.org/10.1007/s00710-015-0383-5

Chen, S., Niu, Y., Li, J., Sun, W., Zhang, Y., Hu, Y., Shao, F., 2016. Syn-collisional adakitic granodiorites formed by fractional crystallization: Insights from their enclosed mafic magmatic enclaves (MMEs) in the Qumushan pluton, North Qilian Orogen at the northern margin of the Tibetan Plateau. Lithos 248–251, 455–468. https://doi.org/10.1016/j.lithos.2016.01.033

Chen, J., Wei, J., Fu, L., Li, H., Zhou, H., Zhao, X., Zhan, X., Tan, J., 2017. Multiple sources of the Early Mesozoic Gouli batholith, Eastern Kunlun Orogenic Belt, northern Tibetan Plateau: Linking continental crustal growth with oceanic subduction. Lithos 292–293, 161–178. https://doi.org/10.1016/j.lithos.2017.09.006

Chen, S., Niu, Y., Xue, Q., 2018. Syn-collisional felsic magmatism and continental crust growth: A case study from the North Qilian Orogenic Belt at the northern margin of the Tibetan Plateau. Lithos 308–309, 53–64. https://doi.org/10.1016/j.lithos.2018.03.001

Clemens, J.D., Elburg, M.A., Harris, C., 2017. Origins of igneous microgranular enclaves in granites: the example of Central Victoria, Australia. Contributions to Mineralogy and Petrology 172. https://doi.org/10.1007/s00410-017-1409-2

Cunha, M.A.L., 1994. Petrologia, geoquímica, e profundidade de posicionamento de stocks granodioriticos-tonaliticos da Boa Ventura, Conceição e Pedra Branca, Paraíba. M.Sc. thesis. Universidade Federal de Pernambuco.

Dahlquist, J., 2002. Mafic microgranular enclaves: early segregation from metaluminous magma (Sierra de Chepes), Pampean Ranges, NW Argentina. Journal of South American Earth Sciences, 15(6), 643–655. https://doi.org/10.1016/s0895-9811(02)00112-8

Defant, M.J., Drummond, M.S., 1990. Derivation of some modern arc magmas by melting of young subducted lithosphere. Nature 347, 662–665. https://doi.org/10.1038/347662a0

Deng, Z., Chaussidon, M., Guitreau, M., Puchtel, I.S., Dauphas, N., Moynier, F., 2019. An oceanic subduction origin for Archaean granitoids revealed by silicon isotopes. Nature Geoscience. https://doi.org/10.1038/s41561-019-0407-6

Didier, J., 1973. Granite and their Enclaves. Elsevier, London, 393.

Didier, D., Barbarin, B., 1991. Enclaves and Granite Petrology, Developments in Petrology. Elsevier Science Publications, Amsterdam, pp. 1–625.

Donaire, T., Pascual, E., Pin, C., Duthou, J.L., 2005. Microgranular enclaves as evidence of rapid cooling in granitoid rocks: the case of the Los Pedroches granodiorite, Iberian Massif, Spain. Contributions to Mineralogy and Petrology, 149(3), 247–265. https://doi.org/10.1007/s00410-005-0652-0

Ebert, H., 1970. The Precambrian geology of the Borborema Belt (states of Paraiba and Rio Grande do Norte, northeastern Brazil), and the origin of its mineral resources. Geologische Rundschau, 59, 1294 – 1326.

Elburg, M.A., 1996. Evidence of isotopic equilibration between microgranitoid enclaves and host granodiorite, Warburton Granodiorite, Lachlan Fold Belt, Australia. Lithos, 38(1– 2), 1–22. https://doi.org/10.1016/0024-4937(96)00003-5

Errázuriz-Henao, C., Gómez-Tuena, A., Duque-Trujillo, J. F., Weber, M., 2019. The role of subducted sediments in the formation of intermediate mantle-derived magmas from the Northern Colombian Andes. Lithos 336–337, 151–168. https://doi.org/10.1016/j.lithos.2019.04.007

Ferreira, V.P., Valley, J.W., Sial, A.N., Spicuzza, M.J., 2003. Oxygen isotope compositions and magmatic epidote from two contrasting metaluminous granitoids, NE Brazil. Contributions to Mineralogy and Petrology 145, 205–216. https://doi.org/10.1007/s00410-003-0443-4

Ferreira, V.P., Sial, A.N., Pimentel, M.M., Moura, C.A.V., 2004. Intermediate to acidic magmatism and crustal evolution in the Transversal Zone, northeastern Brazil. In: Mantesso-Neto, V., Bartorelli, A., Carneiro, C.D.R., Brito Neves, B.B. (Eds.), Geologia do Continente Sul-Americano: Evolução da Obra de Fernando Flávio Marques de Almeida. Beca Produções Cultura Ltda, São Paulo, Brasil, 189–201.

Ferreira, V.P., Sial, A.N., Pimentel, M.M., Armstrong, R., Spicuzza, M.J., Guimarães, I.P., Silva Filho, A.F., 2011. Contrasting sources and P-T crystallization conditions of epidote-bearing granitic rocks, northeastern Brazil: O, Sr, and Nd isotopes. Lithos 121, 189–201. https://doi.org/10.1016/j.lithos.2010.11.002

Ferreira, V.P., Sial, A.N., Weinberg, R.F., Pimentel, M.M., 2015. Deep-seated fragmentation, transport of breccia dikes and emplacement: An example from the Borborema province, northeastern Brazil. Journal of South American Earth Sciences 58, 300–308. https://doi.org/10.1016/j.jsames.2014.10.006

Fonseca, D.P.P.C., 2019. Aspectos geológicos, petrográficos e geoquímicos do pluton granítico de Angico Torto, terreno Cachoeirinha-Salgueiro, nordeste do Brasil. Trabalho de conclusão de curso. Universidade Federal de Pernambuco.

Frisch, W., Meschede, M., Blakey, R., 2011. Subduction zones, island arcs and active continental margins. In: Plate Tectonics, 91–122. Springer, Heidelberg Dordrecht London. https://doi.org/10.1007/978-3-540-76504-2_7

Frost, B.R., Barnes, C.G., Collins, W.J., Arculus, R.J., Ellis, D.J., Frost, C.D., 2001. A Geochemical Classification for Granitic Rocks. Journal of Petrology 42(11), 2033–2048. https://doi.org/10.1093/petrology/42.11.2033

Fu, D., Kusky, T., Wilde, S.A., Polat, A., Huang, B., Zhou, Z., 2019. Early Paleozoic collision-related magmatism in the eastern North Qilian orogen, northern Tibet: A linkage between accretionary and collisional orogenesis. Bulletin of the Geological Society of America 131, 1031–1056. https://doi.org/10.1130/B35009.1

Gale, A., Dalton, C.A., Langmuir, C.H., Su, Y., Schilling, J.G., 2013. The mean composition of ocean ridge basalts. Geochemistry, Geophysics, Geosystems 14 (3), 480 – 518. https://doi.org/10.1002/ggge.20038

Guimarães, I.P., Silva Filho, A.F., 2000. Evidence of multiple sources involved in the genesis of the Neoproterozoic Itapetim Granitic Complex, NE Brazil, based on geochemical and isotopic data. Journal of South American Earth Sciences 13(6), 561–586. https://doi.org/10.1016/s0895-9811(00)00040-7

Guimarães, I.P., Silva Filho, A.F., Almeida, C.N., Van Schmus, W.R., Araújo, J.M.M., Melo, S.C., Melo, E.B., 2004. Brasiliano (Pan-African) granitic magmatism in the Pajeú-Paraíba Belt, Northeast Brazil: an isotopic and geochronological approach. Precambrian Research 135(1–2), 23–53. https://doi.org/10.1016/j.precamres.2004.07.004

Guimarães, I.P., Silva Filho, A.F., Almeida, C.N., Macambira, M.B., Armstrong, R., 2011. U-Pb SHRIMP data constraints on calc-alkaline granitoids with 1.3–1.6 Ga Nd TDM model ages from

the Central Domain of the Borborema Province, NE Brazil. Journal of South American Earth Sciences 31(4), 383–396. https://doi.org/10.1016/j.jsames.2011.03.001

Guimarães, I.P., Van Schmus, W.R., Brito Neves, B.B., Bittar, S.M.B., Silva Filho, A.F., Armstrong, R., 2012. U-Pb zircon ages of orthogneisses and supracrustal rocks of the Cariris Velhos Belt: Onset of Neoproterozoic rifting in the Borborema Province, NE Brazil. Precambrian Research 192–195, 52–77. https://doi.org/10.1016/j.precamres.2011.10.008

Guimarães, I.P., Brito, M.F.L., Lages, G.A., Silva Filho, A.F., Santos, L., Brasilino, R.G., 2016. Tonian granitic magmatism of the Borborema Province, NE Brazil: A review. Journal of South American Earth Sciences 68, 97–112. https://doi.org/10.1016/j.jsames.2015.10.009

Hauff, F., Hoernle, K., Schmidt, A., 2003. Sr-Nd-Pb composition of Mesozoic Pacific oceanic crust (Site 1149 and 801, ODP Leg 185): Implications for alteration of ocean crust and the input into the Izu-Bonin-Mariana subduction system. Geochemistry, Geophysics, Geosystems 4(8), 1–30. https://doi.org/10.1029/2002gc000421

Hari, K.R., Prasanth, M.P.M., Swarnkar, V., Kumar, J.V., Randive, K.R., 2018. Evidence for the Contrasting Magmatic Conditions in the Petrogenesis of A-type Granites of Phenai Mata Igneous Complex: Implications for Felsic Magmatism in the Deccan Large Igneous Province. Journal of the Indian Institute of Science. https://doi.org/10.1007/s41745-018-0079-z

Hermann, J., Spandler, C.J., 2007. Sediment Melts at Sub-arc Depths: an Experimental Study. Journal of Petrology 49(4), 717–740. https://doi.org/10.1093/petrology/egm073

Hernández-Uribe, D., Hernández-Montenegro, J.D., Cone, K.A., Palin, R.M., 2020. Oceanic slab-top melting during subduction: Implications for trace-element recycling and adakite petrogenesis. Geology. https://doi.org/10.1130/g46835.1

Hibbard, M.J, 1991. Zircon saturation thermometry. Textural anatomy of twelve magma-mixed granitoid systems. In: Didier, J., Barbarin, B. (Eds.), Enclaves and Granite Petrology. Elsevier, Amsterdam, pp. 431–444.

Holden, P., Halliday, A.N., Ed Stephens, W., Henney, P.J., 1991. Chemical and isotopic evidence for major mass transfer between mafic enclaves and felsic magma. Chemical Geology 92(1–3), 135–152. https://doi.org/10.1016/0009-2541(91)90053-t

Hoskin, P. W. O., Schaltegger, U., 2003. The Composition of Zircon and Igneous and Metamorphic Petrogenesis. Reviews in Mineralogy and Geochemistry 53(1), 27–62. https://doi.org/10.2113/0530027

Huang, H., Niu, Y., Nowell, G., Zhao, Z., Yu, X., Zhu, D., Mo, X., Ding, S., 2014. Geochemical constraints on the petrogenesis of granitoids in the East Kunlun Orogenic belt, northern Tibetan Plateau: implications for the continental crust growth through syn-collisional felsic magmatism. Chemical Geology 370, 1–18. https://doi.org/10.1016/j.chemgeo.2014.01.010

Huang, X.D., Lu, J.J., Sizaret, S., Wang, R.C., Wu, J.W., Ma, D.S., 2018. Reworked restite enclave: Petrographic and mineralogical constraints from the Tongshanling intrusion, Nanling Range, South China. Journal of Asian Earth Sciences 166, 1–18. https://doi.org/10.1016/j.jseaes.2018.07.001

Lima, B.T.A., Ferreira, V.P., Ardila, D.H., Neves, C.H.F.S., Sial, A.N., 2021. Crystallization conditions of the Carmo stock, NE Brazil: Implications for magmatic epidote-bearing granitoids petrogenesis. Journal of South American Earth Sciences 103427. https://doi.org/10.1016/j.jsames.2021.103427

Jackson, S.E., Pearson, N.J., Griffin, W.L., Belousova, E.A., 2004. The application of laser ablation-inductively coupled plasma-mass spectrometry to in situ U–Pb zircon geochronology. Chemical Geology 211 (1–2), 47–69. https://doi.org/10.1016/j.chemgeo.2004.06.017.

Jardim de Sá, E.F., 1994. A Faixa Seridó (Província Borborema, NE do Brasil) e o seu significado geodinâmico na cadeia Brasiliana/Pan-Africana. Ph.D Thesis, Universidade de Brasilia.

Karsli, O., Chen, B., Aydin, F., Şen, C., 2007. Geochemical and Sr–Nd–Pb isotopic compositions of the Eocene Dölek and Sariçiçek Plutons, Eastern Turkey: Implications for magma interaction in the genesis of high-K calc-alkaline granitoids in a post-collision extensional setting. Lithos 98(1–4), 67–96. https://doi.org/10.1016/j.lithos.2007.03.005

Kawashita, K., 1972. O método Rb–Sr Em Rochas Sedimentares Ph.D thesis Instituto de Geociências, IGc–USP, São Paulo.

Kocak, K., Zedef, V., Kansun, G., 2011. Magma mixing/mingling in the Eocene Horoz (Nigde) granitoids, Central southern Turkey: Evidence from mafic microgranular enclaves. Mineralogy and Petrology 103, 149–167. https://doi.org/10.1007/s00710-011-0165-7

Kosler, J., Sylvester P.J., 2003. Present Trends and the Future of Zircon in Geochronology: Laser Ablation ICPMS. Reviews in Mineralogy and Geochemistry 53(1), 243–275. https://doi.org/10.2113/0530243

Kong, J., Niu, Y., Hu, Y., Zhang, Y., Shao, F., 2020. Petrogenesis of the Triassic granitoids from the East Kunlun Orogenic Belt, NW China: Implications for continental crust growth from syn-collisional to post-collisional setting. Lithos 364–365. https://doi.org/10.1016/j.lithos.2020.105513

Kozuch, M., 2003. Isotopic and trace element geochemistry of early Neoproterozoic gneissic and metavolcanic rocks in the Cariris Velhos orogen of the Borborema Province, Brazil, and their bearing on tectonic setting. Ph.D. thesis. University of Kansas.

Kumar, S., 2020. Schedule of Mafic to Hybrid Magma Injections Into Crystallizing Felsic Magma Chambers and Resultant Geometry of Enclaves in Granites: New Field and Petrographic Observations From Ladakh Batholith, Trans-Himalaya, India. Frontiers in Earth Science 8. https://doi.org/10.3389/feart.2020.551097

Lages, G.A., Dantas, E.L., 2016. Floresta and Bodocó Mafic–Ultramafic Complexes, western Borborema Province, Brazil: Geochemical and isotope constraints for evolution of a Neoproterozoic arc environment and retro-eclogitic hosted Ti-mineralization. Precambrian Research 280, 95–119. https://doi.org/10.1016/j.precamres.2016.04.017

Lages G.A., Dantas E.L., Oliveira R.G., Santos L.C.M.L., 2017. A sequência ofiolítica de Gurjão: Caracterização geoquímica e isotópica, Província Borborema. In: Simpósio de Geologia do Nordeste, 27. Sociedade Brasileira de Geologia, Abstracts, João Pessoa.

Lee, B.Y., Oh, C.W., Cho, D.L., Zhai, M., Lee, B.C., Peng, P., Yi, K., 2019. The Devonian back-arc basin and Triassic arc-continent collision along the Imjingang belt in the Korean Peninsula and their tectonic meaning. Lithos 328–329, 276–296. https://doi.org/10.1016/j.lithos.2019.01.011

Lesher, C E., 1990. Decoupling of chemical and isotopic exchange during magma mixing. Nature 344(6263), 235–237. https://doi.org/10.1038/344235a0

Lesher, C.E., 1994. Kinetics of Sr and Nd exchange in silicate liquids: Theory, experiments, and applications to uphill diffusion, isotopic equilibration, and irreversible mixing of magmas. Journal of Geophysical Research: Solid Earth 99(B5), 9585–9604. https://doi.org/10.1029/94jb00469

Maniar, P.D., Picolli, P.M., 1989. Tectonic discrimination of granitoids. Geological Society of America Bulletin 101(5), 635–643. https://doi.org/10.1130/0016-7606(1989)101<0635:tdog>2.3.co;2

Martin, H., 1999. Adakitic magmas: modern analogues of Archaean granitoids. Lithos 46(3), 411–429. https://doi.org/10.1016/s0024-4937(98)00076-0

Martin, H., Smithies, R.H., Rapp, R., Moyen, J.F., Champion, D., 2005. An overview of adakite, tonalite–trondhjemite–granodiorite (TTG), and sanukitoid: relationships and some implications for crustal evolution. Lithos 79(1–2), 1–24. https://doi.org/10.1016/j.lithos.2004.04.048

Marulanda, C.O., 2013. Estudo da Proveniência em sequências supracrustais neoproterozoicas da Zona Transversal, Província Borborema. M.Sc. thesis. Universidade de São Paulo. https://doi.org/10.11606/D.44.2013.tde-03062015-092058

McCarthy, T.C., Patiño Douce, A.E., 1997. Experimental evidence for high-temperature felsic melts formed during basaltic intrusion of the deep crust. Geology 25(5), 463. https://doi.org/10.1130/0091-7613(1997)025<0463:eefhtf>2.3.co;2

Medeiros, V.C., 1995. Sensoriamento remoto e petrologia de granitoides Brasilianos no Domínio da Zona Transversal, nordeste do Brasil. M.Sc. thesis. Universidade Federal de Pernambuco.

Medeiros, V.C., 2004. Evolução geodinâmica e condicionamento estrutural dos terrenos Piancó-Alto Brígida e Alto Pajeú, Domínio da Zona Transversal, NE do Brasil. Ph.D. thesis. Universidade Federal do Rio Grande do Norte.

Medeiros, V.C., Jardim de Sá, E.F., 2009. O Grupo Cachoeirinha (Zona Transversal, NE do Brasil) redefinição e proposta de formalização. Revista de Geologia 22 (2), 124 – 136.

Mo, X., Niu, Y., Dong, G., Zhao, Z., Hou, Z., Zhou, S., Ke, S., 2008. Contribution of syncollisional felsic magmatism to continental crust growth: a case study of the Paleocene Linzizong volcanic succession in southern Tibet. Chemical Geology 250, 49–67. https://doi.org/10.1016/j.chemgeo.2008.02.003

Moyen, J.F., 2009. High Sr/Y and La/Yb ratios: The meaning of the “adakitic signature.” Lithos 112, 556–574. https://doi.org/10.1016/j.lithos.2009.04.001

Naney, M.T., 1983. Phase equilibria of rock-forming ferromagnesian silicates in granitic systems. American Journal of Science 283, 993–1033.

Niu, Y., Batiza, R., 1997. Trace element evidence from seamounts for recycled oceanic crust in the Eastern Pacific mantle. Earth and Planetary Science Letters, 148(3–4), 471–483. https://doi.org/10.1016/s0012-821x(97)00048-4

Niu, Y., Zhao, Z., Zhu, D., Mo, X., 2013. Continental collision zones are primary sites for net continental crust growth–a testable hypothesis. Earth Science Reviews 127, 96–110. https://doi.org/10.1016/j.earscirev.2013.09.004

Neves, S.P., 2003. Proterozoic history of the Borborema province (NE Brazil): Correlations with neighboring cratons and Pan-African belts and implications for the evolution of western Gondwana. Tectonics 22. https://doi.org/10.1029/2001TC001352

Neves, S.P., 2015. Constraints from zircon geochronology on the tectonic evolution of the Borborema Province (NE Brazil): Widespread intracontinental Neoproterozoic reworking of a Paleoproterozoic accretionary orogen. Journal of South American Earth Science 58, 150 – 164. https://doi.org/10.1016/j.jsames.2014.08.004

Neves, S.P., Bruguier, O., Silva, J.M.R., Mariano, G., Silva Filho, A.F., Teixeira, C.M.L., 2015. From extension to shortening: Dating the onset of the Brasiliano Orogeny in eastern Borborema Province (NE Brazil). Journal of South American Earth Sciences 58, 238–256. https://doi.org/10.1016/j.jsames.2014.06.004

Neves, S.P., 2018. Comment on "A preserved early Ediacaran magmatic arc at the northernmost part of the transversal zone-Central domain of the Borborema Province, Northeast of South America", by B. B. de Brito Neves et al. (2016). Brazilian Journal of Geology 48, 623–630. https://doi.org/10.1590/2317-4889201820180049

Neves, S.P., Teixeira, C.M.L., Bruguier, O., 2020. Long-lived localized magmatism in central-eastern part of the Pernambuco-Alagoas Domain, Borborema Province (NE, Brazil): Implications for tectonic setting, heat sources, and lithospheric reworking. Precambrian Research 337, 105559. https://doi.org/10.1016/j.precamres.2019.105559

Neves, S.P., 2021. Comparative geological evolution of the Borborema Province and São Francisco Craton (eastern Brazil): Decratonization and crustal reworking during West Gondwana assembly and implications for paleogeographic reconstructions. Precambrian Research 355. https://doi.org/10.1016/j.precamres.2021.106119

Patiño Douce, A.E., 1995. Experimental generation of hybrid silicic melts by reaction of high-Al basalt with metamorphic rocks. Journal of Geophysical Research: Solid Earth 100(B8), 15623–15639. https://doi.org/10.1029/94jb03376

Patiño Douce, A.E., Beard, J.S., 1995. Dehydration-melting of Biotite Gneiss and Quartz Amphibolite from 3 to 15 kbar. Journal of Petrology 36(3), 707–738. https://doi.org/10.1093/petrology/36.3.707

Patiño Douce, A.E., 1999. What do experiments tell us about the relative contributions of crust and mantle to the origin of granitic magmas? In: Castro, A., Fernandez, C., Vigneresse, J.L. (eds) Understanding Granites. Integrating New and Classical Techniques. Geological Society, London, Special Publications 158, 55–75.

Patiño Douce, A.E., Johnston, A.D., 1991. Phase equilibria and melt productivity in the pelitic system: implications for the origin of peraluminous granitoids and aluminous granulites. Contributions to Mineralogy and Petrology 107(2), 202–218. https://doi.org/10.1093/petrology/36.3.707

Peacock, S.M., Rushmer, T., Thompson, A.B., 1994. Partial melting of subducting oceanic crust. Earth and Planetary Science Letters 121 (1–2), 227–244. https://doi.org/10.1016/0012-821X(94)90042-6

Pessoa, R.J.R., 2001. Mecanismos de alojamento e Construção do Batólito Granítico Neoproterozoico de Tavares, Estado da Paraíba, NE do Brasil. Ph.D thesis. Universidade Federal de Pernambuco.

Peccerillo, A., Taylor, S.R., 1976. Geochemistry of Eocene calc-alkaline volcanic rocks from the Kastamonu area, Northern Turkey. Contributions to Mineralogy and Petrology 58(1), 63–81. https://doi.org/10.1007/bf00384745

Plank, T., Langmuir, C.H., 1998. The chemical composition of subducting sediment and its consequences for the crust and mantle. Chemical Geology, 145(3–4), 325–394. https://doi.org/10.1016/s0009-2541(97)00150-2

Plank, T., 2014. The Chemical Composition of Subducting Sediments. Treatise on Geochemistry, 607–629. https://doi.org/10.1016/b978-0-08-095975-7.00319-3

Poli, G., Tommasini, S., Halliday, A.N., 1996. Trace element and isotopic exchange during acid–basic magma interaction processes. Special Paper 315: The Third Hutton Symposium on the Origin of Granites and Related Rocks, 225–232. https://doi.org/10.1130/0-8137-2315-9.225

Rapp, R.P., Watson, E.B., 1995. Dehydration Melting of Metabasalt at 8-32 kbar: Implications for Continental Growth and Crust-Mantle Recycling. Journal of Petrology 36(4), 891–931. https://doi.org/10.1093/petrology/36.4.891

Rudnick, R.L., Gao, S., 2014. Composition of the Continental Crust A2 - Holland, Heinrich D. In: Turekian, K.K. (Ed.), Treatise on Geochemistry, second edition Elsevier, Oxford, pp. 1–51.

Salters, V.J.M., Stracke, A., 2004. Composition of the depleted mantle. Geochemistry, Geophysics, Geosystems 5(5), 1–27. https://doi.org/10.1029/2003gc000597

Santos, E.J., Schmus, W.R.V., Kozuch, M., Neves, B.B.B., 2010. The Cariris Velhos tectonic event in Northeast Brazil. Journal of South American Earth Sciences, 29(1), 61–76. https://doi.org/10.1016/j.jsames.2009.07.003

Santos, L.C.M.L., Dantas, E.L., Cawood, P.A., Lages, G.A., Lima, H.M., Santos, E.J., Caxito, F.A., 2019. Early to late Neoproterozoic subduction-accretion episodes in the Cariris Velhos Belt of the Borborema Province, Brazil: Insights from isotope and whole-rock geochemical data of supracrustal and granitic rocks. Journal of South American Earth Sciences 96. https://doi.org/10.1016/j.jsames.2019.102384

Santos, L.C.M.L., Lima, H.M., Lages, G.A., Caxito, F.A., Araújo Neto, J.F., Guimarães, I.P., 2020. Petrogenesis of the Riacho do Icó Stock: Evidence for Neoproterozoic slab melting during accretion tectonics in the Borborema Province?. Brazilian Journal of Geology 50. https://doi.org/10.1590/2317-4889202020190127

Sato, K., Tassinari, C.G., Kawashita, K., Petronilho, L., 1995. O método Geocronológico Sm-Nd no IG/USP e suas aplicações. Anais da Academia Brasileira de Ciências 67 (3), 313–336.

Sato, K., Basei, M.A.S, Sproesser, W.M., Siga, Jr.O., 2012. The application of U–Pb geochronology to zircon and titanite by laser ablation-ICP-MS. Geonalysis 2012: the 8th international conference on the analysis of geological and environmental materials, abstracts, p 86.

Schmidt, M.W., Thompson, A.B., 1996. Epidote in calc-alkaline magmas: An experimental study of stability, phase relationships, and the role of epidote in magmatic evolution. American Mineralogist 81, 462–474. https://doi.org/10.2138/am-1996-3-420

Schmidt, M.W., Poli, S., 2004. Magmatic epidote. Reviews in Mineralogy and Geochemistry 56, 399–430. https://doi.org/10.2138/gsrmg.56.1.399

Schödlbauer, S., Hecht, L., Höhndorf, A., Morteani, G., 1997. Enclaves in the S-type granites of the Kösseine massif (Fichtelgebirge, Germany): implications for the origin of granites. Geologische Rundschau 86(S1), S125–S140. https://doi.org/10.1007/pl00014648

Shand, S.J., 1947. Eruptive Rocks, third ed. Hafner Publishing Company, New York, p. 488

Shao, F., Niu, Y., Liu, Y., Chen, S., Kong, J., Duan, M., 2017. Petrogenesis of Triassic granitoids in the East Kunlun Orogenic Belt, northern Tibetan Plateau and their tectonic implications. Lithos 282–283, 33–44. https://doi.org/10.1016/j.lithos.2017.03.002

Shinjo, R., Kato, Y., 2000. Geochemical constraints on the origin of bimodal magmatism at the Okinawa Trough, an incipient back-arc basin. Lithos 54(3–4), 117–137. https://doi.org/10.1016/s0024-4937(00)00034-7

Słaby, E., Götze, J., Wörner, G., Simon, K., Wrzalik, R., Śmigielski, M., 2008. K-feldspar phenocrysts in microgranular magmatic enclaves: A cathodoluminescence and geochemical study of crystal growth as a marker of magma mingling dynamics. Lithos 105(1–2), 85–97. https://doi.org/10.1016/j.lithos.2008.02.006

Sial, A.N., 1986. Granite-types of Northeast Brazil: current knowledge. Revista Brasileira de Geociências 16, 54–72.

Sial, A.N., 1990. Epidote-bearing calc-alkalic granitoids in Northeast Brazil. Revista Brasileira de Geociências 20, 88–100. https://doi.org/10.25249/0375-7536.199088100

Sial, A.N., 1993. Contrasting metaluminous magmatic epidote-bearing granitic suites from two Precambrian Foldbelts in Northeast Brazil. Anais da Academia Brasileira de Ciência 65, 141–162.

Sial, A.N., Ferreira, V.P., Fallick, A.E., Jerônimo, M., 1998. Amphibole-rich clots in calc-alkalic granitoids in the Borborema province, northeastern Brazil. Journal of South American Earth Science. 11, 457–471. https://doi.org/10.1016/S0895-9811(98)00034-0

Sial, A.N., Toselli, A.J., Saavedra, J., Parada, M.A., Ferreira, V.P., 1999. Emplacement, petrological and magnetic susceptibility characteristics of diverse magmatic epidote-bearing granitoid rocks in Brazil, Argentina and Chile. Lithos 46, 367–392. https://doi.org/10.1016/S0024-4937(98)00074-7

Sial, A.N., Vasconcelos, P.M., Ferreira, V.P., Pessoa, R.R., Brasilino, R.G., Morais Neto, J.M., 2008. Geochronological and mineralogical constraints on depth of emplacement and ascension rates of epidote-bearing magmas from northeastern Brazil. Lithos 105, 225–238. https://doi.org/10.1016/j.lithos.2008.04.002

Sial, A.N., Ferreira, V.P., 2016. Magma associations in Ediacaran granitoids of the Cachoeirinha-Salgueiro and Alto Pajeú terranes, northeastern Brazil: Forty years of studies. Journal of South American Earth Science 68, 113–133. https://doi.org/10.1016/j.jsames.2015.10.005

Silva, S.P., Bustamante, A., Araújo, D.S., 2019. As rochas da região de Bodocó (PE) e o problema na transição entre fácies metamórficas. In: 28° Simpósio de Geologia do Nordeste. Sociedade Brasileira de Geologia, Abstracts, Sergipe.

Siqueira, R., 2017. Petrologia e geoquímica de dois plutons adjacentes de Tamboril com epidoto magmático e clinopiroxênio, Terreno Cachoeirinha-Salgueiro, Zona Transversal, nordeste do Brasil. M.Sc. thesis. Universidade Federal de Pernambuco.

Sisson, T.W., Ratajeski, K., Hankins, W.B., Glazner, A.F., 2005. Voluminous granitic magmas from common basaltic sources. Contributions to Mineralogy and Petrology 148(6), 635–661. https://doi.org/10.1007/s00410-004-0632-9

Souza, S.L., Basei, M.A.S., Sato, K., Silva, W.B., 2017. LA-MC-ICP-MS instrumentation and acquisition of U-Pb ages on zircon, monazite and titanite at CPGeo-USP. In: 2° Workshop of Inorganic Mass Spectrometry, São Paulo.

Staudigel, H., 2003. Hydrothermal Alteration Processes in the Oceanic Crust. Treatise on Geochemistry, 511–535. https://doi.org/10.1016/b0-08-043751-6/03032-2

Stern, C.R., Kilian, R., 1996. Role of the subducted slab, mantle wedge and continental crust in the generation of adakites from the Andean Austral Volcanic Zone. Contributions to Mineralogy and Petrology 123(3), 263–281. https://doi.org/10.1007/s004100050155

Stern, R.J., 2002. Subduction zones. Reviews of Geophysics 40 (4), 1012. https://doi.org/10.1029/2001RG000108

Stern, R.J., Johnson, P.R., 2019. Constraining the Opening of the Red Sea: Evidence from the Neoproterozoic Margins and Cenozoic Magmatism for a Volcanic Rifted Margin. In: Rasul N., Stewart I. (eds) Geological Setting, Paleoenvironment and Archaeology of the Red Sea, 53–79. Springer, Cham. https://doi.org/10.1007/978-3-319-99408-6_4

Syracuse, E.M., van Keken, P.E., Abers, G.A., 2010. The global range of subduction zone thermal models. Physics of the Earth and Planetary Interiors 183(1–2), 73–90. https://doi.org/10.1016/j.pepi.2010.02.004

Tatsumi, Y., 2001. Geochemical modeling of partial melting of subducting sediments and subsequent melt-mantle interaction: Generation of high-Mg andesites in the Setouchi Volcanic Belt, southwest Japan. Geology 29(4), 323. https://doi.org/10.1130/0091-7613(2001)029<0323:gmopmo>2.0.co;2

Tatsumi, Y., 2006 . High-mg andesites in the Setouchi Volcanic Belt, southwestern Japan: Analogy to Archean Magmatism and Continental Crust Formation?. Annual Review of Earth and Planetary Sciences, 34(1), 467–499. https://doi.org/10.1146/annurev.earth.34.031405.125014

Tepper, J.H., Kuehner, S.M., 2004. Geochemistry of Mafic Enclaves and Host Granitoids from the Chilliwack Batholith, Washington: Chemical Exchange Processes between Coexisting Mafic and Felsic Magmas and Implications for the Interpretation of Enclave Chemical Traits. The Journal of Geology 112(3), 349–367. https://doi.org/10.1086/382764

Usma, C.D., Sial, A.N., Ferreira, V.P., Gaucher, C., Frei, R., 2021. Ediacaran banded iron formations and carbonates of the Cachoeirinha Group of NE Brazil: Paleoenvironment and paleoredox conditions. Journal of South American Earth Sciences 109. https://doi.org/10.1016/j.jsames.2021.103282

Valley, J.W., Lackey, J.S., Cavosie, A.J., Clechenko, C.C., Spicuzza, M.J., Basei, M.A.S., Wei, C.S., 2005. 4.4 billion years of crustal maturation: oxygen isotope ratios of magmatic zircon. Contributions to Mineralogy and Petrology 150(6), 561–580. https://doi.org/10.1007/s00410-005-0025-8

van Hunen, J., Allen, M.B., 2011. Continental collision and slab break-off: A comparison of 3-D numerical models with observations. Earth and Planetary Science Letters 302(1-2), 27–37. https://doi.org/10.1016/j.epsl.2010.11.035

Van Schmus, W.R., Kozuch, M., Brito Neves, B.B., 2011. Precambrian history of the Zona Transversal of the Borborema Province, NE Brazil: Insights from Sm-Nd and U-Pb geochronology. Journal of South American Earth Science 31, 227–252. https://doi.org/10.1016/j.jsames.2011.02.010

Vauchez, A., Neves, S., Caby, R., Corsini, M., Egydio, M.S., Arthaud, M., Amaro, V., 1995. The Borborema shear zone system, NE Brazil. Journal of South American Earth Science 8, 247–266. https://doi.org/10.1016/0895-9811(95)00012-5

Vermeesch, P., 2018. IsoplotR: A free and open toolbox for geochronology. Geoscience Frontiers 9(5), 1479–1493. https://doi.org/10.1016/j.gsf.2018.04.001

Vernon, R.H., 1983. Restite, xenoliths and microgranitoid enclaves in granites. Journal and Proceedings, Royal Society of New South Wales 116, 77–103.

Vernon, R.H., 1984. Microgranitoid enclaves in granites - Globules of hybrid magma quenched in a plutonic environment. Nature 309, 438–439. https://doi.org/10.1038/309438a0

Vernon, R.H., 1990. Crystallization and hybridism in microgranitoid enclave magmas: Microstructural evidence. Journal of Geophysical Research 95(B11), 17849. https://doi.org/10.1029/jb095ib11p17849

Vernon, R.H., 2014. Microstructures of microgranitoid enclaves and the origin of S-type granitoids. Australian Journal of Earth Sciences, 61(2), 227–239. https://doi.org/10.1080/08120099.2014.886623

Wang, Q., Xu, J.F., Jian, P., Bao, Z.W., Zhao, Z.H., Li, C.F., Xiong, X.L., Ma, J.L., 2006. Petrogenesis of adakitic porphyries in an extensional tectonic setting, dexing, South China: Implications for the genesis of porphyry copper mineralization. Journal of Petrology 47, 119–144. https://doi.org/10.1093/petrology/egi070

Wang, X.C., Li, Q.L., Wilde, S.A., Li, Z.X., Li, C.F., Lei, K., Li, S., Li, L., Pandit, M.K., 2021. Decoupling between oxygen and radiogenic isotopes ─ evidence for generation of juvenile continental crust by partial melting of subducted oceanic crust. Journal of Earth Science, in press.

Weinberg, R.F., Sial, A.N., Pessoa, R.R., 2001. Magma flow within the Tavares pluton, northeastern Brazil: Compositional and thermal convection. Geological Society of America Bulletin 113(4), 508–520. https://doi.org/10.1130/0016-7606(2001)113<0508:mfwttp>2.0.co;2

White, A.J.R., Chappell, B.W., Wyborn, D., 1999. Application of the Restite Model to the Deddick Granodiorite and its Enclaves --a Reinterpretation of the Observations and Data of Maas et al. (1997). Journal of Petrology 40(3), 413–421. https://doi.org/10.1093/petroj/40.3.413

White, W.M., Klein, E.M., 2014. Composition of the Oceanic Crust. Treatise on Geochemistry, 457–496. https://doi.org/10.1016/b978-0-08-095975-7.00315-6

Whitney, D.L., Evans, B.W., 2010. Abbreviations for names of rock-forming minerals. American Mineralogist 95, 185–187. https://doi.org/10.2138/am.2010.3371

Williams, I.S., Claesson, S., 1987. Isotopic evidence for the Precambrian provenance and Caledonian metamorphism of high grade paragneisses from the Seve Nappes, Scandinavian Caledonides. Contributions to Mineralogy and Petrology 97(2), 205–217. https://doi.org/10.1007/bf00371240

Wilson, M., 1989. Igneous Petrogenesis. Springer, Harper Collins Academic, London p. 466.

Wu, T., Zhang, W., Wilde, S.A., 2020. The origin of mafic microgranular enclaves in granitoids: Insights from in situ Sr isotope of plagioclase and Zr-Hf isotopes of zircons. Chemical Geology, 119776. https://doi.org/10.1016/j.chemgeo.2020.119776

Zang, C., Tang, H., Wang, M., 2020. Effects of sediment addition on magma generation from oceanic crust in a post-collisional extensional setting: constraints from partial melting experiments on mudstone–amphibolite/basalt at 1.0 and 1.5 GPa. Journal of Asian Earth Sciences, 104111. https://doi.org/10.1016/j.jseaes.2019.104111

Zen, E.A., Hammarstrom, J.M., 1984. Magmatic epidote and its petrologic significance. Geology 12, 515–518. https://doi.org/10.1130/0091-7613(1984)12<515:MEAIPS>2.0.CO;2

Zhang, Y., Niu, Y., Hu, Y., Liu, J., Ye, L., Kong, J., Duan, M., 2016. The syncollisional granitoid magmatism and continental crust growth in the west Kunlun orogen, China – evidence from geochronology and geochemistry of the Arkarz pluton. Lithos 245, 191–204 https://doi.org/10.1016/j.lithos.2015.05.007

Zhang, X., Zhang, H., 2014. Geochronological, geochemical, and Sr–Nd–Hf isotopic studies of the Baiyanghe A-type granite porphyry in the Western Junggar: Implications for its petrogenesis and tectonic setting. Gondwana Research 25(4), 1554–1569. https://doi.org/10.1016/j.gr.2013.05.023

Zhang, L., Zhang, H., Hawkesworth, C., Luo, B., Yang, H., Xu, W., Tao, L., 2019. Sediment contribution in post-collisional high Ba-Sr magmatism: Evidence from the Xijing pluton in the Alxa block, NW China. Gondwana Research 69, 177–192. https://doi.org/10.1016/j.gr.2018.12.010

Zhu, M., Zhang, F., Fan, J., Miao, L., Baatar, M., Anaad, C., Yang, S., Li, X., Ganbat, A., 2017. Late Carboniferous bimodal volcanic rocks and coeval A-type granite in the Suman Khad area, Southwest Mongolia: Implications for the tectonic evolution. Journal of Asian Earth Sciences 144, 54–68. https://doi.org/10.1016/j.jseaes.2017.03.025

Zhu, R.Z., Lai, S.C., Qin, J.F., Zhao, S.W., Santosh, M., 2019. Petrogenesis of high-K calc-alkaline granodiorite and its enclaves from the SE Lhasa block, Tibet (SW China): Implications for recycled subducted sediments. Bulletin of the Geological Society of America 131, 1224–1238. https://doi.org/10.1130/B1841.1

5 CONCLUSÃO

O stock Carmo é composto de granodioritos e monzogranitos porfiríticos com megacristais de plagioclásio e variáveis proporções modais de anfibólio, biotita e epidoto. A abundância modal de biotita e epidoto magmático aumenta em direção ao centro do pluton, associado com a diminuição de hornblenda. Os enclaves de composição quartzo diorítica e clots ricos em anfibólios são uma característica notável e estão amplamente distribuídos em todo o pluton. Os enclaves microgranulares máficos (MMEs) tem assembleia mineral semelhante ao que ocorre nos granitóides hospedeiros, mas com maior proporção dos minerais ferromagnesianos.

A mineralogia e química mineral dos granitóides do stock Carmo, estão relacionadas com a composição e condições físico-químicas do magma durante sua cristalização. Pressões entre 6 a 7 kbar foram calculadas de acordo com o geobarometro Al em hornblenda e condições moderadamente oxidadas tamponadas por NNO foram estimadas para esses granitóides. Ambos os resultados são consistentes com a presença de epidoto magmático. Diversas evidências sugerem que o anfibólio provavelmente foi uma fase mineral cristalizada cedo, tais como a proximidade entre os valores de temperaturas estimados a partir dos geotermômetros anfibólio-plagioclásio e saturação de zircão (656 – 735 °C e 749 – 776°C, respectivamente), elevado conteúdo inicial de água (~ 5 – 6 wt%) e a sequência de cristalização mineral.

Dados U-Pb LA-ICP-MS em grãos de zircão forneceram uma idade de cristalização de 615 Ma para os granitóides do stock Carmo. Os granodioritos, monzogranitos e enclaves máficos associados são cálcio-alcalinos de alto K, metaluminosos e magnesianos. Todas as rochas estudadas mostram enriquecimento em elementos litófilos de grande raio iônico (LILE) e elementos terras raras leves (LREE), e empobrecimento em elementos de alta força de campo (HFSE) e elementos terras raras pesados (HREE). As composições isotópicas Sr-Nd dos granitóides hospedeiros e MMEs se sobrepõem dentro de uma estreita variação com altas razões iniciais de $^{87}Sr/^{86}Sr$ (0,707863 – 0,709677), valores de $\varepsilon Nd_{(t)}$ ligeiramente negativos (-2,1 a -3,1) e idades modelo T_{DM} de 1,31 – 1,40 Ga.

As semelhanças nos valores isotópicos entres os MMEs e suas rochas hospedeiras podem ter sido resultado da homogeneização e difusão isotópicas durante processos de mistura de magma. Além disso, uma série de características de campo e petrográficas, tais como a presença de megacristais de feldspato inclusos nos MMEs, apatita de morfologia acircular, quartzo “ocelli” e plagioclásio com zonação oscilatória indicam que mistura de magma jogou um papel importante na formação dos enclaves. A assinatura geoquímica dos enclaves sugere que elas foram geradas a partir de um fundido relativamente evoluído derivado do manto que foi injetado como bolhas dentro de uma câmara magmática félsica.

Os granodioritos e monzogranitos do stock Carmo apresentam valores moderados de Mg# (38,61 – 45,68) e assinaturas isotópicas Sr-Nd ligeiramente radiogênicas, indicando a participação de uma componente juvenil na sua gênese. No entanto, as características geoquímicas de elementos traços desses granitóides, tais como baixas razões Ba/Th e Sm/La e altas razões La/Sm e Th/La, são semelhantes aos valores obtidos para sedimentos marinhos modernos e sedimentos globais subduzidos, o qual indica o envolvimento de sedimentos na fonte do magma. As observações petrográficas, as composições isotópicas e os dados de geoquímica de rocha total sugerem que o magma do stock Carmo foi formado por fusão parcial

de crosta oceânica alterada hidrotermalmente mais sedimentos. Essa conclusão também é corroborada pelas composições químicas dos cristais de hornblenda e biotita, os quais sugerem fontes misturadas.

Os novos dados geoquímicos, isotópicos e geocronológicos, junto com as características geológicas regionais, sugerem que os granitóides do stock Carmo, bem como os granitos cálcio-alcalinos com epidoto magmático tipo Conceição, foram mais provavelmente formados sob um regime tectônico sin-colisional após a quebra cedo de uma placa oceânica relativamente fraca. A ascensão do manto astenosférico além de ser fonte de calor, também pode ter fornecido material para a geração dos MMEs.

REFERÊNCIAS

ALMEIDA, F. F. M.; LEONARDOS, O. H.; VALENÇA, J. Review on granitic rocks of northeast South America. *In:* International Union of Geological Sciences/UNESCO, 1967, 41 p.

ALMEIDA, F. F. M.; HASUY, H.; BRITO NEVES, B. B.; FUCK, R. A. Províncias estruturais brasileiras. *In*: Simpósio de Geologia do Nordeste, 1977, Campina Grande, p. 363 – 391.

ALMEIDA, F. F. M.; HASUI, Y.; BRITO NEVES, B. B.; FUCK, R. A. Brazilian structural provinces: An introduction. **Earth Sciences Review**, vol. 17, p.1–29, 1981.

BITTAR, S. M. B. **Faixa Piancó-Alto Brígida: Terrenos tectono-estratigráficos sob regimes metamórficos e deformacionais contrastantes**. 1998. 170 p. Dissertação de Mestrado, Universidade de São Paulo, São Paulo, 1998.

BRANDON, A. D.; CREASER, R. A.; CHACKO, T. Constraints on rates of granitic magma transport from epidote dissolution kinetics. **Science** vol. 271, p. 1845–1848, 1996.

BRITO NEVES, B. B. **Regionalização geotectônica do Pre-cambriano nordestino**. 1975. Tese de Doutorado, Universidade de São Paulo, São Paulo, 1975.

BRITO NEVES, B. B.; SANTOS, E. J.; VAN SCHMUS, W. R. Tectonic history of the Borborema Province, northeastern Brazil. *In:* CORDANI, U.; MILANI, E. J.; THOMAZ FILHO, A.; CAMPOS, D. A. (Eds.), **Tectonic Evolution of South America**. 31 st International Geological Congress, 2000, Rio de Janeiro, p. 151–182.

BRITO NEVES, B. B.; SANTOS, E. J.; FUCK, R. A.; SANTOS, L. C. M. L. A preserved early Ediacaran magmatic arc at the northernmost portion of the Transversal Zone central subprovince of the Borborema Province, Northeastern South America. **Brazilian Journal of Geology**, vol. 46, p. 491–508, 2016.

BRITO NEVES, B. B., VAN SCHMUS, W. R., CAMPOS NETO, M. C. Piancó-Alto Brígida branching system of orogens (PE-PB-CE), Tectonic regionalization and geochronology. **Geologia USP - Serie Cientifica**, vol.18, p. 149–171, 2018.

CAXITO, F. A.; BASTO, C. F.; SANTOS, L. C. M. L.; DANTAS, E. L.; MEDEIROS, V. C.; DIAS, T. G.; BARROTE, V.; HAGEMANN, S.; ALKMIM, A. R.; LANA, C. Neoproterozoic magmatic arc volcanism in the Borborema Province, NE Brazil: possible flare-ups and lulls and implications for western Gondwana assembly. **Gondwana Research**, vol. 92, p. 1–25, 2021.

EBERT, H. The Precambrian geology of the Borborema Belt (states of Paraiba and Rio Grande do Norte, northeastern Brazil), and the origin of its mineral resources. **Geologische Rundschau**, vol. 59, p. 1294 – 1326, 1970.

FERREIRA, V. P.; SIAL, A. N.; PIMENTEL, M. M.; MOURA, C. A. V. Intermediate to acidic magmatism and crustal evolution in the Transversal Zone, northeastern Brazil. *In:* MANTESSO-NETO, V.; BARTORELLI, A.; CARNEIRO, C. D. R.; BRITO NEVES, B. B. (Eds.), **Geologia do Continente Sul-Americano: Evolução da Obra de Fernando Flávio Marques de Almeida**. Beca Produções Cultura Ltda, 2004, São Paulo, p. 189–201.

FERREIRA, V. P.; SIAL, A. N.; PIMENTEL, M. M.; ARMSTRONG, R.; SPICUZZA, M. J.; GUIMARÃES, I. P.; SILVA FILHO, A. F. Contrasting sources and P-T crystallization conditions of epidote-bearing granitic rocks, northeastern Brazil: O, Sr, and Nd isotopes. **Lithos,** vol. 121, p. 189–201, 2011.

GUIMARÃES, I. P.; SILVA FILHO, A. F.; ALMEIDA, C. N.; MACAMBIRA, M. B.; ARMSTRONG, R. U-Pb SHRIMP data constraints on calc-alkaline granitoids with 1.3-1.6 Ga Nd TDM model ages from the central domain of the Borborema province, NE Brazil. Journal of South American Earth Science, vol. 31, p. 383–396, 2011.

JARDIM DE SÁ, E. F. **A Faixa Seridó (Província Borborema, NE do Brasil) e o seu significado geodinâmico na cadeia Brasiliana/Pan-Africana.** 1994. 803 p. Tese de Doutorado, Universidade de Brasilia, Brasília, 1994.

MARULANDA, C. O. **Estudo da Proveniência em sequências supracrustais neoproterozoicas da Zona Transversal, Província Borborema**. 2013. 123 p. Dissertação de Mestrado. Universidade de São Paulo, São Paulo, 2013.

MEDEIROS, V. C. **Evolução geodinâmica e condicionamento estrutural dos terrenos Piancó-Alto Brígida e Alto Pajeú, Domínio da Zona Transversal, NE do Brasil**. 2004. 199 p. Tese de Doutorado. Universidade Federal do Rio Grande do Norte, Natal, 2004.

NANEY, M. T. Phase equilibria of rock-forming ferromagnesian silicates in granitic systems. **American Journal of Science,** vol. 283, p. 993–1033, 1983.

NEVES, S. P. Proterozoic history of the Borborema province (NE Brazil): Correlations with neighboring cratons and Pan-African belts and implications for the evolution of western Gondwana. **Tectonics**, vol. 22, 2003.

NEVES, S. P. Constraints from zircon geochronology on the tectonic evolution of the Borborema Province (NE Brazil): Widespread intracontinental Neoproterozoic reworking of a Paleoproterozoic accretionary orogen. **Journal of South American Earth Science**, vol. 58, p. 150 – 164, 2015.

NEVES, S. P. Comment on "A preserved early Ediacaran magmatic arc at the northernmost part of the transversal zone-Central domain of the Borborema Province, Northeast of South America", by B. B. de Brito Neves et al. (2016). **Brazilian Journal of Geology**, vol. 48, p. 623–630, 2018.

SANTOS, E. J.; SCHMUS, W. R. V.; KOZUCH, M.; BRITO NEVES, B. B. The Cariris Velhos tectonic event in Northeast Brazil. **Journal of South American Earth Sciences**, vol. 29(1), p. 61–76, 2010.

SANTOS, L. C. M. L.; DANTAS, E. L.; CAWOOD, P. A.; LAGES, G. A.; LIMA, H. M.; SANTOS, E. J.; CAXITO, F. A. Early to late Neoproterozoic subduction-accretion episodes in the Cariris Velhos Belt of the Borborema Province, Brazil: Insights from isotope and whole-rock geochemical data of supracrustal and granitic rocks. **Journal of South American Earth Sciences,** vol. 96, 2019.

SANTOS, L. C. M. L.; LIMA, H. M.; LAGES, G. A.; CAXITO, F. A.; ARAÚJO NETO, J. F.; GUIMARÃES, I. P. Petrogenesis of the Riacho do Icó Stock: Evidence for Neoproterozoic slab melting during accretion tectonics in the Borborema Province?.**Brazilian Journal of Geology,** vol. 50, 2020.

SCHMIDT, M. W.; THOMPSON, A. B. Epidote in calc-alkaline magmas: An experimental study of stability, phase relationships, and the role of epidote in magmatic evolution. **American Mineralogist**, vol. 81, p. 462–474, 1996.

SIAL, A. N. Granite-types in northeast Brazil: current knowledge. **Revista Brasileira de Geociências**, vol. 16, p. 54–72, 1986.

SIAL, A. N. Epidote-bearing calc-alkalic granitoids in Northeast Brazil. **Revista Brasileira de Geociências,** vol. 20, p. 88–100, 1990.

SIAL, A. N.; TOSELLI, A. J.; SAAVEDRA, J.; PARADA, M. A.; FERREIRA, V. P. Emplacement, petrological and magnetic susceptibility characteristics of diverse magmatic epidote-bearing granitoid rocks in Brazil, Argentina and Chile. **Lithos,** vol. 46, p. 367–392, 1999.

SIAL, A. N.; VASCONCELOS, P. M.; FERREIRA, V. P.; PESSOA, R. R.; BRASILINO, R. G.; MORAIS NETO, J. M. Geochronological and mineralogical constraints on depth of emplacement and ascencion rates of epidote-bearing magmas from northeastern Brazil. **Lithos**, vol. 105, p. 225–238, 2008.

SIAL, A. N.; FERREIRA, V. P. Magma associations in Ediacaran granitoids of the Cachoeirinha-Salgueiro and Alto Pajeú terranes, northeastern Brazil: Forty years of studies. **Journal of South American Earth Science**, vol. 68, p. 113–133, 2016.

SILVA, T. R.; FERREIRA, V. P.; LIMA, M. M. C.; SIAL, A. N. Rapid magma ascent and formation of the Águas Belas-Canindé granitic batholith, NE Brazil: Evidence of epidote dissolution and thermobarometry. **Brazilian Journal of Geology**, vol. 50, 2020.

USMA, C. D.; SIAL, A. N.; FERREIRA, V. P.; GAUCHER, C.; FREI, R. Ediacaran banded iron formations and carbonates of the Cachoeirinha Group of NE Brazil: Paleoenvironment and paleoredox conditions. **Journal of South American Earth Sciences**, vol. 109, 2021.

VAN SCHMUS, W. R.; KOZUCH, M.; BRITO NEVES, B. B. Precambrian history of the Zona Transversal of the Borborema Province, NE Brazil: Insights from Sm-Nd and U-Pb geochronology. **Journal of South American Earth Science,** vol. 31, p. 227–252, 2011.

ANEXO A – CARTAS DE SUBMISSÃO E ACEITO

Dear Author, your article has been accepted
1 mensagem

Journal of South American Earth Sciences <service@author.email.elsevier.com> 17 de junho de 2021 05:56
Responder a: no-reply <no-reply@author.email.elsevier.com>
Para: biancathalitalima@gmail.com

If you are unable to view this message correctly, click here

ELSEVIER

Congratulations on your accepted article!

Dear Author,

We recognize you have a choice of where to submit your research and we thank you for choosing to publish with *Journal of South American Earth Sciences*.

As an expert in the field, you are best placed to explain why your article, **Crystallization conditions of the Carmo stock, NE Brazil: Implications for magmatic epidote-bearing granitoids petrogenesis**, is interesting or impactful to a wider audience. Find out how you can help your article get the visibility it deserves:

Share Your Research Data | Researcher Academy | Get Noticed

We look forward to receiving future manuscripts from you!

Sincerely,

Researcher Engagement Team

Submission to Journal of South American Earth Sciences - manuscript number

2 mensagens

Journal of South American Earth Sciences <em@editorialmanager.com> 15 de novembro de 2021 14:07
Responder a: Journal of South American Earth Sciences <support@elsevier.com>
Para: Bianca Thalita Lima <biancathalitalima@gmail.com>

This is an automated message.

Manuscript Number: SAMES-D-21-00492
Petrogenesis of the Late Neoproterozoic Carmo stock, northeastern Brazil: Implications for partial melting of oceanic crust and sediments in a syn-collisional setting

Dear Mrs Lima,

Your above referenced submission has been assigned a manuscript number: SAMES-D-21-00492.

To track the status of your manuscript, please log in as an author at https://www.editorialmanager.com/sames/, and navigate to the "Submissions Being Processed" folder.

Thank you for submitting your work to this journal.

Kind regards,
Journal of South American Earth Sciences

More information and support

You will find information relevant for you as an author on Elsevier's Author Hub: https://www.elsevier.com/authors

FAQ: How can I reset a forgotten password?
https://service.elsevier.com/app/answers/detail/a_id/28452/supporthub/publishing/
For further assistance, please visit our customer service site: https://service.elsevier.com/app/home/supporthub/publishing/
Here you can search for solutions on a range of topics, find answers to frequently asked questions, and learn more about Editorial Manager via interactive tutorials. You can also talk 24/7 to our customer support team by phone and 24/7 by live chat and email

#AU_SAMES#

To ensure this email reaches the intended recipient, please do not delete the above code